Experimental and Numerical Analyses of Mixed Mode Crack Initiation Angle

BY

Jafar Husain Ali Al Bin Mousa

A Thesis Presented to the

DEANSHIP OF GRADUATE STUDIES

KING FAHD UNIVERSITY OF PETROLEUM & MINERALS

DHAHRAN, SAUDI ARABIA

In Partial Fulfillment of the

Requirements for the Degree of

MASTER OF SCIENCE

In

MECHANICAL ENGINEERING

June 2006

KING FAHD UNIVERSITY OF PETROLEUM & MINERALS

DHAHRAN 31261, SAUDI ARABIA

DEANSHIP OF GRADUATE STUDIES

This thesis, written by

JAFAR HUSAIN ALI AL BIN MOUSA

under the direction of his thesis advisor and approved by his thesis committee, has been presented to and accepted by the Dean of Graduate Studies, in partial fulfillment of the requirements for the degree of

MASTER OF SCIENCE IN MECHANICAL ENGINEERING.

Thesis Committee

Dr. Nesar Merah (Thesis Advisor)

Dr. Abdul Salam Eleiche (Member)

Dr. Abul Fazal Arif (Member)

Dr. Amro Al-Qutub
Department Chairman

Dr. Mohammad Abdul-Aziz Al-Ohali
Dean of Graduate Studies

28-6-2006
Date

to my

parents

wife

brothers

sisters

and

parents in law

ACKNOWLEDGEMENTS

At the beginning I thank Allah on his generous blessings that give me the health, the strength and the capability in my entire life moments and, to accomplish this work.

I acknowledge King Fahd University of Petroleum & Minerals for the continuous support in carrying out this research.

I would like to express my deepest gratitude to my thesis advisor, Dr. Nesar Merah for his unlimited help and guidance during the course of this work. It might seem to worth nothing when I say that he taught me how to say "*I will do it*" rather than "*I will try to do it*". However, I found it one of the greatest lesson I have ever been taught and I can't imagine how positively it is going to effect my future life. I also would like to thank my thesis committee members, Dr. Abdul Salam Eleiche and Dr. Abul Fazal Arif for their cooperation and valuable suggestions.

I would like to thank the Chairman of Mechanical Engineering Dr. Amro Al-Qutub, faculty members, graduate students, people of Mechanical Engineering Workshop, Civil Engineering Department and Physics Department for their support and help.

Finally, my greatest thanks go to my wife for her patience, love and understanding throughout all stages of this work.

TABLE OF CONTENTS

LIST OF FIGURES

LIST OF TABLES

NOMENCLATURE

a	Crack Length
β	Crack inclination angle
E	Modulus of Elasticity
f_k	Arbitrary function
f_σ	Material fringe constant
G	Modulus of rigidity
h	Specimen thickness
I, II, III	Subscripts denoting mode of loading
i	Subscript refers to i^{th} iterative step
K	Stress intensity factor
k	Data point index
κ	for plane strain = 3-4v, for plane stress = (3- v)/(1+ v)
L	Specimen length
M	Stress Triaxiality ratio
m	Number of data point
μ	Stress intensity ratio K_I/K_{II}
N	Fringe Order
v	Poisson's ratio
Q	Figure of merit
r_0	Radial distance from the crack tip to the frist side-node behaind the crack tip
r	Radial distance from the crack tip to any point
r_p	Radius of Mises elastic-plastic boundary
R_p	Non-dimensionlized radius of Mises elastic-plastic boundary
S	Strain energy desnsity factor
S	Sensitivity index
SIF	Stress intensity factor
σ	Applied stress
σ_{0x}	Far field stress
σ_H	Hydrostatic stress
σ_{eq}	Equivalent stress
σ_{YS}	Tensile yield strength
T_v	Dilatational strain energy
T_D	Distortional strain energy
τ_{max}	Maximum shear stress
θ	Radial position of r with respect to the crack axis
θ_0	Crack initiation angle

θ_m	Radial position of r_m with respect to the crack axis
u_x	Displacement in x direction
u_y	Displacement in y direction
w	Specimen width
Y	Geometry correction factor
Y_I	Mode I geometry correction factor
Y_{II}	Mode II geometry correction factor

ABSTRACT

Name:	Jafar Husain Ali Al Bin Mousa
Thesis Title:	Experimental and numerical analyses of mixed mode crack initiation angle
Major Field:	Mechanical Engineering
Date of Degree:	June 2006

In fracture mechanics, one of the key factors in predicting crack propagation path is the value of the crack initiation angle. It is well known that crack propagation phenomenon is highly dependent on the state of stress in the vicinity of the crack tip, therefore, stress intensity factor 'SIF' is considered as the most significant parameter in predicting the crack propagation path. The knowledge of the crack initiation angle is an important issue in arresting the crack. In addition, SIF completely characterizes the crack tip stress condition in linear elastic material. Photoelastic technique is one of the common experimental methods used to determine the SIF for either pure or mixed mode fracture. The angle of crack initiation is inferred from fringe patterns using methods such as Schroedl and Smith and Sanford and Dally for the case of pure opening mode and mixed mode fractures, respectively. Numerical analyses are also used to describe the state of stress at crack tip and calculate SIF's from which angle of crack initiation is found.

Beside analytical methods, experimental and numerical methods can be used either separately or in combination to find the crack initiation angle. The main objective of this study is to predict the crack initiation angle for mixed mode fracture using both photoelasticity and numerical techniques. The FE code "ANSYS" is used to estimate the SIF numerically. The estimated value of the SIF is going to be incorporated into crack initiation criteria to predict the crack initiation angle. Six criteria were considered in this analysis and these are the maximum tangential stress (MTS) criterion, the minimum strain energy density (S) criterion, the maximum dilatational strain (T) criterion, the maximum triaxial stress (M) criterion, the modified MTS criterion (M.MTS) and the (R) criterion. A Polycarbonate sheet of 3mm thickness was used for manufacturing single edge crack specimens. All specimens have the same crack length but different angles of inclination namely, 0º, 10º, 20º, 30º and 40º. In the experimental analysis, the specimens were loaded until the crack initiated and the angle is measured to validate both techniques. A new model based on numerical results is proposed for estimating the geometric correction factor Y for an inclined edge crack panel.

Master of Science Degree

King Fahd University of Petroleum and Minerals

Dhahran, Saudi Arabia

June 2006

ملخص الرسالة

الاســـــــــــم: جعفر حسين علي البن موسى

عنوان الرسالة: التحاليل التجريبية و الرقمية لنشأة تشقق ذو صيغة ممزوجه

التخصـــــص: هندسة ميكانيكية

تاريخ الشهادة: يونيو 2006

في ميكانيا الإنكسار و احد من أهم العوامل لتخمين طريق إنتشار الإنشقاق هو معرفة زاوية بداية الإنشقاق. من المعروف إن ظاهرة إنتشار الإنشقاق تعتمد بشكل كبير على حالة الإجهاد عند مقدمة حافة الإنشقاق. و لذلك يعتبر معامل كثافة الإجهاد واحد من أهم العوامل لتخمين طريق إنتشار الإنشقاق.كما أن معرفة زاوية بداية الإنشقاق تعتبر مسألة مهمة لإيقاف الإنشقاق. إن معامل كثافة الإجهاد يشخص حالة الإجهاد عند حافة الإنشقاق للمواد المرنة الخطية. تعتبر تقنية الفوتو إلآستستي واحده من أكثر الطرق التجريبية إستخداماً لتحديد معامل كثافة الإجهاد إما في حالة إنشقاق نقي أو ممزوج. تعرف زاوية نشأة الإنشقاق من أنماط الأهداب بإستخدام طريقة شرودل و سميث لصيغة الفتح النقية و إستخدام طريقة سانفرد و دآلي في حالة الصيغة الممزوجة. و تستخدم التحاليل الرقمية أيضاً لوصف حالة الإجهاد عند حافة الإنشقاق و لحساب معامل كثافة الإجهاد و بذلك يمكن إيجاد زاوية نشأة الإنشقاق. بالإضافة إلى الطرق التحليلية يمكن أن تستخدم كل طريقة على حده أو كلى الطريقتين لإيجاد زاوية نشأة الإنشقاق. الهدف الأساسي من هذه الدراسة هو تخمين زاوية نشأة الإنشقاق ذو الصيغة الممزوجه بإستخدام تقنية الفوتوإلآستستي و التقنية الرقمية.كما سيتتخدم كود ANSYS للعناصر المنتهية لتخمين معامل كثافة الإجهاد رقميا.

يتم دمج القيم المخمنة لمعامل كثافة الإجهاد في معايير نشأة الإنشقاق. ستستخدم ستة معايير في هذا التحليل و هي معيار إجهاد التماس الأعظم و معيار كثافة طاقة التوتر الصغرى و معيار طاقة التمدد القصوى و معيار الإجهاد الثلاثي المحاور الأعظم و معيار إجهاد التماس الأعظم المطور و معيار آر. أستخدم لوح بولي كاربونيت ذو سماكة 3 ملم لصناعة عينات ذات شق جانبي كما أن كل العينات تحتوي على شقوق متساوية الطول ولكن بزاوية ميلان مختلفة, أي درجة صفر و 10 و 20 و 30 و 40. في التحليل التجريبي تم تحميل كل العينات حتى بداية أنتشار الشق و بذلك قيست الزاوية لمصادقة كلى الطريقتين. كما تم أقتراح نموذج جديد و بإعتمادية رقمية لتخمين معامل التصحيح الهندسي واي للوح ذو شق جانبي مائل.

درجة الماجستير في العلوم

جامعة الملك فهد للبترول و المعادن

الظهران, المملكة العربية السعودية

يونيو 2006

CHAPTER 1

INTRODUCTION

1.1. Introduction

The concept of fracture mechanics developed during early research was applicable to linear elastic, i.e., materials obeying Hooke's law. This branch is known as Linear Elastic Fracture Mechanics (LEFM). However, LEFM was extended to include non-linear effects such as plasticity, viscoelasticity, viscopalsticity and dynamic effects. Due to the modern developments in the computations, researchers around the world are working to simulate the crack propagation and one of the key issues in predicting crack propagation path is the value of the crack initiation angle. Because crack propagation concept is highly dependent on the state of stress in the vicinity of the crack tip, stress intensity factor (SIF) is considered as the most important parameter that can be used to predict the crack propagation path. Conversely in elastic-plastic fracture, the crack tip opening displacement (CTOD) and the *J* counter integral are the dominant parameters.

Beside analytical work, different experiments were conducted to estimate the SIF for different modes of fracture, i.e., opening (mode I), shearing (mode II), tearing (mode III) and mixed mode. As Fig. 1.1 shows, in mode I the load is applied normal to the crack plane and it tends to open the crack. However, in mode II in-plane shear loading is applied such that it tends to slide one crack face with respect to the other. In Mode III, out-of-plane shear loading is applied such that it tends to move the crack surfaces relative to one another.

The method of determination of SIF gets more complicated as the complexity of the cracked structure increases. Analytically, the SIF can be determined exactly or approximately. However, for simple geometries and boundary conditions the exact solutions of SIF using stress functions such as Westergaard's function are restricted to the cases where the boundary conditions can be satisfied exactly and for infinite geometries. Few exact solutions are available in the open literature. These solutions are often not practical because they are limited to particular finite and semi-infinite geometries. On the other hand, analytical approximate methods including Green's functions, weight functions and conformal mapping are more flexible than the exact methods. This is because they are applicable to the problems where the boundary conditions are only satisfied approximately. However, with many fracture mechanics problems involving complex geometry and load configuration, an approximate analytical solution for the determination of the stress intensity factors is not feasible.

In addition, due to the advancements in computational methods, numerical techniques were also employed in this regard. Boundary collocation, finite difference and finite element methods are all used to estimate the SIF numerically. In finite element the elastic continuum is replaced by a finite number of structural elements, connected at nodes. The elements are related mathematically with nodal points and the forces are transmitted through these nodal points. Using singular elements around the crack tip, singularity behavior can be achieved and the SIF can be calculated numerically.

Among the experimental methods used for measuring SIF are Photoeasticity, Moire, Holography and Caustics. For more than thirty years the photoelastic technique, has been extensively used to measure the SIF for both pure and mixed mode fractures. Photoelasticity is an experimental technique for stress and strain analysis that is particularly useful for members having complicated geometry, complicated loading conditions, or both. Though, it was not till 1954 and 1956 when Post and Post and Wells showed the application of photoelasticity to fracture problems. They did not mention the term SIF, simply because it was not introduced until by Irwin (1958), but they used the technique to measure stresses near the crack tip. Irwin showed that the stress intensity factor may be determined from the characteristics of isochromatic fringes in the vicinity of the crack tip in a straight crack problem i.e. opening mode SIF (K_I). This method was based on analyzing one fringe loop. Later, Bradley and Kobayashi (1970) and Schroedl and Smith (1973) modified Irwin's method by using data from more than one fringe loop using different techniques. This increases the flexibility and accuracy in estimating the

opening mode SIF (K_I). Smith and Smith (1972) were the first who used photoelasticity in analyzing mixed mode crack problem. In their method, they neglected the effect of the far field stress, hence, they utilized extrapolation technique to estimate the mixed mode SIF (K_I and K_{II}). Sanford and Dally (1979) proposed a full field method in which data are taken from close and far isochromatic fringe patterns. The method of solution involves an iterative numerical procedure based on Newton-Raphson technique and for the over-deterministic approach the method of least squares was employed.

After calculating the SIFs analytically or estimating them either experimentally or numerically the crack initiation angle can be predicted. Erdogan and Shi (1963) proposed the maximum tangential stress criterion (MTS-criterion) and it uses the stress as critical parameter in terms of the SIF. Later, many criteria were introduced based on different assumptions like maximum triaxial stress criterion M-criterion, minimum strain energy density S-criteria and maximum dilatational stain energy T-criteria. Some of these criteria are more suitable for analyzing brittle material and some others are better when used in analyzing ductile materials.

1.2. Statement of the Problem

The stress intensity factor plays a major role in linear elastic fracture mechanics problems and several methods were proposed to calculate it using analytical, experimental and numerical techniques. Photoelastic technique is considered to be one of the most practical

methods for estimating SIF experimentally in pure opening and mixed fracture modes (mode I and II). Different techniques were developed for estimating the pure opening mode stress intensity factor (K_I). Among these methods are Irwin's (1958), Bradley and Kobayashi (1970) and Schrodel and Smith (1972) method. In addition, photoelastic methods for estimating the mixed mode SIF (K_I and K_{II}) were developed using different techniques like that of Smith and Smith (1972) and Sanford and Dally (1979). On the other hand, numerical methods such as finite element method are used to estimate the stress intensity factors. Over the past few decades numbers of commercial FEM computer codes have been developed and ANSYS is one of the codes that can be used to analyze fracture mechanics problems. In addition, approximate analytical techniques such as Green's function, weight functions and conformal mapping are used to calculate the stress intensity factors for either pure or mixed mode fracture.

After estimating the SIF experimentally or numerically, crack initiation angle can be predicted. Several crack initiation criteria were proposed to predict the crack initiation angle. These criteria were developed analytically and based on different assumptions. Mainly, all of these criteria predict the crack initiation angle by using the value of the SIF.

Predicting the crack initiation angle based on the value of the SIF is a vital issue and the proposed criteria are still under investigation. In fact, some of these criteria are suitable

for analyzing ductile material and some others are suitable for analyzing brittle materials. However, these criteria show discrepancies in this regard.

Moreover, photoelastic method like Smith and Smith (1972) needs to be closely analyzed and examined especially from application and accuracy point of views. In this method, very close fringes near the crack tip are needed to be analyzed in order to get a good estimate of the SIF. This complicates the specimen photographing issue and makes the method less attractive in practice. The method needs also to be tested for its applicability in analyzing both top and bottom fringes for different crack inclination angles.

Similarly, finite element method as a numerical technique needs also to be tested for its validity in estimating the SIF for edge crack panels with different angles of inclination. Recently, researches are directed toward the simulations of the crack initiation angle using finite element method where the SIF value is used as a critical parameter. As a result, a correct prediction of the crack initiation angle will be so much dependent on the accuracy of the value of SIF.

Furthermore, there are no available closed form solutions for calculating the mixed mode SIF (mode I and II) for an inclined edge crack panel. Although there are solutions for such problem but they are restricted to cases of specific dimensions and load configurations. These solutions were developed using weight functions, Green's function

or conformal mapping. A general closed form solution for an inclined edge crack panel is very much needed.

Photoelasticity has been used to estimate the mixed mode SIF using different techniques (Sanford and Dally (1979) and Smith and Smith, 1972) and to estimate the crack initiation angle (Nurse and Patterson, 1990). Hernandez *et al.* (2004) analyzed crack initiation angle under mixed mode loading at diverse strain rates using experimental-numerical approach but they didn't used photoelasticity. Numerical technique was also employed to study different cracked materials (Rousseau and Tippur, 2000) and it was also coupled with photoelastic technique (Ramesh *et al*. 1997). The crack initiation criteria were also investigated analytically under different loading conditions (Shafique and Marwan, 2000).

However, an integrated investigation that couples both experimental analysis using photolelasticity and finite element analysis to estimate the crack initiation angle was not addressed, especially, for different crack inclination angles. Additionally, the mixed mode photoelastic methods were not carefully examined in analyzing different crack inclination angles.

1.3. Objectives

The main purpose of this research is to predict crack propagation angle for a mixed mode fracture case using photoelastic and finite element techniques. Different inclination angles will be considered. The applicability of the crack initiation criteria such as the maximum tangential stress (MTS) criterion, the minimum strain energy density (S) criterion, the maximum dilatational strain (T) criterion, the maximum triaxial stress (M) criterion, the modified MTS criterion and the (R) criterion will be investigated. The specimen will be loaded until crack propagation and the measured crack initiation angles will be used to validate some of these criteria. The particular objectives of this research are:

1. To estimate the pure opening mode and mixed mode stress intensity factors experimentally and by finite element method.
2. To investigate the applicability of ANSYS finite element code in estimating mixed mode stress intensity factors.
3. To estimate the crack initiation angle, by incorporating the results from photoelasticity and finite element in the existing crack initiation angle criteria.
4. To compare the crack initiation value estimated from experimental and numerical results with the observed one.
5. To developed a model for estimating the mixed mode stress intensity factors for an inclined edge crack panel.

1.4. Thesis Layout

The thesis has been divided into five chapters. The first chapter introduces the subject of crack initiation angle of mixed mode fracture and describes the objectives of the study. The second chapter highlights six mixed mode fracture initiation criteria. These criteria are going to be used to predict the crack initiation angle. The third chapter examines the applicability of ANSYS FE code in estimating the SIF for mixed mode problem. In addition, it discusses the prediction of the crack initiation angle using the numerical results. Finite element modeling including: geometry, mesh, crack modeling and loading are all addressed in this chapter. Additionally, it discusses the FE model validation procedure and it presents a new model based on FE for estimating the mixed mode SIF for an inclined edge crack panel. The fourth chapter presents background of information about photoelastic technique. It addresses different methods used to estimate the SIF using photoelasticity. These include Schroedle and Smith method for estimating the pure opening mode SIF (K_I), Smith and Smith and Sanford and Dally methods for estimating the mixed mode SIF (K_I and K_{II}). The two methods for estimating the mixed mode SIF are thoroughly compared. Experimental procedure, results and analysis are included in this chapter. Experimental estimation of the crack initiation angle is also presented and discussed in this chapter. The application of the fringe symmetry axis method in estimating the crack initiation angle is investigated. Moreover, Comparisons between experimental and numerical results are discussed in this chapter. The fifth chapter presents the conclusions and recommendations of this research.

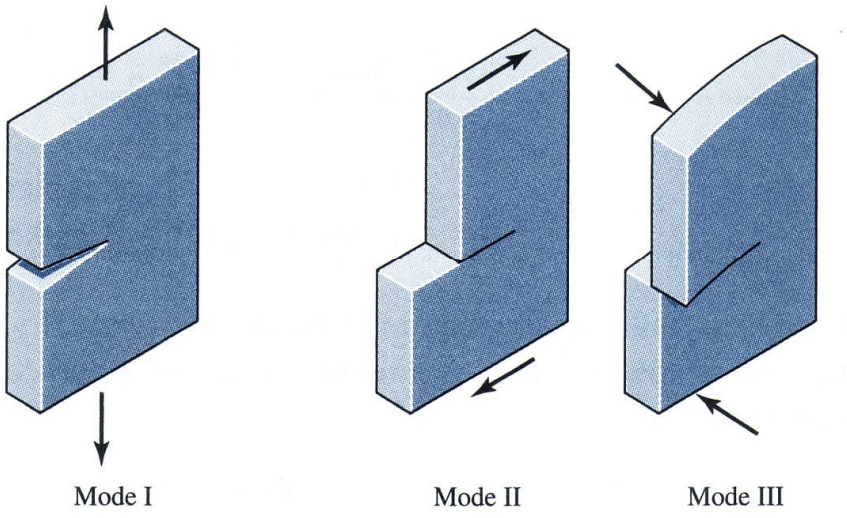

Figure 1.1: Crack propagation modes, Shigley (2004).

CHAPTER 2

REVIEW OF MIXED MODE FAILURE CRITERIA

2.1. Introduction

The elastic stress field around crack tips can become unbounded and for brittle solids this behavior can lead to rapid crack propagation resulting in catastrophic failure of the structure. Therefore, the nature of such elevated stress distributions around cracks is important in engineering applications. Studying crack initiation angles is an important issue in dealing with crack arrest. Accordingly, several criteria have been proposed to predict the crack initiation angle. These criteria can be categorized on the basis of the critical parameter on which the criterion is defined. These parameters might be a critical value of stress, energy or strain. Griffith (1921) was the first to propose a crack initiation criterion based on energy. It states that the fracture occurs when the energy stored in a structure overcomes the surface energy of the material. On the other hand, Erdogan and Sih (1963) were the first to propose a crack initiation criterion using the stress as a critical

parameter. This criterion states that direction of crack initiation coincides with the direction of the maximum tangential stress along a constant radius around the crack tip so it is called the maximum tangential stress (MTS) criterion. To support their criterion, Erdogan and Sih conducted experiments using brittle Plexiglass plates and it is believed that MTS is suitable for analyzing brittle material. Later, Sih (1973-1974) used the strain as a critical parameter in order to propose the minimum strain energy density (S) criterion. It states that the direction of crack initiation coincides with the direction of minimum strain energy density along a constant radius around the crack tip. The (S) criterion showed a good agreement with the experimental results obtained earlier by Erdogan and Sih (1963). In addition, this criterion is the only one that shows the dependence of the initiation angle on material property represented by Poisson's ratio *v*. Similar to Sih, Theocaris *et al*. (1982) used the strain as a critical parameter to propose the maximum dilatational strain energy (T) criterion. It states that the direction of crack initiation coincides with the direction of maximum dilatational strain energy density along the contour of constant distortional strain energy around the crack tip. Theocaris *et al*. (1982) used Polycarbonate specimens for their experimental work and their experimental results showed a good agreement with the theoretical predictions. On the other hand, Kong *et al*. (1995) proposed the maximum triaxial stress (M) criterion which uses the stress as a critical parameter. It states that the direction of crack initiation coincides with the direction of maximum stress triaxiality ratio along a constant radius around the crack tip. Kong *et al*. (1995) performed experiments using steel (FeE550) specimen at low temperature (-140ºC) in order to ensure that *K* controls the fracture.

Kong *et al*. experimental results were in agreement with the theoretical predictions as well as the experimental results by Theocaris *et al*. (1982) and T criterion. Ukadgaonker and Awasare (1995) presented the T-criterion in a new form using the first and second stress invariants. Shafique and Marwan (2000) modified the MTS criterion in order to be suitable for analyzing ductile materials. To achieve this, they introduced a variable radius for the plastic core region and used the von Mises yield criterion for determining the variable radius. Later, Shafique and Marwan (2004) proposed the (R) criterion which states that the direction of the crack initiation angle coincides with the direction of the minimum distance from the crack tip to the core region boundary.

It can be realized from the literature review that each criterion is based on different assumption. To estimate the crack initiation angle, six of these criteria are going to be used through out this study. These are the maximum tangential stress (MTS) criterion, the minimum strain energy density (S) criterion, the maximum dilatational strain (T) criterion, the maximum triaxial stress (M) criterion, the modified MTS criterion and (R) criterion. As a result, these criteria are going to be discussed in detail in the following section.

2.2. Crack Initiation Angle Criteria

2.2.1. MTS-criterion

The maximum tangential stress MTS-criterion (Erdogan and Sih, 1963) is the simplest criterion and it states that direction of crack initiation coincides with the direction of the maximum tangential stress along a constant radius around the crack tip. It can be stated mathematically as:

$$\begin{aligned} &\frac{\partial \sigma_\theta}{\partial \theta} = 0 \\ &\frac{\partial^2 \sigma_\theta}{\partial \theta^2} < 0 \end{aligned} \tag{2.1}$$

Using the stress field in polar coordinates:

$$\begin{aligned} \sigma_\theta &= \frac{1}{\sqrt{2\pi r}}\left[\left(\frac{K_I}{2}\cos\frac{\theta}{2}(1+\cos\theta)\right)-\left(\frac{3K_{II}}{2}\sin\frac{\theta}{2}(1+\cos\theta)\right)\right] \\ \sigma_r &= \frac{1}{\sqrt{2\pi r}}\left[\left(\frac{K_I}{2}\cos\frac{\theta}{2}(3-\cos\theta)\right)-\left(\frac{K_{II}}{2}\sin\frac{\theta}{2}(1-3\cos\theta)\right)\right] \\ \tau_{r\theta} &= \frac{1}{\sqrt{2\pi r}}\left[\left(\frac{K_I}{2}\sin\frac{\theta}{2}(1+\cos\theta)\right)-\left(\frac{K_{II}}{2}\cos\frac{\theta}{2}(1-3\cos\theta)\right)\right] \end{aligned} \tag{2.2}$$

and applying the MTS-criterion, one gets the following equations:

$$\tan^2\frac{\theta}{2}-\frac{\mu}{2}\tan\frac{\theta}{2}-\frac{1}{2}=0 \tag{2.3a}$$

$$-\frac{3}{2}\left[\left(\frac{1}{2}\cos^3\frac{\theta}{2}-\cos\frac{\theta}{2}\sin^2\frac{\theta}{2}\right)+\frac{1}{\mu}\left(\sin^3\frac{\theta}{2}-\frac{7}{2}\sin\frac{\theta}{2}\cos^3\frac{\theta}{2}\right)\right]<0 \tag{2.3b}$$

where

$$\mu = \frac{K_I}{K_{II}} \tag{2.4}$$

if the stress intensity ratio K_I/K_{II} is known then Eq (2.3) can be solved for θ such that $\theta = \theta_0$ which is the predicted crack initiation angle.

2.2.2. S-criterion

The minimum strain energy density S-criterion (Sih, 1973-1974) states that the direction of crack initiation coincides with the direction of minimum strain energy density along a constant radius around the crack tip. In mathematical form, S-criterion can be stated as:

$$\frac{\partial \mathrm{S}}{\partial \theta} = 0$$
$$\frac{\partial^2 \mathrm{S}}{\partial \theta^2} > 0 \tag{2.5}$$

where S is the stain energy density factor, defined as:

$$\mathrm{S} = r_0 \frac{dW}{dV} \tag{2.6}$$

where dW/dV is the strain energy density function per unit volume, and r_0 is a finite distance from the point of failure initiation. For slit cracks, the crack tip is assumed to be the point of failure initiation. Using the stress field in Cartesian coordinates:

$$\sigma_x = \frac{K_I}{\sqrt{2\pi r}}\cos\frac{\theta}{2}\left[1-\sin\frac{\theta}{2}\sin\frac{3\theta}{2}\right]-\frac{K_{II}}{\sqrt{2\pi r}}\sin\frac{\theta}{2}\left[2+\cos\frac{\theta}{2}\cos\frac{3\theta}{2}\right]$$
$$\sigma_y = \frac{K_I}{\sqrt{2\pi r}}\cos\frac{\theta}{2}\left[1+\sin\frac{\theta}{2}\sin\frac{3\theta}{2}\right]+\frac{K_{II}}{\sqrt{2\pi r}}\sin\frac{\theta}{2}\cos\frac{\theta}{2}\cos\frac{3\theta}{2} \qquad (2.7)$$
$$\tau_{xy} = \frac{K_I}{\sqrt{2\pi r}}\sin\frac{\theta}{2}\cos\frac{\theta}{2}\cos\frac{3\theta}{2}+\frac{K_{II}}{\sqrt{2\pi r}}\cos\frac{\theta}{2}\left[1-\sin\frac{\theta}{2}\sin\frac{3\theta}{2}\right]$$

one can obtain the strain energy density function per unit volume, and then using Eq. (2.6), the strain energy density function cab be written as:

$$\mathrm{S} = a_{11}K_I^2 + 2a_{12}K_I K_{II} + a_{22}K_{II}^2 \qquad (2.8)$$

where the factors a_{ij} are functions of the angle θ, and are defined as:

$$a_{11} = \frac{1}{16G}(1+\cos\theta)(\kappa-\cos\theta)$$
$$a_{12} = \frac{1}{16G}[2\cos\theta-(\kappa-1)]\sin\theta \qquad (2.9)$$
$$a_{22} = \frac{1}{16G}[(\kappa+1)(1-\cos\theta)+(1+\cos\theta)(3\cos\theta-1)]$$

where G is the modulus of rigidity and κ is a constant depending upon stress state, and is defined as:

$$\kappa = \frac{(3-\nu)}{(1+\nu)} \quad \text{for plane stress} \qquad (2.10a)$$

$$\kappa = (3-4\nu) \quad \text{for plane strain} \qquad (2.10b)$$

from Eqs. (2.5, 2.8, 2.9) we get:

$$\left[2(1+\kappa)\mu\right]\tan^4\frac{\theta}{2}+\left[2\kappa(1-\mu^2)-2\mu^2+10\right]\tan^3\frac{\theta}{2}-24\mu\tan^2\frac{\theta}{2}$$
$$+\left[2\kappa(1-\mu^2)+6\mu^2-14\right]\tan\frac{\theta}{2}+2(3-\kappa)\mu=0 \qquad (2.11a)$$

$$\left[2(\kappa-1)\mu\right]\sin\theta-8\mu\sin 2\theta+\left[(\kappa-1)(1-\mu^2)\right]\cos\theta+\left[2(\mu^2-3)\right]\cos 2\theta>0 \qquad (2.11b)$$

where μ is defined as in Eq. (2.11).

Similar to MTS criterion, after finding the stress intensity ratio μ, Eq. (2.11) can be solved for θ, $\theta = \theta_0$ which is the predicted crack initiation angle.

2.2.3. T-criterion

The maximum dilatational strain energy density T-criterion (Theocaris, 1982) states that the direction of crack initiation coincides with the direction of maximum dilatational strain energy density along the contour of constant distortional strain energy around the crack tip. T-criterion uses elastic plastic boundary as given by von Mises flow rule, to define the radius of the core region at the crack tip. In mathematical form, T-criterion can be stated as:

$$\frac{\partial T_v}{\partial\theta}=0$$
$$\frac{\partial^2 T_v}{\partial\theta^2}<0 \qquad (2.12)$$

where T_v is the dilatational strain energy, defined as:

$$T_v = \frac{(1-2v)}{6E}(\sigma_x + \sigma_y)^2 \tag{2.13}$$

The distortional strain energy T_D, is given by:

$$T_D = \frac{(1+v)}{3E}(\sigma_x^2 + \sigma_y^2 - \sigma_x\sigma_y + 3\tau_{xy}^2) \tag{2.14}$$

The relations for T_v and T_D are used for plane stress condition, however, the results are the same for plane strain condition.

Now defining $f_x(\theta)$, $f_y(\theta)$ and $f_{xy}(\theta)$ as:

$$\begin{aligned}
f_x(\theta) &= K_I \cos\frac{\theta}{2}\left(1 - \sin\frac{\theta}{2}\sin\frac{3\theta}{2}\right) - K_{II}\sin\frac{\theta}{2}\left(2 + \cos\frac{\theta}{2}\cos\frac{3\theta}{2}\right) \\
f_y(\theta) &= K_I \cos\frac{\theta}{2}\left(1 + \sin\frac{\theta}{2}\sin\frac{3\theta}{2}\right) + K_{II}\sin\frac{\theta}{2}\cos\frac{\theta}{2}\cos\frac{3\theta}{2} \\
f_{xy}(\theta) &= K_I \sin\frac{\theta}{2}\cos\frac{\theta}{2}\cos\frac{3\theta}{2} + K_{II}\cos\frac{\theta}{2}\left(1 - \sin\frac{\theta}{2}\sin\frac{3\theta}{2}\right)
\end{aligned} \tag{2.15}$$

We get the stress field in Cartesian coordinates:

$$\begin{aligned}
\sigma_x &= \frac{1}{\sqrt{2\pi r}} f_x(\theta) \\
\sigma_y &= \frac{1}{\sqrt{2\pi r}} f_y(\theta) \\
\tau_{xy} &= \frac{1}{\sqrt{2\pi r}} f_{xy}(\theta)
\end{aligned} \tag{2.16}$$

Using this notation, we obtain from Eqs. 2.13 and 2.14, respectively:

$$T_v = \frac{(1-2v)}{12\pi Er}(f_x + f_y)^2 \tag{2.17}$$

$$T_D = \frac{(1+v)}{6\pi Er}(f_x^2 + f_y^2 - f_x f_y + 3f_{xy}^2) \tag{2.18}$$

Since the distortional strain energy is constant along the von Mises elastic plastic boundary, $T_{D,0}$ can be considered as a material constant. By combining Eqs. 2.17 and 2.18, we get:

$$r = \frac{(1+v)}{6\pi E T_{D,0}}(f_x^2 + f_y^2 - f_x f_y + 3f_{xy}^2) \tag{2.19}$$

$$T_v = \frac{(1-2v)T_{D,0}}{2(1-v)} \frac{(f_x + f_y)^2}{(f_x^2 + f_y^2 - f_x f_y + 3f_{xy}^2)} \tag{2.20}$$

Applying the T-criterion, to Eq. (2.20), we get:

$$\tan^5\frac{\theta}{2} - 4\mu\tan^4\frac{\theta}{2} + (5\mu^2 - 1)\tan^3\frac{\theta}{2} + \frac{(3-5\mu^2)\mu}{2}\tan^2\frac{\theta}{2} + \frac{(\mu^4 - 2\mu^2 - 1)}{2}\tan\frac{\theta}{2} + \frac{(1+\mu^2)\mu}{2} = 0 \tag{2.20a}$$

$$[1-20\mu^2-5\mu^4]\cos\theta + [8(3+2\mu^2-\mu^4)]\cos 2\theta - [3(3-12\mu^2+\mu^4)]\cos 3\theta + [2(13+5\mu^2)\mu]\sin\theta + [32(1+\mu^2)\mu]\sin 2\theta - [6(5-3\mu^2)\mu]\sin 3\theta < 0 \tag{2.20b}$$

Again the same procedure as for MTS can be applied to find the crack initiation angle.

2.2.4. M-criterion

The maximum triaxial stress M-criterion (Kong *et al*. 1995) states that the direction of crack initiation coincides with the direction of maximum stress triaxiality ratio along a constant radius around the crack tip. M-criterion can be stated mathematically as:

$$\begin{aligned} \frac{\partial M}{\partial \theta} &= 0 \\ \frac{\partial^2 M}{\partial \theta^2} &< 0 \end{aligned} \tag{2.22}$$

where M is the stress triaxiality ratio, defined as:

$$M = \frac{\sigma_H}{\sigma_{eq}} \tag{2.23}$$

where σ_H is the hydrostatic stress and σ_{eq} is the equivalent stress. Kong *et al*. used von Mises equivalent stress. The hydrostatic stress calculated using the following equation for plane strain condition

$$\sigma_H = \frac{\sigma_x + \sigma_y + \sigma_z}{3} = \frac{2(1+\nu)}{3\sqrt{2\pi r}}\left[K_I \cos\frac{\theta}{2} - K_{II}\sin\frac{\theta}{2}\right] \tag{2.24}$$

The von Mises equivalent stress for plane strain condition at the crack tip is given by:

$$\begin{aligned} \sigma_{eq} &= \left[\frac{(\sigma_x - \sigma_y)^2 + (\sigma_y - \sigma_z)^2 + (\sigma_z - \sigma_x)^2 + 6\tau_{xy}^2}{2}\right] \\ &= \frac{1}{\sqrt{2}\sqrt{2\pi r}}\left[\left(\frac{3}{2}K_I^2 - \frac{9}{2}K_{II}^2\right)\sin^2\theta + (2(1-2\nu)^2 K_I^2 + 6K_{II}^2)\cos^2\frac{\theta}{2}\right. \\ &\left. + 8(1-\nu+\nu^2)K_{II}^2\sin^2\frac{\theta}{2} + K_I K_{II}(3\sin 2\theta - 2(1-2\nu)^2\sin\theta\right]^{\frac{1}{2}} \end{aligned} \tag{2.25}$$

Applying the M-criterion, we get the following equation:

$$\tan^4\frac{\theta}{2}-3\mu\tan^3\frac{\theta}{2}-(1-2\mu^2)\tan^2\frac{\theta}{2}+\frac{1}{2}(1-\mu^2)\mu\tan\frac{\theta}{2}-\frac{1}{2}(1+\mu^2)=0 \tag{2.26a}$$

$$\begin{aligned}&\left[2(\mu^2+5)\right]\sin\frac{\theta}{2}+\left[27(\mu^2+1)\right]\sin\frac{3\theta}{2}+\left[5(5\mu^2-3)\right]\sin\frac{5\theta}{2}\\&-\left[2(\mu^2+5)\mu\right]\cos\frac{\theta}{2}-\left[9(\mu^2+1)\mu\right]\cos\frac{3\theta}{2}-\left[5(\mu^2-7)\mu\right]\cos\frac{5\theta}{2}<0\end{aligned} \tag{2.26b}$$

Although plane strain formulation is done here, however, plane stress formulation gives the same results. Again the same procedure as for MTS is applied to find the crack initiation angle.

2.2.5. Modified MTS-criterion

The modified MTS-criterion (Shafique and Marawan, 2000) is the same as the original MTS-criterion except that a variable radius for the plastic core region is introduced. The von Mises yield criterion is used for determining the variable radius.

Using the stress filed in polar coordinates in Eq. (2.9), we get

$$\begin{aligned}\sigma_\theta&=\frac{1}{2\sqrt{2\pi r}}f_\theta(\theta)\\\sigma_r&=\frac{1}{2\sqrt{2\pi r}}f_r(\theta)\\\tau_{r\theta}&=\frac{1}{2\sqrt{2\pi r}}f_{r\theta}(\theta)\end{aligned} \tag{2.27}$$

where

$$f_\theta(\theta)=\left[\left(K_I\cos\frac{\theta}{2}(1+\cos\theta)\right)-\left(3K_{II}\sin\frac{\theta}{2}(1+\cos\theta)\right)\right]$$
$$f_r(\theta)=\left[\left(K_I\cos\frac{\theta}{2}(3-\cos\theta)\right)-\left(K_{II}\sin\frac{\theta}{2}(1-3\cos\theta)\right)\right] \quad (2.28)$$
$$f_{r\theta}(\theta)=\left[\left(K_I\sin\frac{\theta}{2}(1+\cos\theta)\right)-\left(K_{II}\cos\frac{\theta}{2}(1-3\cos\theta)\right)\right]$$

Using the von Mises yield criteria with Eqs. 2.27 and 2.28, we get

$$r=\frac{(1+v)}{24\pi ET_{D,0}}(f_r^2+f_\theta^2-f_rf_\theta+3f_{r\theta}^2) \quad (2.29)$$

where r is the radius of the core region and $T_{D,0}$, the distortional strain energy that is constant along the elastic plastic boundary. Using this equation with the equation for tangential stress Eq. (2.27), we get

$$\sigma_\theta=\sqrt{\frac{3ET_{D,0}}{(1+v)}}\frac{f_\theta}{(f_r^2+f_\theta^2-f_rf_\theta+3f_{r\theta}^2)^{1/2}} \quad (2.30)$$

Applying the MTS-criterion to Eq. (2.30) we get the equation for the modified MTS-criterion

$$12\tan^6\frac{\theta}{2}-24\mu\tan^5\frac{\theta}{2}+[3+16\mu^2]\tan^4\frac{\theta}{2}-[(5+4\mu^2)\mu]\tan^3\frac{\theta}{2}+3\mu^2\tan^2\frac{\theta}{2}$$
$$-\frac{[(7+5\mu^2)\mu]}{2}\tan\frac{\theta}{2}-\frac{[9+5\mu^2]}{2}=0 \quad (2.31a)$$

$$[177+49\mu^2]\sin\frac{\theta}{2}+[1269+621\mu^2]\sin\frac{3\theta}{2}-[255-425\mu^2]\sin\frac{5\theta}{2}$$
$$+[189-147\mu^2]\sin\frac{7\theta}{2}-[(305+49\mu^2)\mu]\cos\frac{\theta}{2}-[(423+207\mu^2)\mu]\cos\frac{3\theta}{2} \quad (2.31b)$$
$$+[(595-85\mu^2)\mu]\cos\frac{5\theta}{2}-[(315-21\mu^2)\mu]\cos\frac{7\theta}{2}<0$$

2.2.6. R-criterion

R-criterion (Shafique and Marwan, 2004) states that the direction of the crack initiation angle coincides with the direction of the minimum distance from the crack tip to the core region boundary. Mathematically, the R-criterion can be stated as:

$$\begin{aligned} &\frac{\partial R_P}{\partial \theta} = 0 \\ &\frac{\partial^2 R_P}{\partial \theta^2} > 0 \end{aligned} \tag{2.32}$$

By defining the stress intensity factors as

$$K_i = \sigma_{app}\sqrt{\pi a}\, f_{K_i}(\beta) \quad i = \text{I, II, or III} \tag{2.33}$$

where for modes I and II it becomes

$$\begin{aligned} K_I &= \sigma_{app}\sqrt{\pi a}\, f_{K_I}(\beta) \\ K_{II} &= \sigma_{app}\sqrt{\pi a}\, f_{K_{II}}(\beta) \end{aligned} \tag{2.34}$$

Using Eq. (2.34) in Eq. (2.14), we get

$$\begin{aligned} \sigma_x &= \frac{\sigma_{app}\sqrt{a}}{\sqrt{2r}} f_{\boldsymbol{x}}(\theta, f_{K_i}) \\ \sigma_y &= \frac{\sigma_{app}\sqrt{a}}{\sqrt{2r}} f_{\boldsymbol{y}}(\theta, f_{K_i}) \\ \tau_{xy} &= \frac{\sigma_{app}\sqrt{a}}{\sqrt{2r}} f_{\boldsymbol{xy}}(\theta, f_{K_i}) \end{aligned} \tag{2.35}$$

where $f_x(\theta, f_{Ki})$, $f_y(\theta, f_{Ki})$ and $f_{xy}(\theta, f_{Ki})$ are defined as:

$$f_x(\theta, f_{K_i}) = f_{K_I}(\beta)\cos\frac{\theta}{2}\left(1-\sin\frac{\theta}{2}\sin\frac{3\theta}{2}\right) - f_{K_{II}}(\beta)\sin\frac{\theta}{2}\left(2+\cos\frac{\theta}{2}\cos\frac{3\theta}{2}\right)$$

$$f_y(\theta, f_{K_i}) = f_{K_I}(\beta)\cos\frac{\theta}{2}\left(1+\sin\frac{\theta}{2}\sin\frac{3\theta}{2}\right) + f_{K_{II}}(\beta)\left(\sin\frac{\theta}{2}\cos\frac{\theta}{2}\cos\frac{3\theta}{2}\right) \tag{2.36}$$

$$f_{xy}(\theta, f_{K_i}) = f_{K_I}(\beta)\left(\sin\frac{\theta}{2}\cos\frac{\theta}{2}\cos\frac{3\theta}{2}\right) + f_{K_{II}}(\beta)\cos\frac{\theta}{2}\left(1-\sin\frac{\theta}{2}\sin\frac{3\theta}{2}\right)$$

The tensile yield strength of the material is given by

$$\sigma_{YS}^2 = \frac{(\sigma_x-\sigma_y)^2+(\sigma_y-\sigma_z)^2+(\sigma_z-\sigma_x)^2+6\tau_{xy}^2}{2} \tag{2.37}$$

and by substituting (2.35) into (2.37), we get the non-dimensional elastic-plastic core region radius R_P for mixed mode loading for the plane stress

$$R_P(\theta, f_{K_i}) = \frac{r_p(\theta, f_{K_i})}{a\left[\frac{\sigma_{app}}{\sigma_{YS}}\right]^2} = \frac{1}{2}\left[f_x^2(\theta, f_{K_i}) + f_y^2(\theta, f_{K_i}) - f_x(\theta, f_{K_i})f_y(\theta, f_{K_i}) + 3f_{xy}^2(\theta, f_{K_i})\right] \tag{2.38}$$

By applying R-criterion to Eq. (2.38), we get

$$2\mu\tan^4\frac{\theta}{2} + (5-2\mu^2)\tan^3\frac{\theta}{2} - 9\mu\tan^2\frac{\theta}{2} + (\mu^2-4)\tan\frac{\theta}{2} + \mu = 0 \tag{2.46a}$$

$$(1-\mu^2)\cos\theta + 3(\mu^2-3)\cos 2\theta + 2\mu\sin\theta - 12\mu\sin 2\theta > 0 \tag{2.46b}$$

for plane stress.

Again the same procedure as for MTS can be applied to find the crack initiation angle. In all criteria, only the negative roots are considered because the applied load is uniaxial tension (Fig. 2.1).

2.3. Conclusion

An overview of crack initiation angle criteria was presented. In general, these criteria can be categorized on the basis of the critical parameter which is used to define the criterion. These parameters are based on critical value of stress, strain or energy. Furthermore, each criterion is based on different assumption related to how and where the crack is going to initiate. Except S-criterion, all criteria are a function of the stress intensity mixity ratio K_{II}/K_I and the crack initiation angle. The S-criterion is the only one that shows the dependence on material property represented by Poisson's ratio v. As a result, once the stress intensity factors K_I and K_{II} are determined the crack initiation angle can be predicted using one of these criteria.

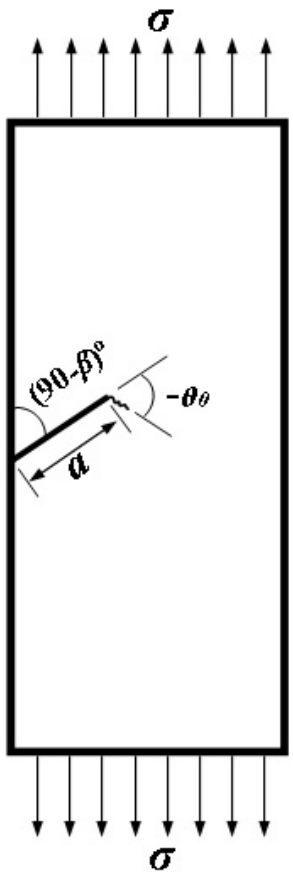

Figure 2.1: Crack initiation angle for an inclined edge crack panel under a tensile loading.

CHAPTER 3

NUMERICAL ANALYSIS

3.1. Introduction

"Computation of fracture parameters, such as the stress intensity factors or energy release rate, using finite element analysis requires either a refined mesh around the crack tip or the use of "special elements" with embedded stress singularity near the crack tip. Although conceptually the stress intensity factors are obtained in a straightforward approach, finite elements analyses with conventional element near the crack tip always underestimate the sharply rising stress-displacement gradients.

Instead of trying to capture the well-known $1/\sqrt{r}$ singular behavior with very small elements, Hanshell and Shaw (1975) and Barsoum (1976, 1977) proposed a direct method by shifting the mid-side node of an 8-noded isoparametric quadrilateral element to the one-quarter point from the crack tip node. Relocating the mid-side nodes to the one-quarter point achieves the desire $1/\sqrt{r}$ singular behavior.

As an extension of the node collapsing approach (Fig. 3.1) Pu *et al.*(1978) showed that the stress intensity factors K_I and K_{II} for opening and sliding modes, respectively, can be calculate directly from the nodal displacement on the opposite sides of the crack plane as

$$K_I = G\sqrt{\frac{2\pi}{r_0}}\,\frac{u_y(r_0,\theta=\pi)-u_y(r_0,\theta=-\pi)}{\kappa+1} \tag{3.1a}$$

and

$$K_{II} = G\sqrt{\frac{2\pi}{r_0}}\,\frac{u_x(r_0,\theta=\pi)-u_x(r_0,\theta=-\pi)}{\kappa+1} \tag{3.1b}$$

in which r_0, usually restricted to one or two percent of the crack length, is the distance from the crack tip to the first side-node behind the crack tip. The shear modulus is G and the parameters κ = 3- ν / 1 + ν and κ = 3- 4ν are for plane stress and plane strain idealizations, respectively", Madenci and Guven (2006).

Peter *et al*. (1995) developed a finite element program which combines the analytical crack tip solution with a conventional finite element analysis and evaluated various crack tip parameters as part of the solution. The authors used the program to analyze cracked specimens subjected to mixed mode loading and demonstrated the importance of retaining the second term of the series expansion for local stress. Their numerical analysis demonstrated that if this term is included in the analytical crack tip solutions the value K_I will be dependent on the load applied parallel to the crack. However, the value of mode II stress intensity factor (K_{II}) is independent of this term.

Petit *et al*. (1996) presented different numerical approaches to study cracked material behavior and the possibility of these approaches in analyzing homogenous material and biomaterial. The authors used finite element method to obtain the displacement field in order to evaluate the stress intensity factors (K_I and K_{II}) and simulate the crack propagation for an inclined edge crack panel with crack angle of 45º. Their numerical analysis showed an agreement with analytical solution.

Rousseau and Tippur (2000) studied the mixed mode crack tip deformation and fracture parameters in a glass-filled epoxy beam with crack normal to the elastic gradient. The authors measured the crack tip fields optically using Coherent Gradient Sensing (CGS) for different crack locations in the elastic gradient when subjected to symmetric pure bending. They also developed a FE model using ANSYS and validated their model by their measurements. Then, they used the numerical model to examine the influence of the elastic gradient on crack location by evaluating the stress intensity factors, mode mixity and energy release rate. Homogenous, bimaterial and functionally graded materials were considered in this study. The authors demonstrated a good agreement between the experimental and computational results.

Ayhan (2003) used three-dimensional enriched finite elements to calculate mixed mode stress intensity factors for deflected and inclined surface cracks in finite-thickness plates under uniform tensile remote loading. The author investigated the effect of plate thickness on the mixed mode fracture solution and showed that decreasing the plate

thickness will magnify the mixed mode stress intensity factors along the crack front. The crack propagation angles along the deflection and inclined crack fronts were also determined in this study. The Author concluded that for both crack types, mode I stress intensity factor decreases in magnitude along the whole crack front as the deflection or inclination angle increases. Mode II and mode III stress intensity factors, on the other hand, increase initially as the deflection or inclination angle increases and then decrease for higher deflection or inclination angles. Crack propagation angles along deflected and inclined crack fronts were shown to increase in magnitude along the whole crack front with increasing deflection or inclination angle.

Shan and Pelegri (2003) investigated the complex fracture behavior of a cross-ply composite cantilever beam with artificially embedded delamination analytically, numerically and experimentally. The authors developed a nonlinear finite element model that accounts for the contact zone effect and delamination in the aforementioned asymmetrically loaded structure using ANSYS. The material used for all specimens was IM7/8552 Hexcel prepreg graphite/epoxy and the obtained experimental data are correlated and compared with the findings of the FEM simulations. The authors found that all numerical, analytical, and experimental results illustrated that the fracture behavior of the laminate cantilever beam is dominated by mode II, mainly due to the effect of a large contact zone and the dominance of mode II over mode I leads to the initiation and propagation of an interfacial crack rather than an intralayer one.

Furthermore, experimental evidence indicates that crack kinking during crack propagation depends on the architecture of the specimens.

Hernandez *et al*. (2004) analyzed the crack initiation angle under mixed mode loading at diverse strain rates using experimental-numerical approach. The experimental work had been divided into two parts, evaluation of the modulus of elasticity at different strain rates and evaluation of crack initiation angle. The authors used FRANC code to evaluate the mixed mode stress intensity factors (K_I and K_{II}) in order to estimate the crack initiation angle. Polymethylmethacrylate (PMMA) plates with center angled cracks under mixed mode loading were tested in this study. The authors performed numerical evaluations with finite element method in conjunction with the volume energy density criterion. In addition, they evaluated the crack initiation angle with the strain energy density factor S. They concluded that when the strain rate increases at the crack tip, a quasi-static evaluation of the stress intensity factors K_I and K_{II} may not be valid. Their results are found to be in agreement with those observed experimentally.

Tilbrook *et al*. (2005) investigated the effects of plastic yielding on crack propagation near ductile/brittle interfaces. The authors modified the finite element model which was used for simulating mixed-mode crack propagation in a linear elastic material to incorporate yielding. Crack propagation was simulated in homogenous and layered Copper-Tungsten Cu/W campsites using ANSYS. They also examined the influences of thermal, elastic and plastic mismatch on the critical load and the crack tip mode mixity.

The authors concluded that when a plastic deformation occurs at the crack tip, a non-linear relationship may be obtained and used to calculate the stress intensity factors. They also stated that plasticity has an important influence on the crack tip stress and the propagation paths for cracks near the interfaces. In addition, they concluded that it is important to incorporate the plastic deformation into the models of failure near the interfaces and to consider the effect of prior strain history on crack tip stresses during simulations.

From the literature review we can see that finite element was used to analyze different fracture problems. These including mixed mode loading, simulating of crack propagation, homogenous materials, bimaterials, functionally graded material, composite, effect of plastic yielding on crack propagation and effect of different stain rates on the evaluation of mixed mode SIF. The application of finite element using ANSYS code in analyzing an inclined edge crack panel will be examined in following section. In addition, its application in predicting crack initiation angle is also investigated. Furthermore, a new model for estimating the mixed mode stress intensity factors for an inclined edge crack is proposed. This model is based on finite element results.

3.2. Finite Element Analysis of Stress Intensity for an Inclined Crack

Solving a fracture mechanics problem numerically, involves performing a linear elastic or elastic-plastic static analysis and then using specialized *postprocessing* commands or

macros to calculate desired fracture parameters. The most important region in a fracture model is the region around the edge of the crack. This region is called the *crack tip* in a 2D model and *crack front* in a 3D model as shown in Fig.3.2. In linear elastic problems, the displacements near the crack tip (or crack front) vary as $r^{1/2}$, where r is the distance from the crack tip. The stresses and strains are singular at the crack tip, varying as $1/ r^{1/2}$ (Eq. 3.1). To pick up the singularity in the strain, the crack faces should be coincident, and the elements around the crack tip (or crack front) should be quadratic, with the midside nodes placed at the quarter points. Such elements are called *singular elements*. A complete description of the modeling of an inclined edge crack panel using ANSYS finite element code is presented in the next section.

3.2.1. Modeling

Geometry

Because there is no symmetry in the case of an inclined crack, full model of the edge cracked plates analyzed experimentally are built using ANSYS. The problem is idealized as 2D plane stress and the geometry was modeled using 8 keypoints with keypoint 7 being the crack tip. Keypoints 6 and 8 are coincident such that each one belonging to opposite crack face as shown in Fig. 3.3. Edge crack specimens were modeled with same crack length a, width w and length L but with different crack angles of inclination. The inclination angles considered in this study are, 0°, 10°, 20°, 30° and 40°. The coordinates of the keypoints are listed in Table 3.1. It should be noted that the coordinates listed in this table are suitable for the considered cases in this work. However, when a higher

angle of inclination is considered the location of keypoint 3 may shift to the top line which is connected by keypoints 4 and 5 (Fig. 3.3).

TABLE 3.1: Coordinates of the keypoints.

Keypoint No.	**x**	**y**
1	0	0
2	w	0
3	w	$L/2 + w * \tan(\beta)$
4	w	L
5	0	L
6	0	$L/2$
7	$a * \cos(\beta)$	$a * \sin(\beta)+L/2$
8	0	$L/2$

Finite Element Mesh

The model was meshed using free mesh option. This is because mapped mesh option can not be utilized in ANSYS if the model has a concentration point which is in our case the crack tip. The radius of the concentration point is chosen to be $8*10^{-4}$ *m* and its location is at keypoint 7 as mentioned earlier. On the other hand, the ratio of the second row elements radius to the first row elements radius (RRAT) is selected to be 0.5 as per

ANSYS documentation manual. The number of elements in circumferential direction (NTHET) is selected to be 6 which will create 12 singular elements around the crack tip. Skew mid-side option is chosen to achieve the singular behavior at the crack tip. The specifications of the crack tip mesh are shown in Fig. 3.4. General finite element meshes for inclination angles β = 0º and β = 40º are shown in Figs. 3.5 and 3.6. A close up view of the crack tip mesh for crack inclination angles β = 0º and β = 40º are shown in Figs. 3.7 to 3.8, respectively.

Crack Path Modeling

Since a full model is considered, five nodes need to be selected along the two crack faces. The first node should be the crack tip and the second and third nodes are the first and second nodes next to the crack tip on the crack's top face. The forth and fifth nodes have to be the first and second nodes next to the crack tip but on the crack's bottom face as shown in Fig 3.9.

Material Model and Element Type

Polycarbonate is modeled as a linear isotropic material with elastic modulus Ex = 2500 MPa and Poisson's ratio PRXY = 0.38. Because the problem is idealized as 2D plane stress 2D PLANE2 triangular structural element was used as recommend by ANSYS documentation manual. This element has 6-nodes with 2 degrees of freedom per node.

Loading and Boundary Conditions

Pressure boundary condition is prescribed on the top surface of the model while the bottom surface is restricted in the *y*-direction and one node, at $x = 0$ and $y = 0$, is restricted in *y* and *x*-direction as shown in Fig. 3.10.

3.2.2. Solution Validation using Available Results

There are closed form solutions for calculating the SIF for single edge crack panel but for straight crack only i.e., pure opening mode I SIF. The general form can be represented as:

$$K_I = Y\sigma\sqrt{a} \tag{3.2}$$

where *Y* is the geometry correction factor and it is usually a function of both crack length and panel width. In the case of centre inclined crack the mixed mode stress intensities can be calculated as:

$$K_I = K_{I_0} \cos^2 \beta \tag{3.3a}$$

$$K_{II} = K_{I_0} \sin \beta \cos \beta \tag{3.3b}$$

where K_I is the opening mode SIF, K_{II} is the sliding mode SIF, K_{I0} is determined by Eq. (3.2) and β is the crack angle. By using a proper geometric correction factor *Y*, i.e., for a single edge crack problem we can calculate the mixed mode SIF. Unfortunately, the available geometry factor is only valid for a straight single edge crack panel and is calculated as:

$$Y = 1.99 - 0.41\left(\frac{a}{w}\right) + 18.7\left(\frac{a}{w}\right)^2 - 38.48\left(\frac{a}{w}\right)^3 + 53.85\left(\frac{a}{w}\right)^4 \quad (3.4)$$

So this method will not be suitable for calculating the mixed mode SIF for an inclined edge crack. In this study, a single edge crack panels having different crack inclination angles are analyzed. The considered crack angles are 0º, 10º, 20º, 30º and 40º. The FE model used in this work was validated using the results of Wilson (1969) determined by boundary collocation technique. The author analyzed single edge cracked panels having crack angles of 22.5º and 45º and *a*/*w* ratios of 0.3, 0.4, 0.5 and 0.6. Consequently, FE models were built for all cases analyzed by Wilson and the values of the SIF were computed numerically for comparison. Except the crack inclination angles and *a*/*w* ratios, the modeling specifications including geometry, finite element mesh, crack path modeling, material and element type and loading and boundary conditions were all defined as mentioned previously in section 3.2.1. It should also be noted that the crack length was kept constant as a = 10 *mm* and the panel width was changed in order to get different *a*/*w* ratios. This is because a crack length of 10 *mm* is considered in this study. Additionally, the case of straight edge crack was validated using Eqs. (3.2 and 3.4). As shown in Fig. 3.11 the present FE results compared very well with Wilson's results especially for *a*/*w* less than 0.6. However, at a ratio *a*/*w* = 0.6 a slight deviation is obtained for β = 22.5 °. This deviation can be referred to the effect of the boundary. For *a*/*w* = 0.6 the crack tip is closer to the side boundary for β = 22.5º than for β = 45º. So, one can expect FEA to produce more error in the case of 22.5º than 45º which is obvious as shown in Fig.3.11. This ensures the validation of the finite element model.

3.3. Results and Discussion

Finite element models were built (Appendix I) for each specimen tested experimentally. It should be kept in mind that the crack tip was sharpened manually by means of a razor blade. This introduced a slight difference in the crack length from one specimen to another. As a result, two specimens were prepared for each angle in order to ensure the accuracy of the experiment. However, the differences in the crack length did not exceed 2.6% of the original crack length which is 10 *mm*. After estimating the SIF using FEA, the crack initiation angle will be calculated using the maximum tangential stress (MTS) criterion, the minimum strain energy density (S) criterion, the maximum dilatational strain (T) criterion maximum triaxial stress (M) criterion, the modified MTS criterion and the (R) criterion.

3.3.1. Stress Intensity Factors Estimation

The mixed mode stress intensity factors (K_I and K_{II}) were numerically computed for all crack angles i.e. 0º, 10º, 20º, 30º and 40º. Table 3.2 lists the finite element model specification and the results for each angle. In addition, Figs. 3.12 and 3.13 show the deformed crack shapes for β =0º and 40º, respectively. Through the validation process, the model numbers of elements were optimized by applying mesh refinement technique. These include the model general plane elements, numbers of singular elements around the crack tip and the singular elements radius size.

TABLE 3.2: FE model specifications and results.

(β^o)	**Measured Crack Length (*mm*)**	**# Elements**	**KI (kPa √m)**	**KII (kPa √m)**
0	10.17	1672	1778.10	0.07
10	10.08	1675	1722.55	181.55
20	10.11	1651	1599.55	340.60
30	10.14	1680	1415.25	460.26
40	10.14	1737	1171.40	522.45

Accordingly, the numbers of elements shown in Table 3.2 are the optimum numbers. Using Eqs. 3.2 and 3.4 for β = 0º the pure mode stress intensity factor came out to be K_I = 1780.75 kPa√m and the difference between the numerical value of K_I at β = 0º and the analytical value is about 0.148%.

3.3.2. Prediction of the Crack Initiation Angle

By incorporating the numerical values of SIF into the crack initiation criteria the crack initiation angles are calculated. Once the stress intensity mixity ratio μ is calculated the corresponding crack initiation angle is found. In fact, each criterion will yield different values of θ_0 depending on the order of the criterion's equation. For example, the S criterion (Eq. 2.18a) is a fourth order equation, hence, it yields four roots. However, from these four roots only those which satisfy the inequality in Eq. (2.18b) must be taken into account. Furthermore, for the case when the crack specimen is subjected to a uniaxial tension only the negative values of the angle θ_0 must be considered. Crack initiation

angle θ_0 is plotted as a function of crack inclination β in Fig. 3.14 for β = 0º, 10º, 20º, 30º and 40º. As this figure shows, all criteria give the same initiation angle at β = 0º. In addition, the M and T criteria match exactly for all inclination angles. This is due to the similarity in the equations of the stress triaxiality ratio (M) and the dilatational strain energy (T_v) as explained by Shafique and Marwan, (2000). However, as the crack angle of inclination increases the difference in crack initiation angle prediction increases reaching more than 4º when β = 40°. For all inclination angles, the S criterion was found to predict the minimum initiation angle while both M and T criteria were found to predict the maximum initiation angle. This scatter is either due to the differences in assumptions on which each criterion is based or due to the formulation of the criteria itself. For example, as previously mentioned the M and T criteria yield exactly the same results due to the similarity in the formulation but they are still based on different assumptions. Moreover, Safique and Marwan (2000) reported that both criteria (M and T) matched exactly for all type of loading. The authors analytically analyzed mixed mode crack initiation angle under uniaxial, pure shear, biaxial and proportional tension-torsion loading and they reported similar observation concerning the M and T criteria.

3.3.3. A New Model for Estimating the Mixed Mode SIF for an Inclined Edge Crack Panel

The need for either exact or approximate solutions to estimate the SIF for an inclined edge crack panel is pressing. Yet, the boundary collocation and conformal mapping techniques are considered to be useful tools, however, they are not very practical. These

methods are not easy to use because they require a certain level of knowledge which might be considered as an obstacle. For example, conformal mapping technique requires an acceptable knowledge in the theory of complex variables. In boundary collocation technique the solution is reduced to a set of linear algebraic equations which still need to be solved numerically. As a result, it is essential to find a fast and easy way to estimate the SIF for an inclined edge crack.

The present model is based on FE analysis of different edge crack angles and sizes. It is based on introducing two geometry correction factors i.e., Y_I and Y_{II} for opening and sliding mode, respectively. Thus, the mixed mode SIF's can be calculated from following relations

$$K_I = Y_I \sigma \sqrt{a} \cos^2 \beta \tag{3.5a}$$

$$K_{II} = Y_{II} \sigma \sqrt{a} \cos \beta \sin \beta \tag{3.5b}$$

where the mixed mode geometry correction factors Y_I and Y_{II} are estimated numerically using

$$Y_I = \frac{K_I}{\sigma \sqrt{a} \cos^2 \beta} \tag{3.6a}$$

and

$$Y_{II} = \frac{K_{II}}{\sigma \sqrt{a} \cos \beta \sin \beta} \tag{3.6b}$$

Using the FE model built for this study (section 3.2.1) and keeping the applied load σ and the crack length a constant and changing the crack initiation angle β and the panel width

w, sets of values for both Y_I and Y_{II} were generated. Crack inclination angles β = 0º to 80º, with increments of 10º, were investigated. Similarly, each angle was analyzed with respect to different crack length to panel width ratios, a/w. The considered a/w ratios are 0.1 to 0.7 with increments of 0.1. Tables 3.3 and 3.4 show the resulting values of the opening and sliding mode geometry correction factors functions of a/w and β. The variations of Y_I and Y_{II} with a/w and the crack inclination angle β are shown in Figs. 3.15 and 3.16. For a/w = 0.017 and β = 0º, Eq. (3.6a) yields Y_I = 2.0 which is comparable with the value of Y given by Eq. (3.4) for a/w = 0.

The mixed mode geometry correction factors can be determined either from Tables 3.3 and 3.4 or from Figs. 3.15 and 3.16. However, by using curve fitting technique correlations between the geometry correction factors Y_I and Y_{II} and the crack inclination angle β and a/w ratio are found.

TABLE 3.3: Opening mode geometry correction factor Y_I.

	a/w						
Angle (º)	**0.1**	**0.2**	**0.3**	**0.4**	**0.5**	**0.6**	**0.7**
0	2.11	2.43	2.95	3.74	5.00	7.12	11.07
10	2.13	2.44	2.95	3.72	4.94	6.95	10.68
20	2.18	2.47	2.95	3.67	4.76	6.50	9.54
30	2.28	2.54	2.97	3.60	4.53	5.92	8.12
40	2.45	2.68	3.05	3.58	4.32	5.37	6.92
50	2.75	2.94	3.25	3.67	4.24	5.00	6.02
60	3.33	3.48	3.72	4.05	4.48	5.01	5.69
70	4.63	4.74	4.93	5.17	5.49	5.86	6.30
80	8.82	8.90	9.03	9.20	9.42	9.66	9.96

TABLE 3.4 : Mixed mode geometry correction factor Y_{II}.

	a/w						
Angle (º)	**0.1**	**0.2**	**0.3**	**0.4**	**0.5**	**0.6**	**0.7**
0	0	0	0	0	0	0	0
10	1.28	1.45	1.71	2.09	2.62	3.50	4.99
20	1.28	1.44	1.68	2.02	2.51	3.26	4.46
30	1.29	1.43	1.64	1.93	2.33	2.89	3.72
40	1.31	1.42	1.59	1.83	2.14	2.56	3.16
50	1.33	1.42	1.55	1.72	1.95	2.24	2.61
60	1.38	1.44	1.53	1.65	1.80	1.98	2.21
70	1.49	1.53	1.58	1.66	1.74	1.84	1.96
80	1.84	1.85	1.88	1.91	1.95	2.00	2.05

The curve fitting processes were performed using MATLAB curve fitting toolbox. Figures 3.15 and 3.16 reveal that Y_I and Y_{II} exhibit a similar behavior with respect to *a*/*w*. Consequently, all Y_I and Y_{II} curves were fitted using the same equation. This equation was selected by inspection and is found to be:

$$Y_i = \gamma\left[\sec\left(\frac{a}{w}\right)\right]^{\xi} + \alpha\left(\frac{a}{w}\right) \tag{3.7}$$

where i = I or II

The constants γ and α and the exponent ξ are to be determined for both Y_I and Y_{II}. Accordingly, Eq. (3.7) can be written as:

$$Y_I = b\left[\sec\left(\frac{a}{w}\right)\right]^{-c} + d\left(\frac{a}{w}\right) \tag{3.8a}$$

$$Y_{II} = p\left[\sec\left(\frac{a}{w}\right)\right]^{-q} + z\left(\frac{a}{w}\right) \tag{3.8b}$$

where b, c, d, p, q and z are to be determined for each a/w ratio.

The values of b, c, d, p, q and z were plotted with respect to the crack inclination angle β as shown in Figs. 3.17 and 3.18. Unlike Y_I and Y_{II}, these figures illustrate that b, c, d, p, q and z show different behaviors with respect to β. As a result, they are fitted but using different equations. This will account for the dependence of the value of Y_I and Y_{II} on both a/w and β.

b, c, d, p, q and z are found to be calculated as:

$$b = 1.9[\sec\beta]^{-0.921} - 0.38\beta^{2.03} \tag{3.9a}$$

$$c = \frac{8.53 - 5.57\beta}{\beta^2 - 0.82\beta + 1.37} \tag{3.9b}$$

$$d = \frac{1.12}{\beta^3 - 0.73\beta^2 + 0.8} \tag{3.9c}$$

$$p = 1.2[\sec\beta]^{-0.3} - 0.15\beta \tag{3.10a}$$

$$q = 2.85\beta^3 - 6.4\beta^2 + 5.1 \tag{3.10b}$$

$$z = 0.8\beta^3 - 2.53\beta^2 + 1.66\beta + 0.54 \tag{3.10c}$$

where β is in radians.

A total of 23 curves were fitted in order to correlate Y_I and Y_{II} with a/w and β. All crack inclination angles i.e., 0º, 10º, 20º, …, 80º and a/w ratios i.e., 0.1, 0.2,…, 0.7 were considered in the fitting processes. It should be noted that if Eqs. 3.8b and 3.10 are solved for $\beta = 0$ they will yield a value of Y_{II} greater than zero, however, this has no physical

meaning since K_{II} is zero. The curve fitting quality is a critical issue in this regard. In order to achieve a good fitting quality the goodness of fit terms were evaluated using the sum of squares due to error (SSE), R-square, adjusted R-square and root mean squared error (RMSE). The goodness of fit terms are listed in Tables 3.5 and 3.6 for Eq. 3.8 as Y_I and Y_{II} are fitted with respect to different a/w ratios. On the other hand, Tables 3.7 to 3.8 list these terms for b, c, d, p, q and z as Eqs. 3.9 to 3.10 are fitted with respect to different inclination angles. Failure to achieve good values of the goodness of fit terms will lead to an obvious error in calculating the mixed mode geometry correction factors Y_I and Y_{II}. This is because the error will accumulate due to progression of the fitting processes.

TABLE 3.5: Goodness of fit terms for Eq. 3.8a.

beta (β°)	**SSE**	**R-square**	**Adjusted R-square**	**RMSE**
0	0.0002182	1	1	0.007385
10	0.0005558	1	1	0.01179
20	0.0008335	1	1	0.01443
30	0.003002	0.9999	0.9998	0.0274
40	0.001833	0.9999	0.9998	0.02141
50	0.00176	0.9998	0.9997	0.02098
60	0.001331	0.9997	0.9996	0.01824
70	0.001179	0.9995	0.9992	0.01717
80	0.0003667	0.9997	0.9995	0.009574

TABLE 3.6: Goodness of fit terms for Eq. 3.8b.

beta (β°)	**SSE**	**R-square**	**Adjusted R-square**	**RMSE**
10	0.0004874	1	0.9999	0.01104
20	$3.68*10^{-5}$	1	1	0.003033
30	0.0002686	0.9999	0.9999	0.008195
40	0.0002844	0.9999	0.9998	0.008431
50	0.0002705	0.9998	0.9997	0.008223
60	0.0001117	0.9998	0.9997	0.005284
70	$8.66*10^{-5}$	0.9995	0.9993	0.004652
80	$6.18*10^{-5}$	0.9983	0.9975	0.003931

TABLE 3.7: Goodness of fit terms for Eq. 3.9.

	SSE	**R-square**	**Adjusted R-square**	**RMSE**
b	0.0005646	1	1	0.01063
c	0.001651	1	0.9999	0.01817
d	0.008558	0.9918	0.989	0.03777

TABLE 3.8: Goodness of fit terms for Eq. 3.10.

	SSE	**R-square**	**Adjusted R-square**	**RMSE**
p	0.0008007	0.9977	0.9968	0.01266
q	0.01997	0.999	0.9987	0.0632
z	0.004406	0.9919	0.9859	0.03319

To check the validity of this model, the values of Y_I and Y_{II} in Tables 3.3 and 3.4 were regenerated using Eqs. 3.8 to 3.10. The model showed a good agreement as compared with the results in Tables 3.3 and 3.4 as shown in Figs 3.19 and 3.20. In addition, the model was compared with Eq. (3.4) for straight edge crack panel. To accomplish this, both the model and Eq. (3.4) were analyzed at different a/w ratios namely 0, 0.1, 0.2, …, 0.7. The model compared very well with the analytical solution for a/w between 0 and 0.65. Even at $a/w = 0.7$, the model gives a difference of 4.4% as compared with Eq. (3.4) which is still reasonable. The model was also used for $\beta = 22.5°$ and $\beta = 45°$ and it found to be in agreement with Wilson (1969) results as shown in Fig. 3.22.

3.4. Conclusion

The pure opening mode and mixed mode SIF are estimated numerically using ANSYS FE code. The finite element model was validated for pure and mixed mode fracture. For pure mode, the FE model compared very well with analytical solution. Similarly, the FE model showed good agreement with Wilson's results in the case of mixed mode fracture. After estimating K_I and K_{II}, the SIF values are incorporated into six crack initiation criteria for crack initiation prediction. All criteria give the same initiation angle at $\beta = 0°$. However, as the crack angle of inclination increases the difference in crack initiation angle prediction increases reaching more than 4°. For all inclination angles the S criterion was found to predict the minimum initiation angle while both M and T criteria were found to predict the maximum initiation angle.

A new model for estimating the SIF for an inclined edge crack panel is proposed. The model is based on finite element results. The proposed model was validated using the analytical solution for the case of pure opening mode. On the other hand, Wilson's results were used to validate the model for the case of mixed mode fracture. The model showed good agreement with both cases.

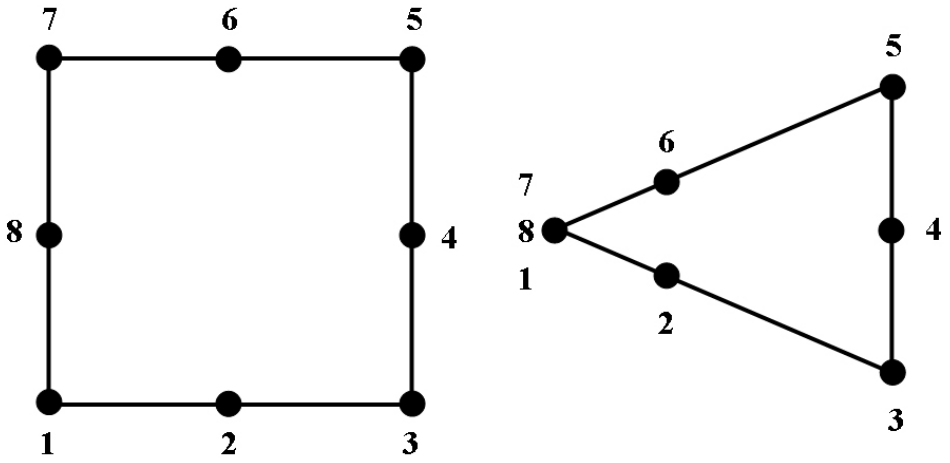

Figure 3.1: Quadrilateral element collapsed into triangular quarter-point element.

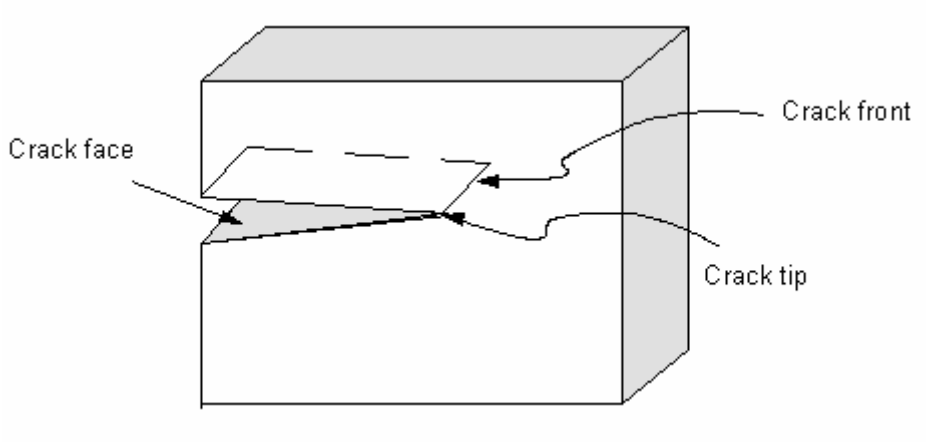

Figure 3.2: Crack tip and crack front.

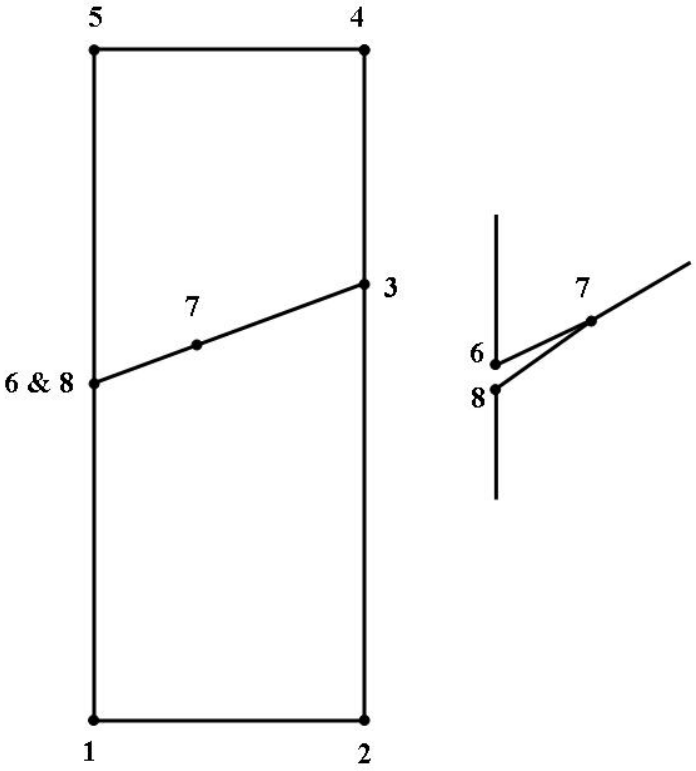

Figure 3.3: Cracked specimen geometry (keypoints and lines).

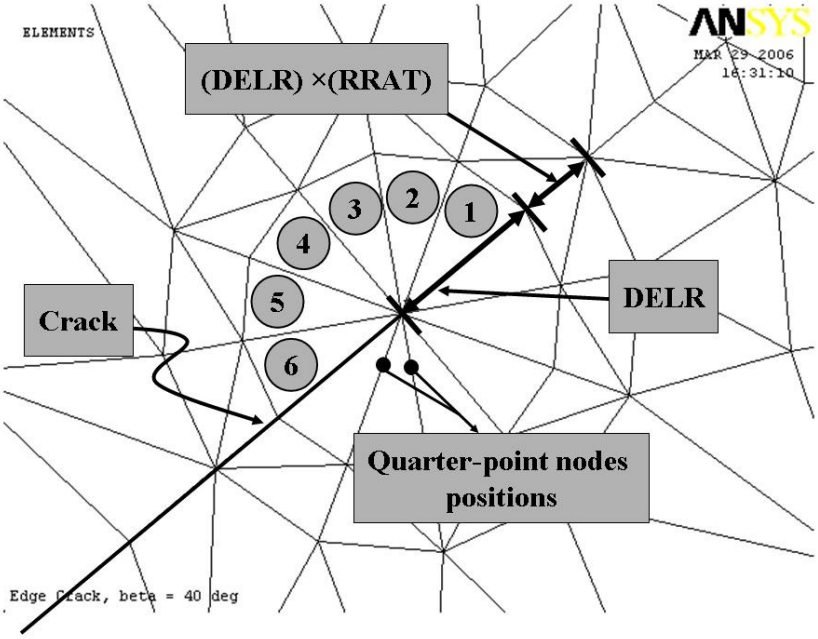

Figure 3.4: Crack tip mesh specifications.

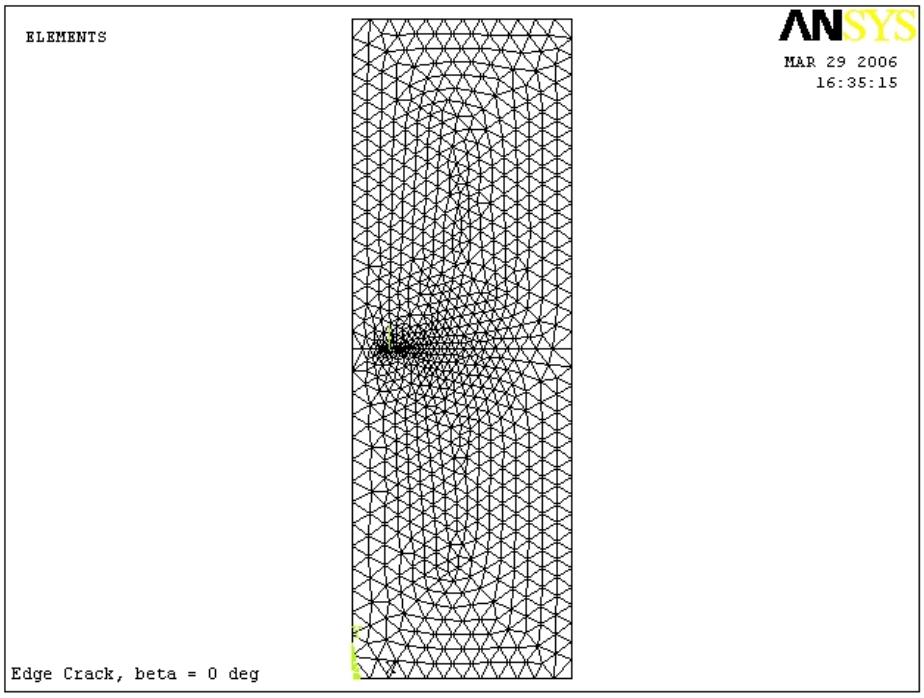

Figure 3.5: Finite element mesh for straight crack ($\beta = 0^{o}$).

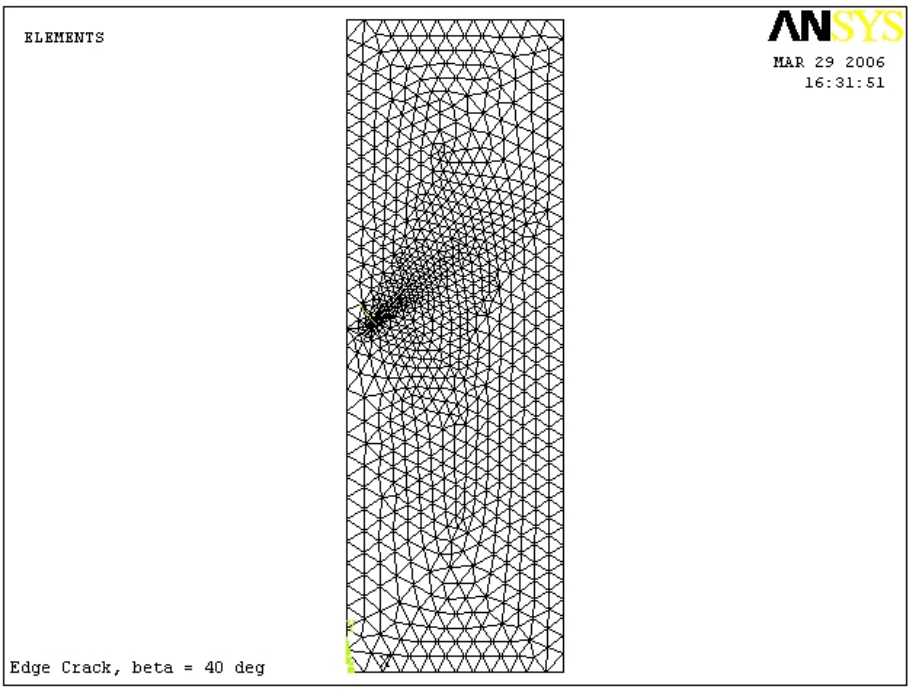

Figure 3.6: Finite element mesh for inclined crack (β = 40º).

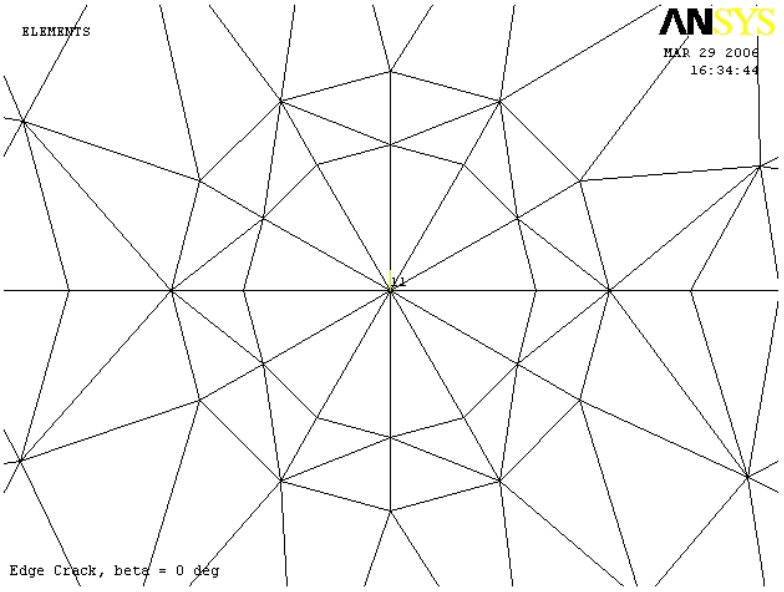

Figure 3.7: Close up view of finite element mesh for straight crack around the crack tip (β = 0º).

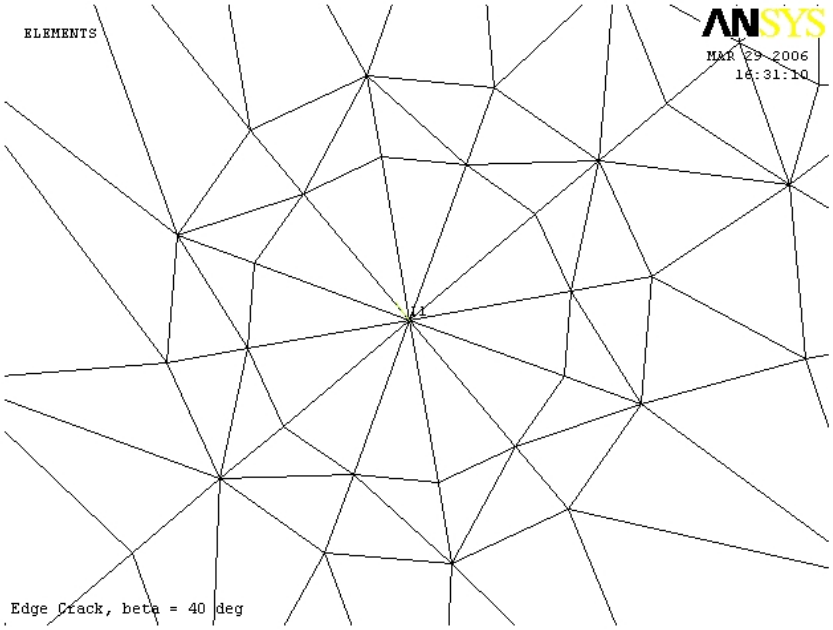

Figure 3.8: Close up view of finite element mesh for inclined crack around the crack tip ($\beta = 40^{o}$).

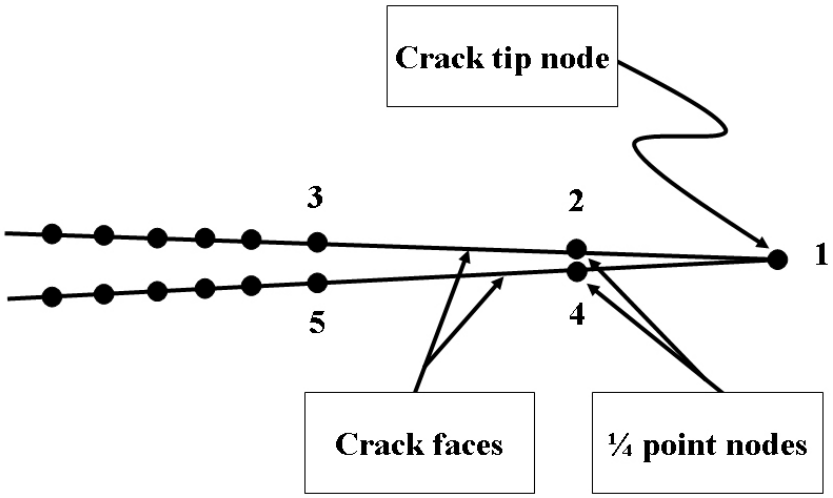

Figure 3.9: Crack path definition (5 nodes sequence).

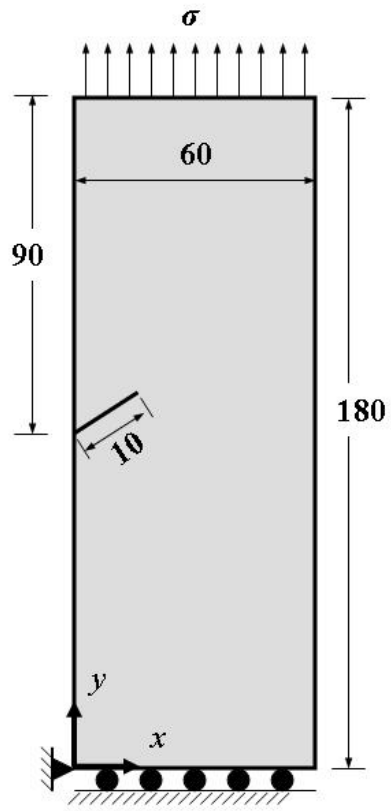

Figure 3.10: FE Model boundary conditions, geometry and dimensions in *mm*.

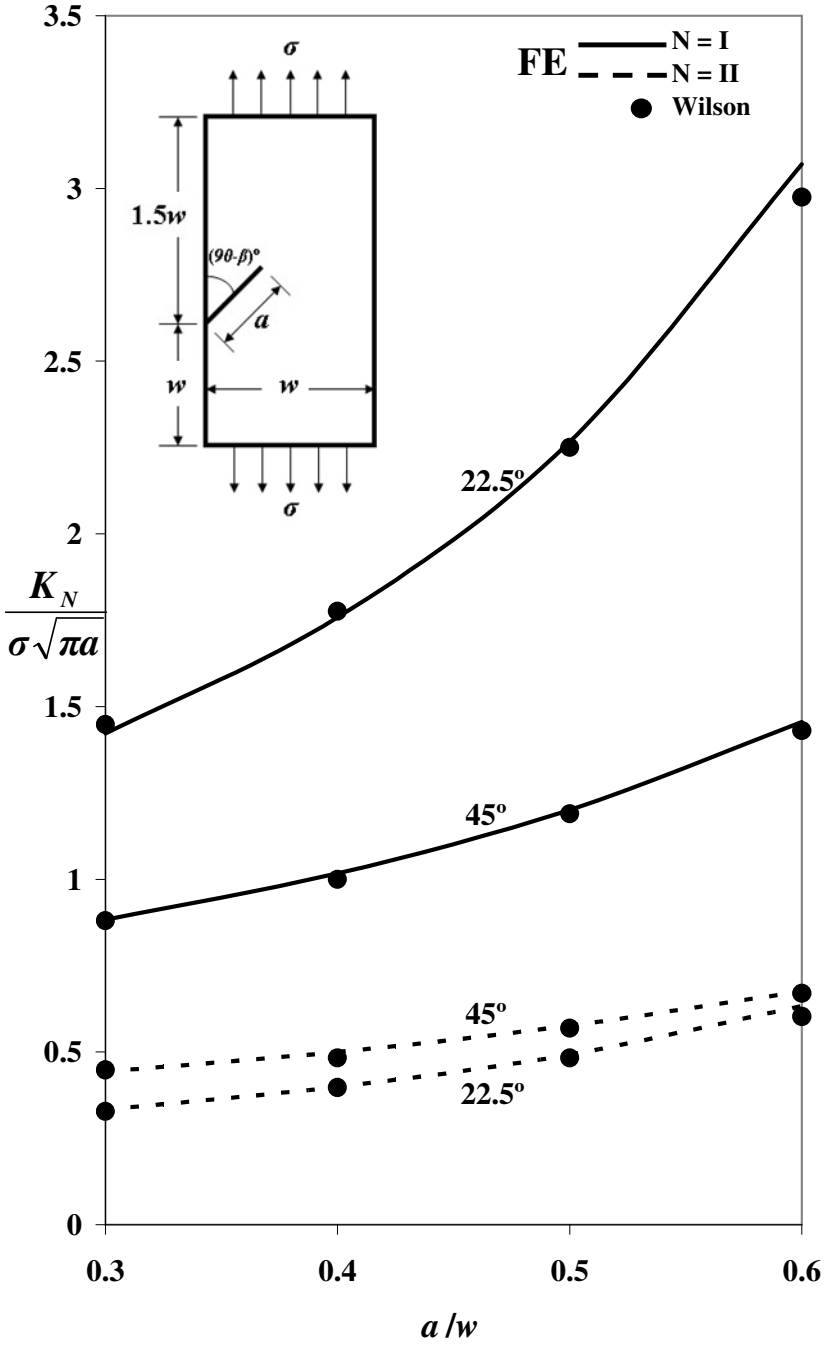

Figure 3.11: Comparison between FE results and Wilson's (1969) results.

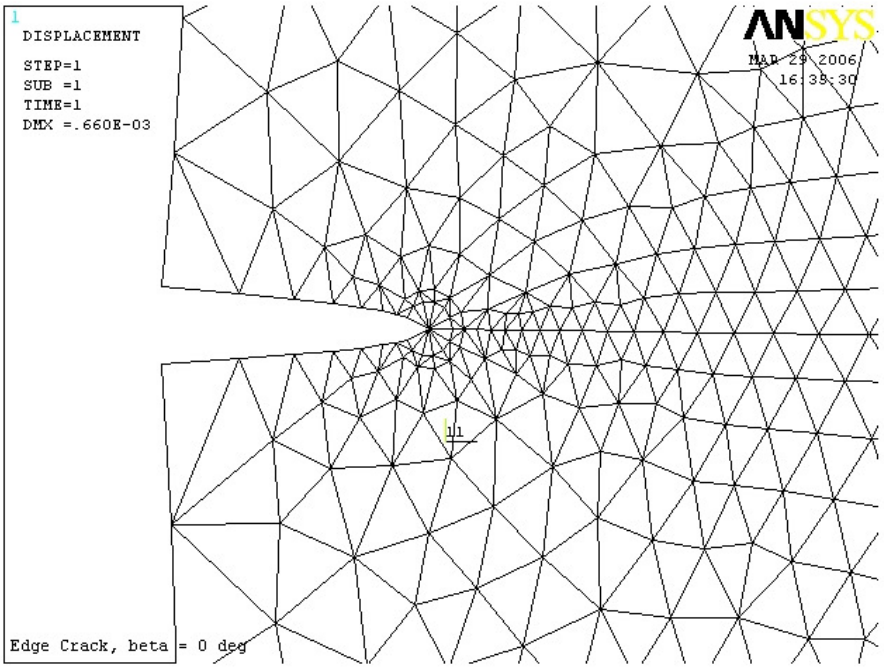

Figure 3.12: Deformed crack area for $\beta = 0º$.

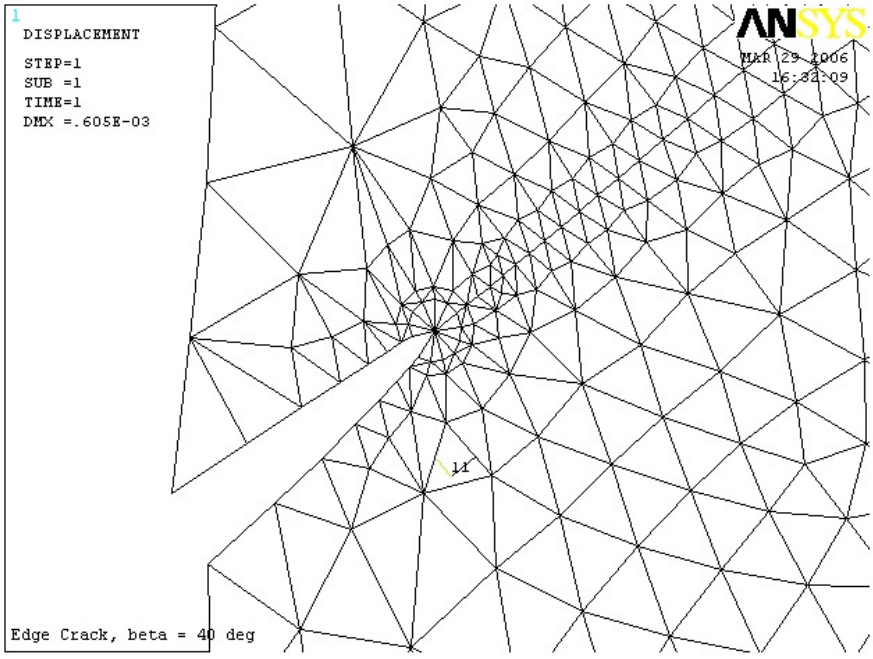

Figure 3.13: Deformed crack area for $\beta = 40º$.

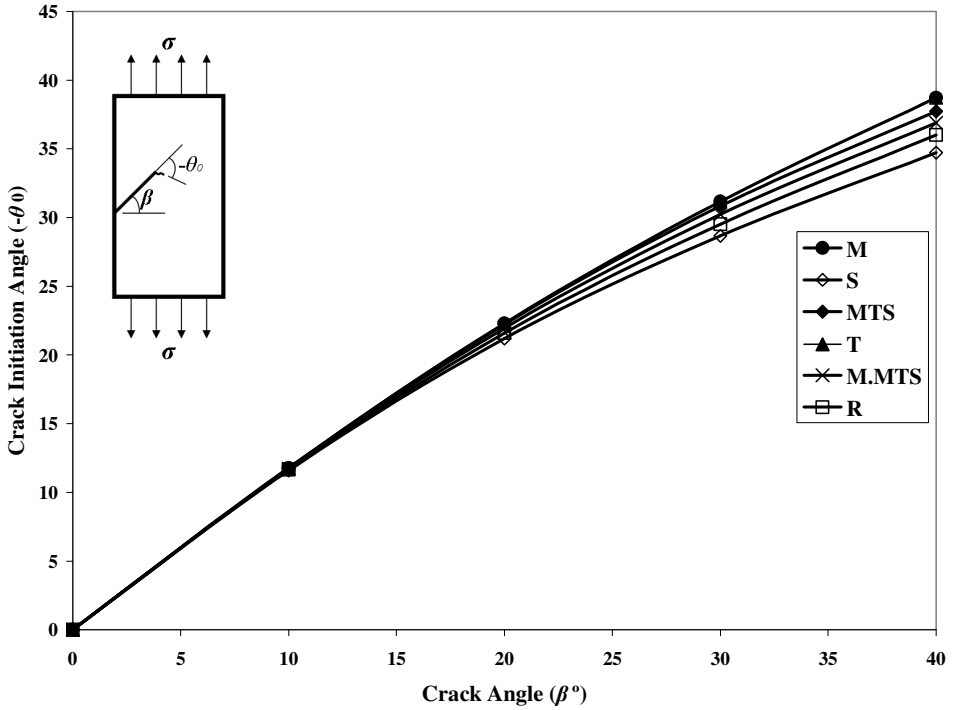

Figure 3.14: Predicted crack initiation angle using FE.

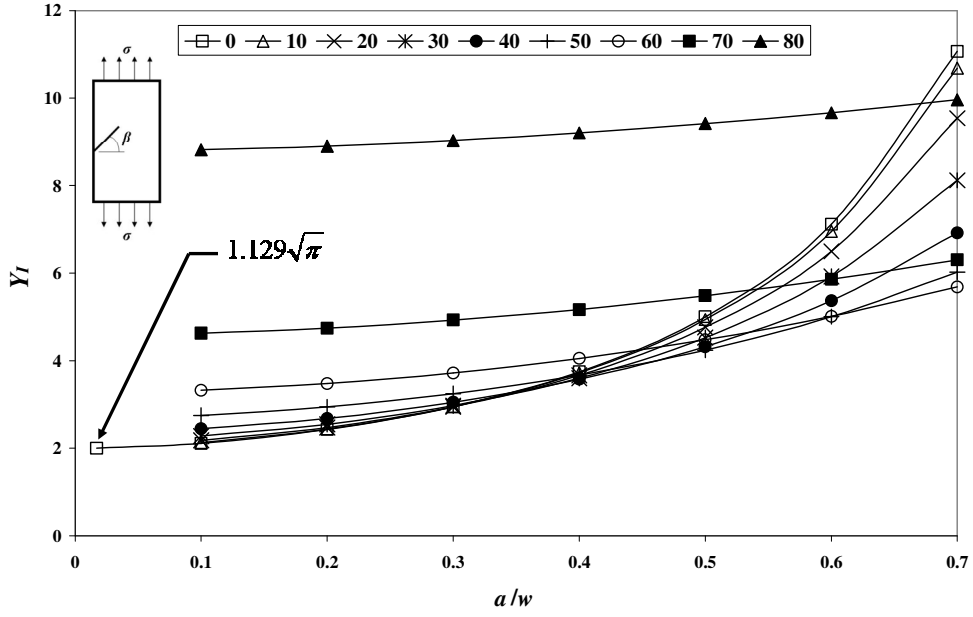

Figure 3.15: FE results of Y_I for β = 0º, 10º, …, 80 º.

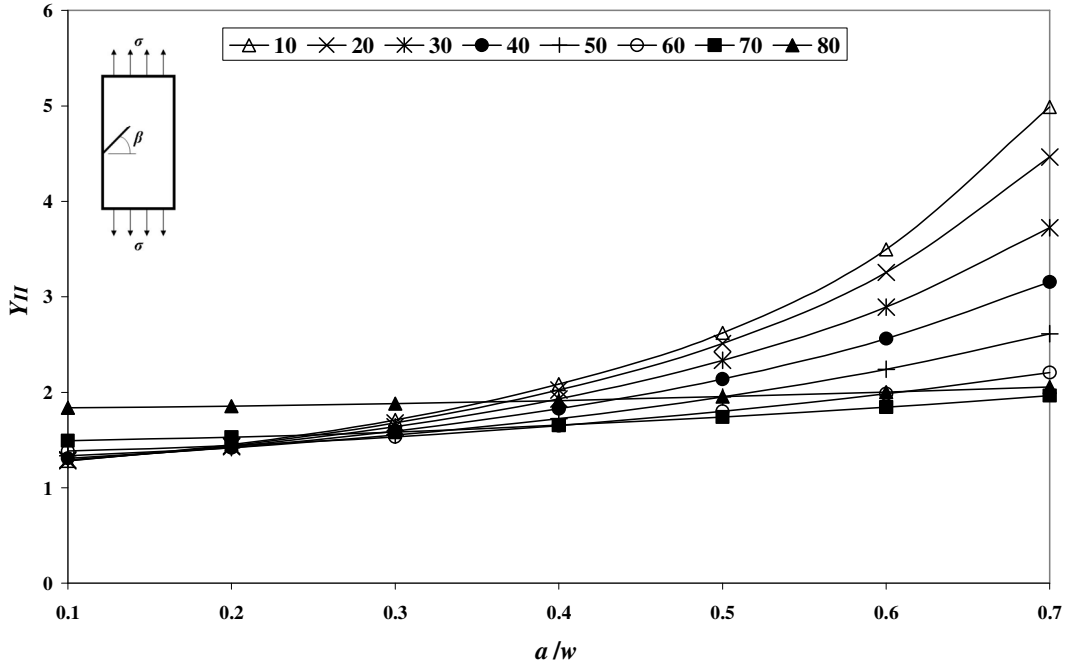

Figure 3.16: FE results of Y_{II} for β = 10º, 20º, …, 80 º.

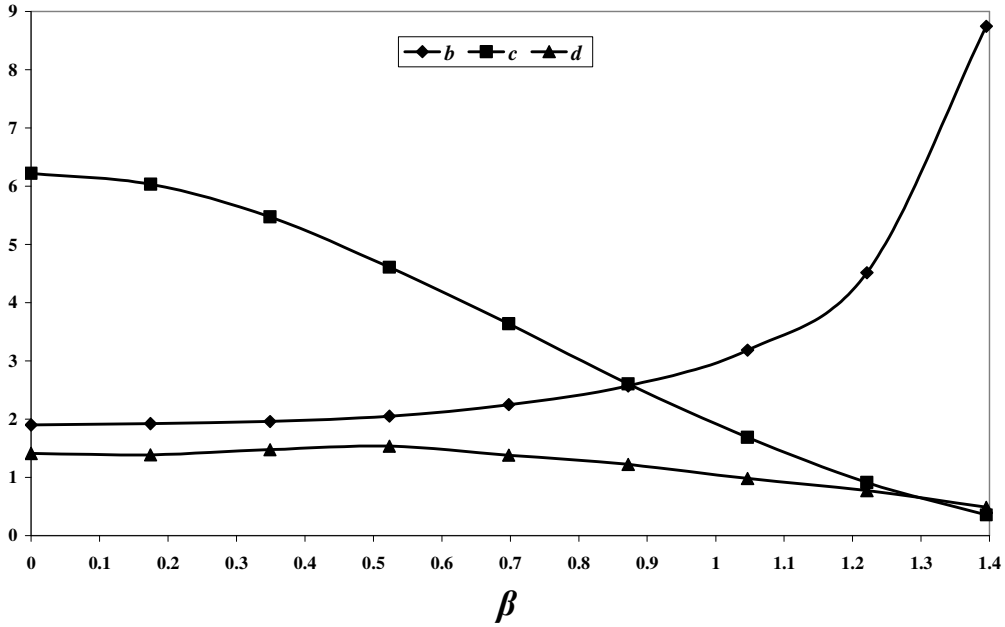

Figure 3.17: Change of *b*, *c* and *d* with respect to crack inclination angle.

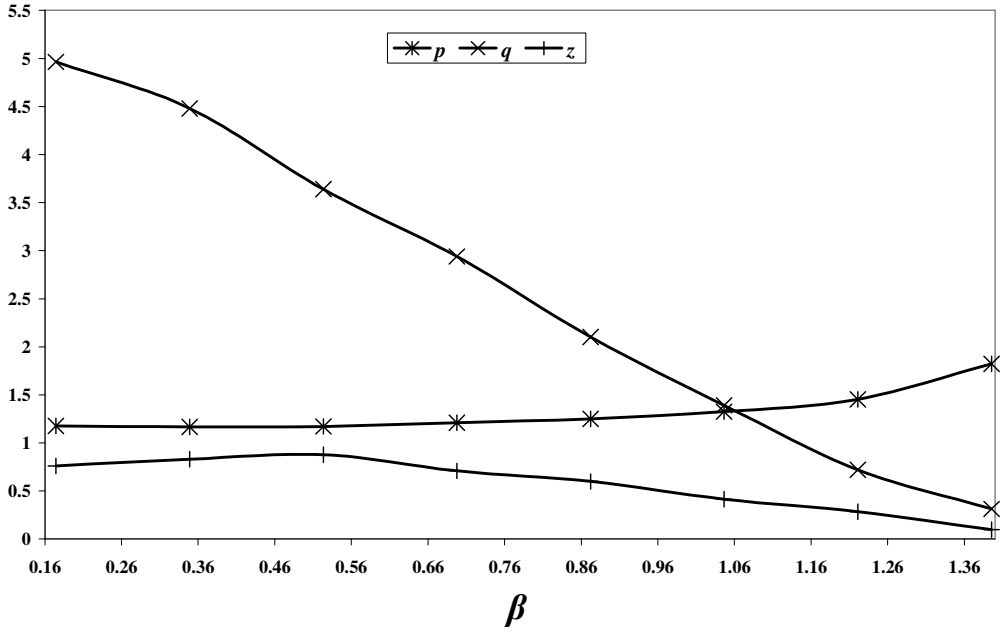

Figure 3.18: Change of p, q and z with respect to crack inclination angle.

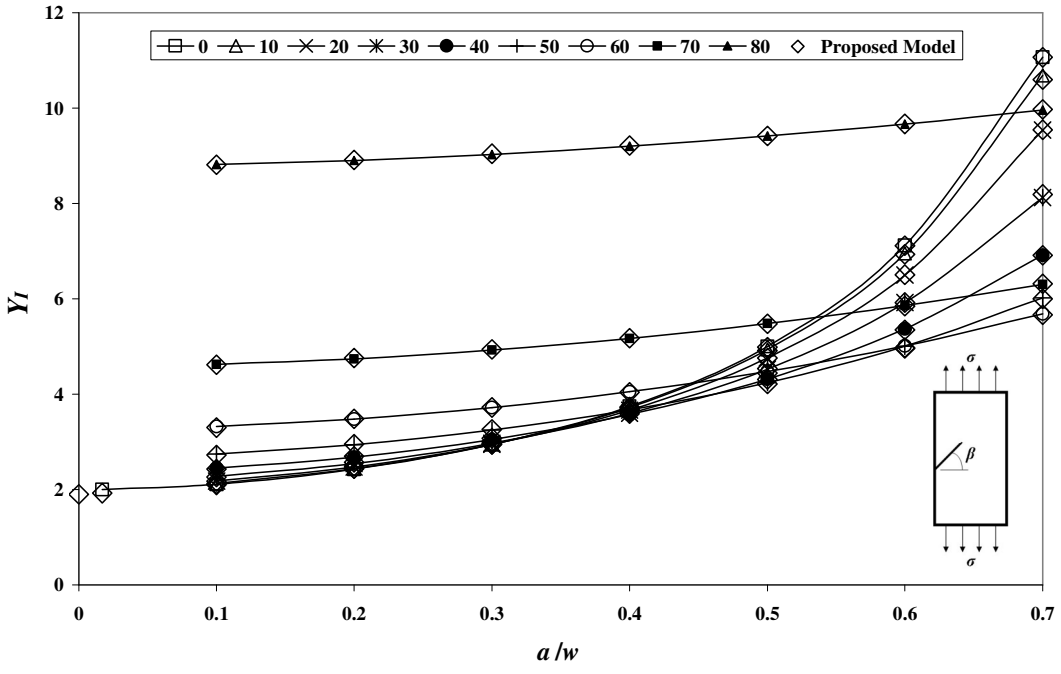

Figure 3.19: Comparison shows the ability of the proposed model to regenerate the FE results for Y_I.

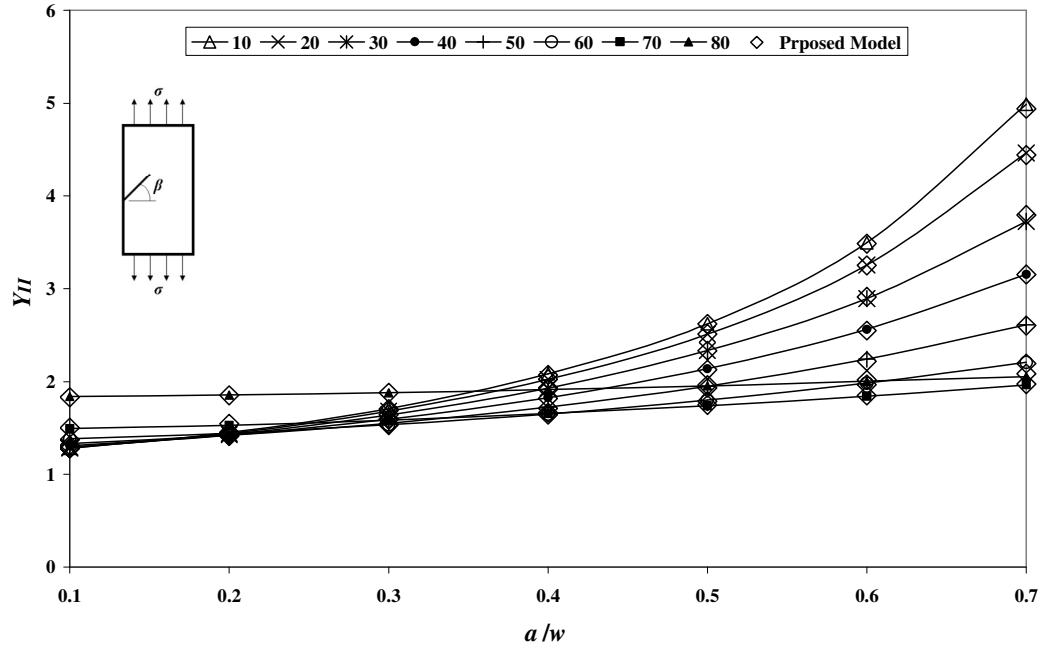

Figure 3.20: Comparison shows the ability of the proposed model to regenerate the FE results for Y_{II}.

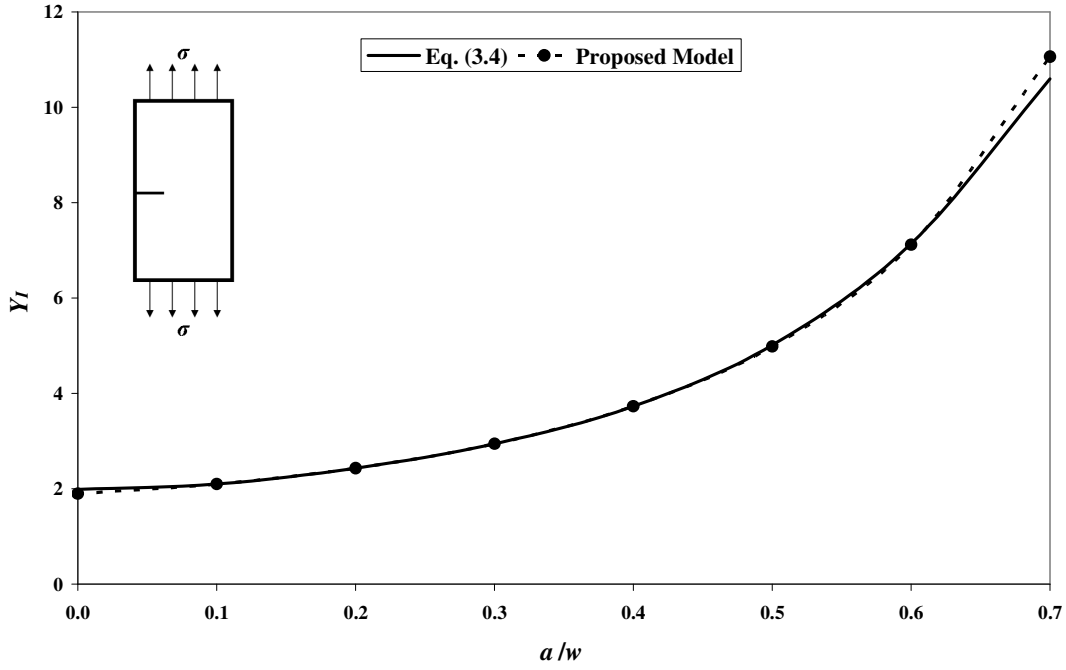

Figure 3.21: Comparison between the proposed model and Eq. (3.4) for straight edge crack.

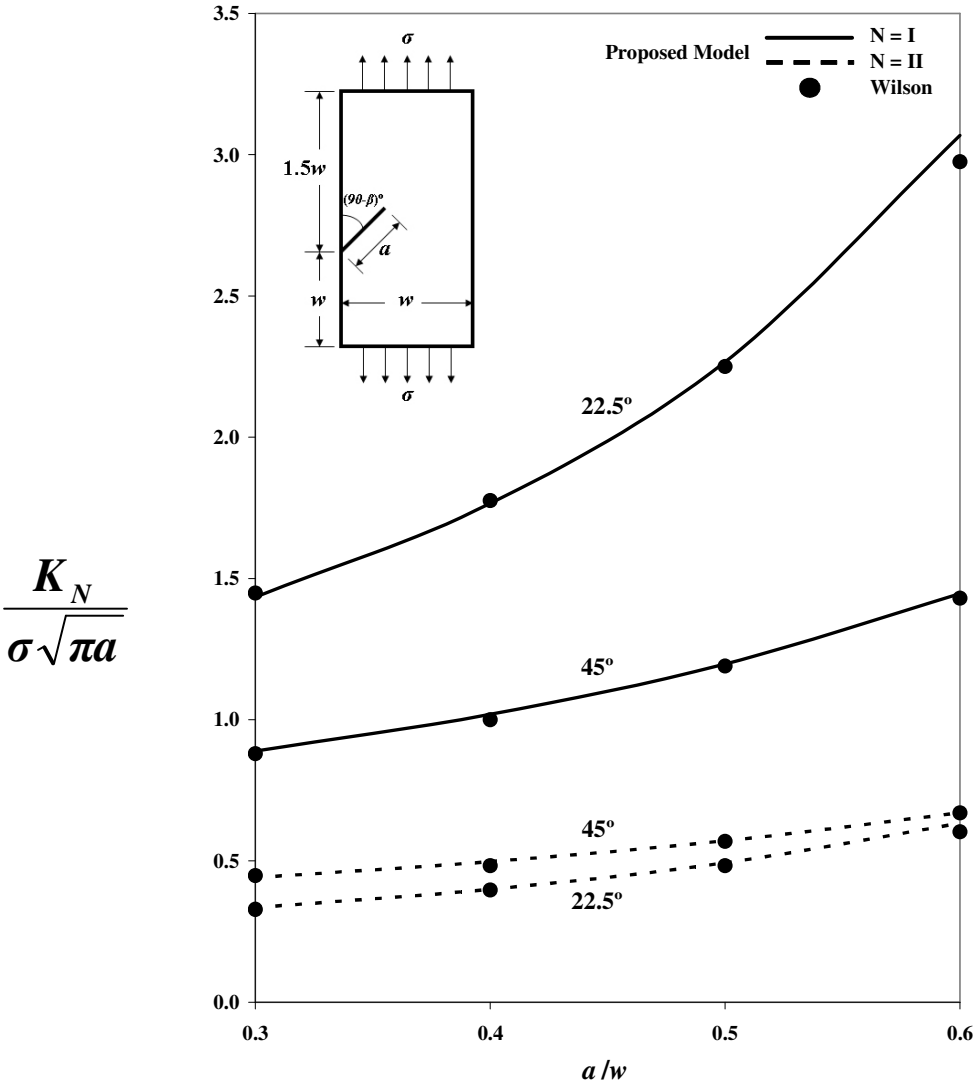

Figure 3.22: Comparison between the proposed model and Wilson (1969).

CHAPTER 4

EXPERIMENTAL DETERMINATION OF CRACK INITIATION ANGLE

4.1. Introduction

"Experimental techniques, ranging from the very elementary to highly sophisticated, provide the vehicle for determining the stress intensity factor for a wide spectrum of problems. At the low end of the scale, as illustrated in Fig. 4.1, two-dimensional photoealsticity or strain gages can be cost-effective alternatives to the other approaches", Sanford (2003).

Most of the experimental work concerning the estimation of the SIF (pure mode I or mixed mode I & II) fracture is preformed using photoelasticity. To make use of photoelasticity technique setups are necessary and these are called polariscopes. There exist two general types of polariscopes, plane polariscope and circular polariscope. The arrangement of these two types is discussed in the following section.

4.2. Photoelastic Technique

"The name photoelasticity reflects the nature of this experimental method: *photo* implies the use of light rays and optical techniques, while *elasticity* depicts the study of stresses and deformations in elastic bodies. Certain materials, notably plastics, behave homogenously when unstressed but become heterogeneous when stressed and the change in index of refraction is a function of stress applied", James and James (1989).

4.2.1. The Plane Polariscope

When the waves in a beam of light are constrained to vibrate in a systematic manner in planes normal to the direction of propagation, the beam is said to be polarized. The ploariscope is an instrument used to measure the relative retardations or phase difference produced when polarized light passes through a stressed photoelastic model. It can have a variety of forms depending on the technique used in the investigation. In its simplest form the polariscope consists of a suitable light source and two polarizers. The first polarizer converts the natural light from the source into a field of plane polarized light in which the model is placed. The second polarizer, which is called the analyzer, revolves the component waves emerging from the model into one plane so that the effects produced by the model can be measured from the resulting interference of the waves. Such an arrangement is known as a plane polariscope. The polarizer and analyzer are frequently referred to collectively as the 'polaroids'.

In the plane polariscope, the polaroids are usually set with their axes crossed or perpendicular to one another. In the absence of a model, none of the light emerging from the polarizer is then transmitted by the analyzer. A model inserted into the field of a crossed plane polariscope, therefore, appears against a dark background. But if the axes of the polaroids are set parallel to one another, all of the light transmitted by the polarizer is transmitted also by the analyzer except for the losses due to absorption and reflection. Hence, the background in this case will be bright.

If the analyzer is set in the cross position, i.e. with its axis perpendicular to that of the polarizer the intensity transmitted will be

$$I = I_o \sin^2 2\Theta \sin^2 \frac{\varphi}{2} \tag{4.1}$$

where

I_o is the total intensity (the intensity of the light that would be transmitted by the analyzer if it were optically isotropic).

Θ is the angle of inclination of the incident wave on the specimen to the direction of the first principal stress σ_1.

φ is the phase difference between the incident wave and the emergent from the specimen.

Eq. (4.1) shows that there are two separate conditions under which extinction of the light will be obtained. One condition is that $\Theta = 0°$ or $90°$. This is satisfied by all points on the

plate where the directions of the principal stresses are parallel to the axes of the polaroids and such points appear dark. In general, these points lie on continuous curves forming a system of dark bands known as isoclinics. The second condition under which the extinction is obtained is that $\varphi = 2n\pi$, for $n = 0, 1, 2$ …etc. n is equivalent to a relative retardation of n wavelengths. Thus all points on the plate at which the difference $(\sigma_1 - \sigma_2)$ in the principal stresses is such that relative retardation produced is equal to a whole number of wavelength will appear dark. In general, the difference in the principal stresses varies continuously within the plate so that the loci of such points are smooth curves. These are known as isochromatics and are classified in terms of their fringe order.

4.2.2. Distinction between Isoclinic and Isochromatic Fringes

An isoclinic is a line along which the principal stresses act in given direction. Thus the direction of the isoclinic itself does not usually give the direction of a principal stress. Knowledge of the principal stress direction is generally useful in understanding how the shape of a part affects the stress distribution, and also provides the additional data needed for evaluation of the two principal stresses at points within the model. In contrast, isochromatic fringes are the lines of constant maximum shear stress and are colored however, isoclinic are dark in appearance.

4.2.3. Circular Polariscope

The plane polariscope is not suitable for general photoelastic work, as both isoclinic and fringes appear at the same time, making it difficult to interpret the all- important fringes. Fortunately, isoclinic can be eliminated by introducing two quarter wave plates into the polariscope (written as λ/4 plates) as Fig. 4.2 shows. The plane polarized wave emerging from the polarizer is converted by the first quarter-wave plate into a counterclockwise circularly polarized wave. The second quarter-wave plate reconverts this into a plane polarized wave vibration in the vertical plane identical with that emerging from the polarizer except for some loss of intensity. With the axis of the analyzer horizontal, the light is therefore extinguished. Thus, when a model is inserted in this polariscope it appears against a dark background. However, if the analyzer is rotated through 90° from the position shown so that it is then parallel to the polarizer, the light emerging from the second quarter-wave plate is transmitted and the background will be bright. When the circular polariscope is set to give a dark background the light intensity is

$$I = I_o \sin^2 \frac{\varphi}{2} \tag{4.2}$$

It can be easily seen that the transmitted intensity will be zero when $\varphi = 2n\pi$, corresponding to a relative retardation equal to a whole number of wavelengths. This is the same as the second condition for extinction obtained in the plane polariscope so that the isochromatic pattern is the same in each. This, however, is the only condition for extinction in the circular polariscope so that no isoclinics appear.

4.2.4. Isochromatic Fringe Order

As the load increased in a model, the relative retardation introduced at every point causes it to undergo a number of darkness-brightness cycles. In the general case where gradients of stresses are present, all points exhibiting the same relative retardation or the same maximum shear stress for a certain load are simultaneously dark and appear as a dark fringe. When white light is used, isochromatics appear as bands of the same color, hence, the name isochromatic, meaning the same color. In contrast, when monochromatic light is used they appear as dark fringes. In the case of white color the transition between the red and green colors defines one fringe, Albrecht (1974) and Durelli and Riley (1965).

In a cracked panel, the isochromatic fringes form continuous loops around the crack tip. When a white light color is used, the determination of the fringe order is achieved by following the color sequence of the isochromatic loops. Black color represents zero fringe order ($N = 0$) and Purple color (Tint-of-Passage) represent a fringe order of one ($N = 1$). Referring to Table 4.1, one can realize that for an integer fringe order to be recognized the isochormatic colors sequence has to be Yellow-Red-Green. Taking into account that the Red/Green transition always represents an integer fringe order i.e. $N = 2$, 3, 4,…etc. Successive occurrences of Red/Green transition indicate the increase of stress and hence the increase of the fringe orders by one. It should be noted that Yellow and Red fringes will appear before the Purple fringe. Then the sequence of the fringes color will be Blue-Green /Yellow /Red/Green /Yellow/Red/Green…etc.

TABLE 4.1: Dominant isochromatic fringe colors for full-field interpretation. (Measurement Group, INC. Photoelastic Stress Analysis Technical Bulletins)

Color	Approximate Fringe Order
Black	0.0
Yellow	0.6
Red	0.9
Purple (Tint-of-Passage)	1.0
Blue-Green	1.2
Yellow	1.5
Red	1.7
Red/Green Transition	2.0
Green	2.2
Yellow	2.5
Red	2.8
Red/Green Transition	3.0
Green	3.2

Knowing that the first Red/Green transition after the Purple color represents the fringe order $N = 2$. Hence, the second Red/Green transition represents the fringe order $N = 3$ and so on. In addition, the Green/Yellow transition indicates an increase of the fringe order by half. As a results, the first Green/Yellow transition after the Purple fringe represents ($N = 1.5$). Because the next fringe order after $N = 1.5$ is $N = 2$, the second Green/Yellow transition represents $N = 2.5$.

4.2.5. Methods for Determining the Stress Intensity Factor using Photoelasticity

Post (1954) and Post and Wells (1958) pioneered the applicability of photoelsticity to fracture mechanics. Irwin (1958) showed that the stress intensity factor may be

determined from the characteristics of isochromatic fringes in the vicinity of the crack tip. Furthermore, in the case of three-dimensional problems, the state of stress may be investigated by employing the frozen stress method. Techniques for extracting the stress intensity factors from photoelastic data have been described in the literature. Many of these techniques rely upon measurements outside the zone where the stress intensity factors are dominant as well as within this zone in order to use data from the complete fringe field.

Considering the case of a semi-infinite cracked plate loaded uniaxially, Irwin (1958) pointed out that for photoelastic analysis of the crack tip stress field, two parameters at least needed. These are the distance from the crack tip to the furthest point on the fringe loop, r_m which is also called the apogee point as well as the angle of inclination of the corresponding radial line with respect to the crack plane, θ_m. However, this method is only applicable in the case of $73^\circ < \theta_m < 139^\circ$ and $r_m/a < 0.03$ and outside this range the error increases rapidly; a is the crack length. This method is based upon the study of one fringe loop.

Bradley and Kobayashi (1970) and Schroedl and Smith (1973) modified Irwin's method by using data from more than one fringe loop using different techniques. All these methods are applicable for determining K_I in the range $73^\circ<\theta_m<139^\circ$ provided $r_m/a <0.03$ and if no measurement error are made in r_m and θ_m, K_I will be predicted with an accuracy of ±5 %.

Smith and Smith (1972) conducted a series of photoelastic experiments on a single edge crack specimen. They used the idea proposed by Irwin to develop equations for maximum in-plane local shearing stress and average fringe loop inclination θ_m near the crack tip to compute mode I and mode II stress intensity factors. The measurements were taken from small fringes and then extrapolated to the crack tip. Their results compared very well with similar cases of Wilson (1969). This method showed a good accuracy in the case of straight crack while for inclined crack the results deviate from the theoretical values by approximately 10 %.

Schroedl *et al*. (1972) studied the factors that might influence the stress field data taken from a stress-freezing photoelastic technique. The authors analyzed the effects of non-linear zone near crack tip and the effects of the far field stress σ_{0x}. The authors found that by using the Westergaard solution the value of $\tau_{\max}$ computed from the singular stresses along $\theta = \pi/2$ differs from the exact solution at $r/a = 0.30$ by less than 2%. They also found that the values of σ_{0x} computed from the experiment were substantially different from the theoretical values by 27%. Furthermore, their computer study revealed that this much of difference is simply due to error in K_I values. Surprisingly, they also found that even if data are taken in the range $r/a = 0.04$ to 0.25, where $\tau_{\max} / \tau_{\max 0}$ values differ by 15 to 20%, the difference between the experimental and theoretical K_I was only 6%. Knowing that $\tau_{\max}$ is the maximum shear stress in plane perpendicular to crack border and $\tau_{\max 0}$ is the maximum remote shear stress in plane perpendicular to crack border.

Theocaris and Gdoutos (1975) established a quantitative relation between the exact solution of the stress field in the vicinity of a crack tip which derived from Westergaard's formulation and the Irwin's singular solution to determine K_I. The results obtained were then correlated with photoelastic data. The maximum shear stress distribution expressed by the isochromatic pattern for the exact and the singular solution were calculated respectively for uniaxial and biaxial tension. From their formulation, the authors showed that by measuring the fringe order along the line $\theta = 90°$ and in the region $0.05 < r / a < 0.1$, K_I can be evaluated with an error 1.04 %for the case of uniaxial and 0.11% for the case of biaxial tension. A center crack specimen was used in this study.

Rouhi *et al*. (1977) determined the crack initiation angle using Sih's strain energy theory in conjunction with isochromatic fringe pattern using photoelastic material. In addition, they used birefringent coatings to perform photoelastic study on aluminum alloys. However, they restricted their theoretical analysis for particular cases when Poisson's ratio of the material is equal to 0.5 and when the plane strain conditions prevail at the crack tip. For these cases the authors found that the crack initiation takes place in a direction perpendicular to that defined by the axis of symmetry of the fringe loops.

Sanford and Dally (1979) used four different methods for determining mixed mode stress intensity factors K_I and K_{II} using photoelastic technique. These methods include: selected line approach (two points), classical approach (two points), deterministic approach (three points) and over deterministic method (multiple-points). Except the selected line

approach, all methods of solution involve an iterative numerical procedure based on Newton-Raphson technique and for the over-deterministic approach, the method of least squares was employed. All four methods provide solutions to 0.1% of the exact solution providing that the input parameters describing the isochromatic field are exact.

Chan and Chow (1979) investigated the notch effect on the photoelastic determination of the mixed mode stress intensity factors. The authors accomplished this by comparing the isochromatic loops generated from a sharp and an elliptical edge crack in an infinite plate. A method of analysis was proposed in this study and used to correct the distorted maximum angle and maximum shear stress due to the notch effect. This study showed that the notch effect at the crack tip has a definite effect in the SIF values K_I and K_{II}. The effect is more pronounced in the case of small crack inclination angle or a large value of K_{II}.

Gdoutos (1980) theoretically proposed a method based on photoelsticity for the determination of the crack initiation angle in a tensile stress field. The method is based on the interrelation of the crack initiation angle and the angle formed by the crack axis and the axis of symmetry of the isochrmatic fringe loops in the vicinity of the crack tip. Unlike Rouhi *et al*. (1977), Gdoutos considered a general case of a material with any value of Poisson's ratio *v*. Gdoutos theoretical analysis showed an agreement with similar experimental results of Rouhi *et al.* (1977).

Nurse and Patterson (1990) investigated the direction of crack extension of blunted edge crack sheets with angled crack under tensile loading using photoelastic model. The authors used the idea that for low values of the ratio of the stress intensity factors (K_{II}/K_I), the axis of symmetry of the isochromatic fringe loops in the neighborhood of the crack tip approximates the direction of the maximum circumferential stress. Thus, a prediction of the direction of the crack extension can be made along this line of symmetry. Experimental tests verified the accuracy of the photoelastic technique. The authors compared their results with theoretical results using maximum tangential stress MTS criterion.

Yin and Chen (1991) measured the mixed mode stress intensity factors and other fracture parameters such as additional non-singular terms in the algorithm, for bending specimens with partial straight cracks and 60° inclined edge crack. The authors performed photoelastic analysis and used the full-field selected line method to measure the mixed mode SIF and other fracture parameters. The authors demonstrated that the larger data analysis region and lower number of equations in the algorithm make it easier to use. In addition, the authors concluded that for accurate evaluation of the SIF the data points should not be too far from the crack tip and the governing equation should not have many non-singular terms.

Ayatollahi and Safari (2003) employed the method of photoelasticity to investigate the effect of *T*-stress on the stress field near the crack tip. In their work, two parameters

formulation was used to study how the *T*-stress influences the isochromatic fringe patterns around the tip of a mode I crack. Their study showed that the isochromatic fringes rotate backward for positive values of *T-stress* and forward for negative values of *T-stress*. Photoelastic tests were conducted on a compact tension specimen with $T > 0$ and a center crack specimen with $T < 0$ and the observed rotations in the fringe patterns were in agreement with the theoretical predictions.

The presented review shows that most of the researches, in which photoelasticity was used, are concerning the measurement of the stress intensity factor. However, Rouhi *et al*. (1977) determined the crack initiation angle using Sih's strain energy theory and in conjunction with isochromatic fringe pattern. Similarly, Nurse and Patterson (1990) used photoelasticity to estimate the crack initiation angle directly for an inclined blunt edge crack.

The applicability of numbers of methods for determining K_I and K_{II} for an inclined edge crack as well as the applicability of using the isochromatic fringe pattern for estimating the crack initiation angle will be studied in the following section.

4.3. Experimental Procedure

There is a wide variety of photoelastic materials and Table 4.2 summaries some of these materials, Dally and Riley (1991). Selecting a proper photoelastic material is based one

more than one factor and the most important factors are the figure of merit Q and the sensitivity index S. The figure of merit Q is defined as the ratio of the elastic modulus E to the fringe value f_σ , Q = E/ f_σ. On the other hand, the sensitivity index S is defined as the ratio of the proportional limit σ_{pl} to the fringe value f_σ, $S = \sigma_{pl}/ f_\sigma$. Superior model materials exhibit high values for both the sensitivity index S and the figure of merit Q.

TABLE 4.2: Summary of the optical and mechanical properties of several photoelastic materials (Dally and Riley, 1991).

Property	**Homolite 100**	**Polycarbonate**	**Epoxy**	**Urethane rubber**
Time-edge effect	Excellent	Excellent	Good	Excellent
Creep	Excellent	Excellent	Good	Excellent
Machinability	Good	Poor	Good	Poor
Modulus of elasticity E:				
psi	560,000	360,000	475,000	450
MPa	3860	2480	3275	3
Poisson's ratio v	0.35	0.38	0.36	0.46
Proportional limit σ_{pl}:				
psi	7000	5000	8000	20
MPa	48.3	34.5	55.2	0.14
Stress fringe value f_σ: (for green light, λ=546.1 *nm*)				
lb/*in*	135	40	64	1
kN/*m*	23.6	7	11.2	0.18
Strain fringe value f_ε: (for green light, λ=546.1 *nm*)				
in	0.00033	0.00015	0.00018	0.00324
mm	0.0084	0.0038	0.0046	0.082
Figure of merit Q:				
1/ *in*	4150	9000	7400	450
1/*mm*	163	354	292	17
Sensitivity index S:				
1/*in*	52	125	125	20
1/*mm*	2.05	4.92	4.92	0.78

It is clear from Table 4.2 that Polycarbonate and the epoxies exhibit superior Q and S. However, Polycarbonate material is difficult to machine and epoxy resin materials require special precautions to minimize time-edge effects. The time-edge effect can be defined as the observation of induced stresses on the model boundary when examined under no load and for a period of time after machining the model.

The selected material for the present experimental program is Polycarbonate which has an elastic modulus E = 2500 MPa, a Poisson's ratio v = 0.38 and a fringe value f_σ = 7 kPa/(fringe/m). It should be noted that the value of elastic modulus for Polycarbonate is selected as per Ayatollahi and Safari (2003) which is near to the value listed in Table 4.2. Edge crack panels of width w = 60 mm and height L = 220 mm are machined from a large sheet of Polycarbonate. An edge crack specimen is prepared from a Polycarbonate sheet of thickness h = 3 mm using a flycutter of thickness 0.5 mm. To reduce overheating of specimen material, Bromrus coolant with a ratio of 1:20 oil to water was used during the crack cutting process. The crack tip was sharpened manually using a razor blade. All specimens have a nominal crack lengths a = 10 mm but different angles of inclination. The inclination angles considered in this study are, 0°, 10°, 20°, 30° and 40°. The geometry and dimensions of the specimens are shown in Fig. 4.3.

Vishay model 061 basic circular polariscope with diffuse light source-17" is used in this experiment and a tensile load is applied using dead weight. The circular polariscope is shown in Fig. 4.4. A high resolution D 50 NIKON digital camera was used to capture

photos of the loaded specimen during the test and it should be noted that a macro lens was used in order to enhance the image quality. Each specimen was loaded uniaxially by a dead weight of 1.37 kN. Because the specimen has a thickness $h = 3\ mm$ and a width $w = 60\ mm$, the specimen cross sectional area is $1.8*10^{-4}\ m$ resulting in a uniform tensile stress of 7.63 MPa. The load was chosen such that enough isochromatic fringes are produced in order to enable a full field photoelastic analysis. By loading each specimen, the photoelastic stress field is captured for SIF estimation. To measure the crack initiation angle, the load is increased until the crack starts to propagate. At the same time series of photos were taken while increasing the load in order to capture the onset of the crack propagation. Hence, the crack initiation angle is measured directly.

Schroedl and Smith method (1973) will be used in analyzing straight edge crack while Sanford and Dally (1979) method will be used in analyzing inclined edge crack. Moreover, the applicability of Smith and Smith (1972) method will be investigated.

4.3.1. Method for Calculation of Pure Mode I Stress Intensity Factor

For straight crack panel, Schroedl and Smith (1973) method is going to be used to estimate the pure opening mode I stress intensity factor. The component of stress in the local neighborhood ($r << a$) of the crack tip are:

$$\sigma_x = \frac{K_I}{\sqrt{2\pi r}}\cos\frac{\theta}{2}\left(1-\sin\frac{\theta}{2}\sin\frac{3\theta}{2}\right)-\sigma_{0x}$$

$$\sigma_y = \frac{K_I}{\sqrt{2\pi r}}\cos\frac{\theta}{2}\left(1+\sin\frac{\theta}{2}\sin\frac{3\theta}{2}\right) \tag{4.3}$$

$$\tau_{xy} = \frac{K_I}{\sqrt{2\pi r}}\sin\frac{\theta}{2}\cos\frac{\theta}{2}\cos\frac{3\theta}{2}$$

where σ_{0x} is the far field stress.

The maximum shear stress, $\tau_{\max}$ is expressed in terms of the stress components as:

$$(2\tau_{\max})^2 = (\sigma_y - \sigma_x)^2 + (2\tau_{xy})^2 \tag{4.4}$$

From Eqs. 4.3 and 4.4, it is apparent that

$$(2\tau_{\max})^2 = \frac{K_I^2}{2\pi r}\sin^2\theta + \frac{2\sigma_{0x}K_I}{\sqrt{2\pi r}}\sin\theta\sin\frac{3\theta}{2} + \sigma_{0x}^2 \tag{4.5}$$

By restricting the data to a line defined by θ = 90º, Eq. (4.5) reduces to

$$\left(2\tau_{\max}\right)^2 = \frac{K_I^2}{2\pi r} + \frac{\sqrt{2}K_I\sigma_{0x}}{\sqrt{2\pi r}} + \sigma_{0x}^2 \tag{4.6}$$

Solving Eq. (4.6) and retaining only the positive root from the quadratic formula gives

$$K_I = \sqrt{\pi r}\left(\left(8\tau_{\max}^2 - \sigma_{0x}^2\right)^{1/2} - \sigma_{0x}\right) \tag{4.7}$$

Eq. (4.7) can be simplified by neglecting σ_{0x}^2 relative to $8\tau_{\max}^2$ to obtain

$$K_I = \sqrt{\pi r}\left(\sqrt{2}\left(2\tau_{\max}\right) - \sigma_{0x}\right) \tag{4.8}$$

By adopting the Bradley-Kobayashi differencing technique, Smith uncouple the K_I and σ_{0x} relation. Using $\tau_{\max}$ from the i^{th} and j^{th} fringe loops gives

$$K_I = \sqrt{2\pi r_i}\,\frac{(2\tau_{\max})_i + (2\tau_{\max})_j}{1-\left(\frac{r_i}{r_j}\right)^{1/2}} \tag{4.9}$$

where $\tau_{\max}$ is calculated from the optical stress relation:

$$\tau_{\max} = \frac{Nf_\sigma}{2h} \tag{4.10}$$

N is the fringe order, f_σ is the material fringe constant and h is the specimen thickness and Fig. 4.5 shows the Schroedl and Smith method parameters.

4.3.2. Methods for Calculation of Mixed Mode (I & II) Stress Intensity Factors

Smith and Smith Method

For an inclined crack panel loaded in tension, the stress filed around the crack tip is given by Eq. (2.7). Combining Eqs. 2.7 and 4.4 gives the maximum in plane shear stress as:

$$\tau_{\max} = \frac{1}{2(2\pi r)^{1/2}}\left[(K_I \sin\theta + 2K_{II}\cos\theta)^2 + (K_{II}\sin\theta)^2\right]^{1/2} \tag{4.11}$$

Differentiating $\tau_{\max}$ in Eq.(4.11) with respect to θ and equating the derivative to zero and setting $\theta = \theta_m$ gives:

$$\left(\frac{K_{II}}{K_I}\right)^2 - \frac{4}{3}\left(\frac{K_{II}}{K_I}\right)\cot 2\theta_m - \frac{1}{3} = 0 \tag{4.12}$$

It is seen that θ_m is controlled by the ratio K_{II}/K_I alone. Therefore, if θ_m is measured from a photoelastic experiment, the ratio K_{II}/K_I is determined by Eq. (4.12). Using this, together with Eq. (4.11) a set of values of K_I and K_{II} can be determined for each fringe.

Although Eq. (4.11) is valid for any point (r, θ) on the fringe but because Smith and Smith (1972) did not include the effect of the far field stress σ_{0x} the values for K_I and K_{II} will be determined on a fringe at some finite distance from the crack tip and then extrapolated to $r = 0$. This eliminates the effect of the non singular stresses on the calculation of K_I and K_{II}. But it is more convenient to employ (r_m, θ_m), shown in Fig. 4.6, in Eq. (4.11) since measurement of r_m will be more accurate than for points of smaller r values; r_m is the distance from the crack tip to the furthest point on the fringe loop.

Sanford and Dally Least-Squares Approach

The method of least squares involves the determination of the mixed mode SIF (K_I and K_{II}) and the far field stress (σ_{0x}). Sanford and Dally included the far field stress term (σ_{0x}) in the stress field equation around the crack tip in Eq. (2.7) which gives

$$\begin{aligned}
\sigma_x &= \frac{K_I}{\sqrt{2\pi r}}\cos\frac{\theta}{2}\left[1-\sin\frac{\theta}{2}\sin\frac{3\theta}{2}\right]-\frac{K_{II}}{\sqrt{2\pi r}}\sin\frac{\theta}{2}\left[2+\cos\frac{\theta}{2}\cos\frac{3\theta}{2}\right]-\sigma_{0x}\\
\sigma_y &= \frac{K_I}{\sqrt{2\pi r}}\cos\frac{\theta}{2}\left[1+\sin\frac{\theta}{2}\sin\frac{3\theta}{2}\right]+\frac{K_{II}}{\sqrt{2\pi r}}\sin\frac{\theta}{2}\cos\frac{\theta}{2}\cos\frac{3\theta}{2}\\
\tau_{xy} &= \frac{K_I}{\sqrt{2\pi r}}\sin\frac{\theta}{2}\cos\frac{\theta}{2}\cos\frac{3\theta}{2}+\frac{K_{II}}{\sqrt{2\pi r}}\cos\frac{\theta}{2}\left[1-\sin\frac{\theta}{2}\sin\frac{3\theta}{2}\right]
\end{aligned} \tag{4.13}$$

Substituting Eqs. 4.13 and 4.10 into Eq. (4.4) gives the relation which defined the isochromatic fringe pattern in the local field near the crack tip as:

$$\left(\frac{Nf_\sigma}{h}\right)^2 = \frac{1}{2\pi r}\left[(K_I \sin\theta + 2K_{II}\cos\theta)^2 + (K_{II}\sin\theta)^2\right]$$

$$+\frac{2\sigma_{0x}}{\sqrt{2\pi r}}\sin\frac{\theta}{2}\left[K_I \sin\theta(1+2\cos\theta) + K_{II}(1+2\cos^2\theta+\cos\theta)\right]+\sigma_{0x}^2 \tag{4.14}$$

Eq. (4.14) is fitted to a large number of points over the isochromatic field. The fitting process involves both the Newton-Raphson method and minimization process associated with the least squares method. Considering the function f_k and $k = 1, 2 \ldots m$ where $m > 3$.

$$f_k(K_I, K_{II}, \sigma_{0x}) = \frac{1}{2\pi r_k}\left[(K_I \sin\theta_k + 2K_{II}\cos\theta_k)^2 + (K_{II}\sin\theta_k)^2\right]$$

$$+\frac{2\sigma_{0x}}{\sqrt{2\pi r_r}}\sin\frac{\theta_k}{2}\left[K_I \sin\theta_k(1+2\cos\theta_k) + K_{II}(1+2\cos^2\theta_k+\cos\theta_k)\right] \tag{4.15}$$

$$+\sigma_{0x}^2 - \left(\frac{Nf_\sigma}{h}\right)^2 = 0$$

The Taylor series expansion of f_k can be written as:

$$(f_k)_{i+1} = (f_k)_i + \left(\frac{\partial f_k}{\partial K_I}\right)_i \Delta K_I + \left(\frac{\partial f_k}{\partial K_{II}}\right)_i \Delta K_{II} + \left(\frac{\partial f_k}{\partial \sigma_{0x}}\right)_i \Delta\sigma_{0x} \tag{4.16}$$

Where the subscript i refers to the i^{th} iteration step and ΔK_I, ΔK_{II} and $\Delta\sigma_{0x}$ are corrections to the pervious estimates. The corrections are determined so that $(h_k)_{i+1} = 0$. Thus, Eq. (4.16) gives:

$$\left(\frac{\partial f_k}{\partial K_I}\right)_i \Delta K_I + \left(\frac{\partial f_k}{\partial K_{II}}\right)_i \Delta K_{II} + \left(\frac{\partial f_k}{\partial \sigma_{0x}}\right)_i \Delta\sigma_{0x} = -(f_k)_i \tag{4.17}$$

The iteration condition given in Eq. (4.17) is invoked to give an over-determined set of equations in terms of corrections ΔK_I, ΔK_{II} and $\Delta\sigma_{0x}$ of the form:

$$[\,f\,] = [c]\,[\,\Delta K\,] \tag{4.18}$$

where the matrices are defined as

$$[f] = \begin{bmatrix} f_1 \\ - \\ - \\ - \\ - \\ f_m \end{bmatrix}_i ; \qquad [c] = -\begin{bmatrix} \frac{\partial f_1}{\partial K_I} & \frac{\partial f_1}{\partial K_{II}} & \frac{\partial f_1}{\partial \sigma_{0x}} \\ - & - & - \\ - & - & - \\ - & - & - \\ - & - & - \\ \frac{\partial f_m}{\partial K_I} & \frac{\partial f_m}{\partial K_{II}} & \frac{\partial f_m}{\partial \sigma_{0x}} \end{bmatrix}_i ; \qquad [\Delta K] = \begin{bmatrix} \Delta K_I \\ \Delta K_{II} \\ \Delta\sigma_{0x} \end{bmatrix}_i \tag{4.19}$$

The least squares minimization process is accomplished by multiplying from the left both sides of Eq. (4.19) by the transpose of matrix [c], to give

$$[c]^T\,[\,f\,] = [c]^T\,[c]\,[\,\Delta K\,] \tag{4.20}$$

or

$$[\,d\,] = [z]\,[\,\Delta K\,]$$

where

$$[\,d\,] = [z]^T\,[\,f\,]$$

$$[z] = [c]^T\,[c]$$

Finally the correction terms are given by

$$[\ \Delta K\ ] = [z]^{-1}\ [\ d\ ] \tag{4.21}$$

The solution of Eq.(4.21) gives ΔK_I, ΔK_{II} and $\Delta\sigma_{0x}$ which are used to correct initial estimates of K_I, K_{II} and σ_{0x} and obtain a better fit of the function f to m data points. The data extraction technique for Sanford and Dally method is shown in Fig. 4.7.

4.4. Results and Discussion

As mentioned previously, the crack was machined using a flycutter having a thickness of 0.5 *mm*. As a result, the crack tip was sharpened manually by means of a razor blade. This introduced a slight difference in the crack length from one specimen to another. Consequently, two specimens were prepared for each angle in order to ensure the accuracy of the experiment. However, the differences in the cracks lengths did not exceed 2.6% of the original crack length which is 10 *mm* and the actual crack length was measured using the captured photo of each specimen.

A MATLAB code (Appendix II) was developed to estimate the mixed mode SIF using Sanford and Dally (1979) method. On the other hand, Smith and Smith method was used and found not efficient due to the limitation in getting fringes close enough to the crack tip. In this method the SIF values are plotted against r_m/a ratios and then extrapolated to $r_m = 0$ where r_m is the radial distance from the crack tip to the furthest distance on closest fringe loop and a is the crack length. In order to estimate the SIF with a reasonable accuracy, the ratio r_m/a has to be very small. Smith and Smith (1972) estimated the mixed

mode stress intensities by analyzing fringes which yield a ratio r_m/a as small as 0.0068. In addition, by plotting Eq. (4.12) for different mixity ratios (K_{II}/K_I) with respect to values -180 º $\leq \theta_m \leq$ 180º one can realize that this equation has five singular points. These points correspond to the value of $\sin 2\theta_m$ as it approaches -180º, -90º, 0º, 90º or 180º. To illustrate this problem, the case of an edge crack with crack inclination angle β = 20º which yields mixity ratio K_{II}/K_I of 0.2 is considered. By analyzing the isochromatic fringe field for such a case, Fig. 4.8, it was found that the data that are supposed to be analyzed fall in the ranges 35º < θ_m< 55º and -103º < θ_m< -84º for top and bottom fringes, respectively. Plot of Eq. (4.12) for K_{II}/K_I = 0.2, as illustrated in Fig. 4.9, shows that this equation suffers an aggressive instability as θ_m approaches -90º. Unlike the bottom fringes, the top fringes were found to lie on the region where Eq. (4.12) is approximately satisfied.

4.4.1. Stress Intensity Factors Estimation

Table 4.3 lists the values of SIF determined from photoelastic technique and compared with finite element results. The value of K_I was predicted using the top and bottom fringes with top fringes yielding a better estimation for the first specimen. However, both top and bottom fringes yield a good estimate of K_I for the second specimen. This can be attributed to the asymmetry of the top and bottom fringes due to manual crack sharpening, Fig. 4.10 illustrate the fringe patterns for β = 0º for the first specimen. Good agreement was achieved when the experimental values of K_I were compared with those given by Eqs. 3.2, and 3.4. The average percentage of error was less than 1%. For all

specimens with an inclined crack, shown in Figs. 4.11 to 4.14, Sanford and Dally (1979) least squares method was used for estimating the mixed mode SIF K_I and K_{II}. The area around the crack tip was divided into increments of $\Delta\theta = 10^{\circ}$ and an average of 100 data points were selected for all specimens within an interval of $0.05 < r/a < 0.3$ *mm*. This interval helps in minimizing the error due to the effect of gradients in σ_{0x} as well as the measuring error in determining the radius *r*. Each data point consists of a measurement of the radial distance from the crack tip to the isochromatic fringe, a measurement of the corresponding angle and the fringe's order *N* as shown in Fig. 4.7.

TABLE 4.3: Comparison between experimental and numerical SIF.

Specimen #	Angle (β^{o})	Crack Length (mm)	Experimental				ANSYS			% Error
			#Iter	KI (kPa√m)	KII (kPa√m)	KII/KI	KI (kPa√m)	KII (kPa√m)	KII/KI	KII/KI
1	0	10.167	---	1799.8	0.00	0.00	1778.1	0.0696	0.00	**0**
2				1788.3	0.00	0.00	1778.1	0.0696	0.00	**0**
1	10	10.11	10	1506.8	146.84	0.097	1726.4	181.9	0.105	**7.51**
2		10.05	20	1448.1	170.97	0.118	1718.7	181.2	0.105	**11.99**
1	20	10.149	10	1687.7	359.40	0.213	1603.9	341.6	0.213	**0.01**
2		10.07	10	1600.3	394.19	0.246	1595.2	339.6	0.213	**15.70**
1	30	10.15	10	1230.9	434.48	0.353	1421.5	462.16	0.325	**8.57**
2		10.133	10	1361	453.23	0.333	1409	458.36	0.325	**2.37**
1	40	10.13	15	1212.7	575.57	0.475	1171.3	522.41	0.446	**6.42**
2		10.15	10	1096.9	511.33	0.466	1171.5	522.48	0.446	**4.52**

All of the fringes are analyzed i.e. N = 1, 2 …etc and N = 1.5, 2.5 …etc, as shown in Fig. 4.15 and points were taken such that half of the data are taken from the top fringes and the other half from the bottom fringes with respect to the crack axis. By doing so, it has been found that the values of K_I and K_{II} converged rapidly to a stable value within 10 to 20 iterations as listed in column 4 of Table 4.3. Similar convergence speed was reported by Sanford and Dally (1979). In addition, the method is supposed to be independent of the initial guess of K_I, K_{II} and σ_{0x} and this was also noticed while performing the analysis on the tested specimens. The experimentally determined average values of SIF were found to be within 10% of the numerical results. However, for the case of β =10º the experimental results were found to be within averages of 14% and 12% for K_I and K_{II}, respectively. In fact, the sensitivity of Sanford and Dally method in estimating the mixed mode SIF seems to be low in the case of low crack angle of inclination and the method needs to be tested carefully for such a case. To support this argument, the method was used to analyze the straight crack and it was found to give K_I =1439 kPa√m and K_{II} = 6273 kPa√m. It can be seen that the method estimates K_I within 19% of the numerical results, however, for the case of K_{II} the method severely diverge from the correct solution. It should be noted that no blunting was observed while performing the experiment.

4.4.2. Prediction of the Crack Initiation Angle

Similar to numerical analysis, the experimentally computed stress intensity factors K_I and K_{II} were incorporated into the six crack initiation criteria to predict the crack propagation

angle. The prediction of the crack initiation angle using the photoelastic fringe axis of symmetry method FASM by Gdoutos (1980) and Nurse and Patterson (1990), is also employed and the results are reported. Procedure for estimating the crack initiation angle using the FSAM is shown in Fig 4.16. Table 4.4 lists the average results of two tested specimens for each angle of inclination.

TABLE 4.4: Crack initiation angle as predicted experimentally.

(β^o)	Experimental									
	Crack Initiation Angle ($-\theta_0^o$)						FSAM		Observed	
	M	S	MTS	T	M.MTS	R	($-\theta_0^o$)	Standard Deviation	($-\theta_0^o$)	Standard Deviation
0	0	0	0	0	0	0	3.13	0.88	0.00	0.00
10	12.03	11.82	12.03	12.03	11.97	11.90	7.75	2.47	9.00	0.00
20	23.78	22.47	23.69	23.78	23.36	22.94	22.50	0.71	18.75	0.35
30	32.40	29.66	31.98	32.40	31.33	30.59	30.00	4.95	30.75	1.77
40	40.07	35.77	38.90	40.07	38.04	37.13	39.00	1.41	36.50	0.71

Again all of the criteria predict approximately the same crack initiation angle for the cases of small crack inclination angles (β = 0º and β = 10º). Similar to what was noticed in section 3.2.3 and as listed in Table 4.4, the M and T criteria were found to yield the same initiation angle for all crack angles. To support their criterion, Kong *et al*. (1995) performed experiments on FeE550 steel center crack specimens at law temperature (-140ºC) in order to ensure that K controls the fracture. The authors conclude that the

theoretical results of the M criterion compared very well with the experiment results of Theocaris *et at*. (1982) and the T criterion. Kong *et al*. experimental results were also in a good agreement with T criterion and the experimental results of Theocaris *et al*., especially for small inclination angles.

Furthermore, the M and T criteria were found to predict the maximum initiation angle while the S criterion predicted the minimum angle compared with other criteria as shown in Figs. 4.17 and 4.18. These figures compare the average results of two tested specimens for each inclination angle. The same behavior of the S criterion is observed in the literature. Ewing *et al*. (1976) conducted experiments on PMMA edge crack specimens. The authors measured the crack initiation angles and the measured angles were in a good agreement with the MTS and the S criterion with later criterion yielding the minimum initiation angle. Similar behavior is observed by Theocaris *et al*. (1982) except that their experimental results showed an agreement with MTS and S criteria for inclination angles less than 50º. However, their experimental measurements of the crack initiation angles showed a good agreement with T criterion for higher inclination angles. Theocaris *et al*. (1982) conducted their experiments on Polycarbonate center crack specimens in order to support their criterion.

Similar to the numerical analysis in section 3.2.3 and as listed in Table 4.4, the difference in the experimental crack initiation prediction was found to increase as the inclination angle increases reaching more than 4º when $\beta = 40°$. This is the difference between the

highest and lowest predicted values of the crack initiation angles estimated experimentally by the crack initiation criteria.

In general, it can be seen from Figs. 4.17 and 4.18 that the S and R criteria give the closest estimation of the initiation angle compared with the observed θ_0. The highest differences between the observed and the experimental crack initiation angle were found to be 31% and 19.9% for β = 10º and β = 20º, respectively. These differences can be attributed to the percentage of error in K_{II}/K_I as listed in Table 4.3. This error in the mixity ratio K_{II}/K_I can be refereed to the manual sharpening of the crack tip. Moreover, while increasing the load for specimens with β = 10º and β = 20º the cracks showed a small extension before they propagate in a brittle manner. This increased the difficultly in measuring the crack initiation angles. Sih (1974) compared the S and MTS criteria with the experimental results of Erdogan and Sih (1963) who conducted experiments on Plexiglass centre crack specimens to support his criterion. The results obtained from the S and MTS criteria were found to be in agreement with experimental observations.

It should be mentioned that no yielding occurred at the crack tip during the entire experimental program. The yield strength of Polycarbonate is 62.1 MPa (Callister ,2000) and the applied stress is 7.63 MPa, hence, $(\sigma/\sigma_y)^2 = 0.051$. The size of the core region is reported to be proportional to $(\sigma/\sigma_y)^2$, Shafique and Marwan (2004).

Comparison between the observed crack initiation angles of this study and Ewing *et al*. (1976) experimental results is shown in Fig. 4.19. It can be seen from this figure that both results are comparable.

On the other hand, Fig. 4.20 shows the comparison between the observed crack initiation angles of this study and the experimental results of Erdogan and Sih (1963), Theocaris *et al*. (1982), Nurse and Patterson (1990), Kong *et al*. (1995) and Hernandez *et al*.(2004). This figure shows the relation between the crack initiation angles and the mixity ratios K_{II}/K_I. Except Nurse and Patterson (1990), all other experiments were preformed using center crack specimens. Although Nurse and Patterson (1990) had performed their experiments on an edge blunted crack specimens, however, they plotted the crack initiation angles with respect to K_{II}/K_I without mentioning the crack inclination angles they analyzed. Consequently, crack initiation angles of these experimental data are plotted with respect to K_{II}/K_I in order to be able to compare the results obtained using a center crack specimen with those obtained using an edge crack one. It should be remembered that the mixity ratio K_{II}/K_I of an edge crack specimen is different than that of a center crack one for a given crack inclination. From Figs. 4.19 and 4.20 it can be realized that the observed crack initiation angles from the present study are well compared with other experimental results in the literature. It should also be noted that Hernandez *et al*. (2004) preformed their experiments using various strain rates. The effect of the strain rate on the value of the crack initiation angle can be observed from Fig. 4.20 and it obvious that it is inversely proportional with the crack initiation angle for a given

K_{II}/K_I ratio. The data of Hernandez *et al*. (2004) were obtained at a load speed of 3000 *mm/min*. The observed crack initiation angles for all specimens are shown in Figs. 4.21 to 4.30.

The numerical results show a good agreement with observed crack initiation angle, especially for higher inclination angles i.e., $\beta = 30°$ and $\beta = 40°$ as shown in Figs. 4.31 and 4.32. In general, it can be seen form these two figures that the numerical results do not favor any criterion.

On the other hand, the fringe symmetry axis method (FSAM) shows a good agreement with experimental, numerical and observed crack initiation angles as shown in Figs. 4.33 to 4.36. However, FSAM overestimates the value of the crack initiation angle for $\beta = 0°$. This method depends on the isochromatic fringe orientation. Consequently, a slight tilt of the isochromatic fringes orientation because of any reason like crack tip sharpening process can cause an obvious error on the measurement the crack initiation angle. Since all specimens were sharpened manually, one can expect this method to show scatter in the measurement of the crack initiation angles.

4.5. Conclusion

The pure mode and mixed mode SIF were estimated experimentally using Schroedl and Smith and Sanford and Dally method, respectively. For pure opening mode, the values of

the SIF were found by extracting photoelastic data from the top and bottom fringes and results were very much comparable with both analytical and numerical results. The mixed modes SIF were estimated using Sanford and Dally method. The results were found to be in excellent agreement with those obtained by FEA. It was shown that Smith and Smith method was not very practical in determining the SIF because of the difficulty associated with the limited area in which it is valid.

The crack initiation angles were predicted by incorporating the values of the experimentally estimated SIF into the crack initiation criteria. Furthermore, the experimental setup was used to load the specimen until crack initiation. The later was measured and used to validate the different methods. The S and R criteria were found to yield the closest angles compared with the observed initiation angles. In addition, numerical analysis and fringe symmetry axis (FSAM) method were employed in estimating the crack initiation angles. Both methods were in a good agreement with the experimental predictions. The FSAM was found to be a good simple method but in general all other methods are acceptable. In addition, the experimental results were found to be comparable with the available results in the literature. There is more than one factor that can influence the accuracy of the results. These include: the method for estimating the SIF, the manufacturing of the specimen especially the crack tip formation and the measurement of the crack initiation angles.

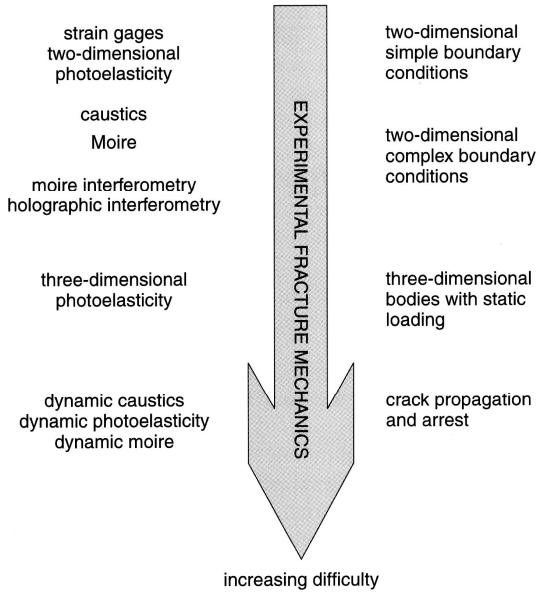

Figure 4.1: The spectrum of experimental methods applied to fracture problems.

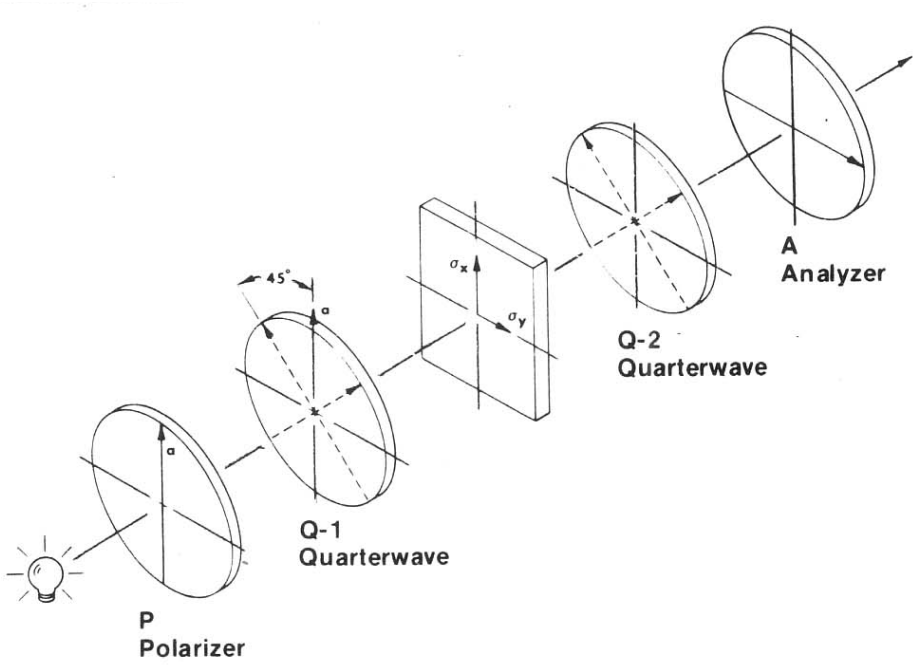

Figure 4.2: Typical circular polariscope.

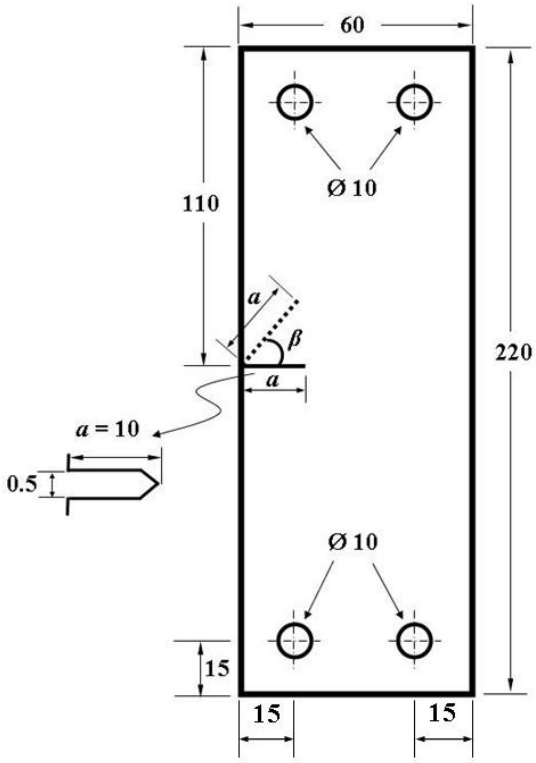

Figure 4.3: Specimen geometry and dimensions in *mm*.
(Dashed line shows inclined crack configuration).

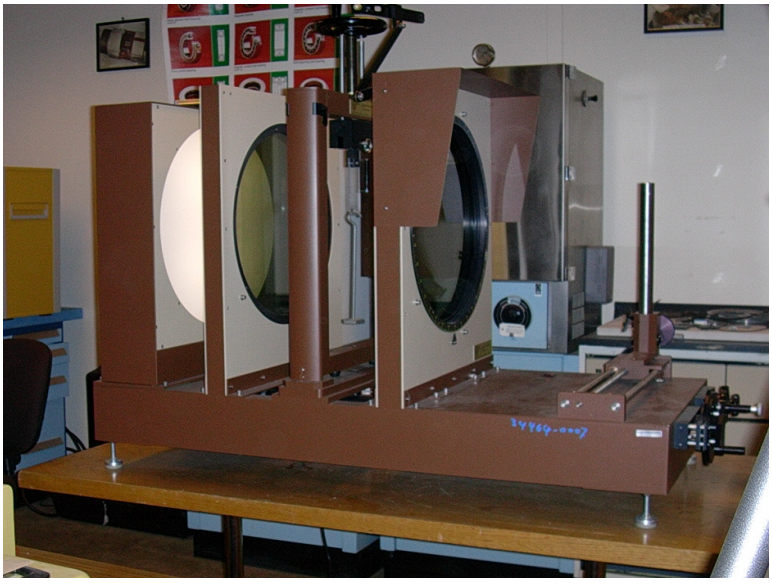

Figure 4.4: Model 061 basic polariscope with diffuse light source -17 *in*.

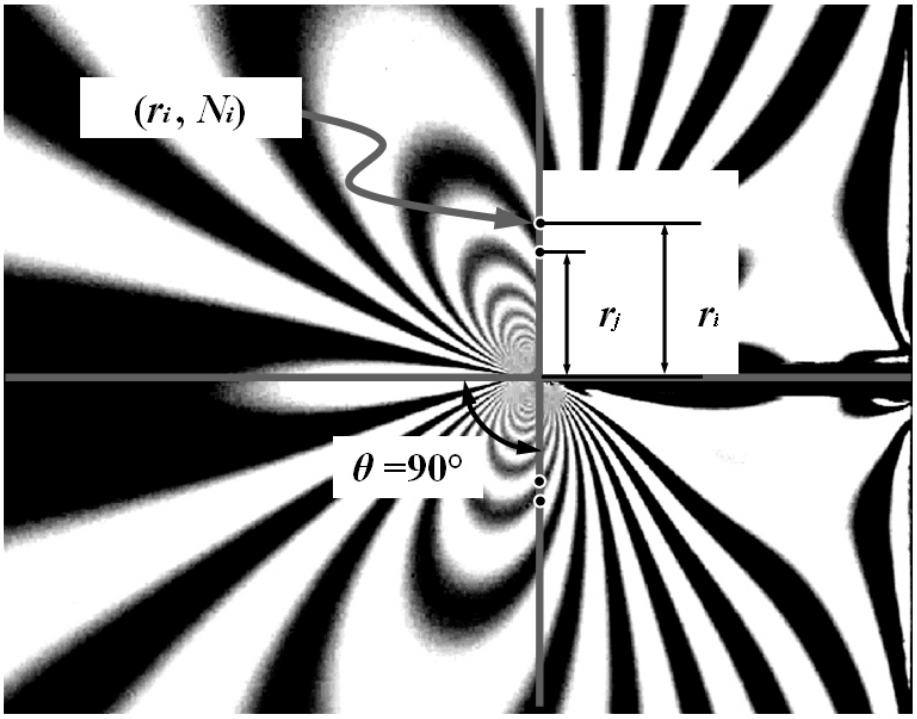

Figure 4.5: Schroedl and Smith method parameters.

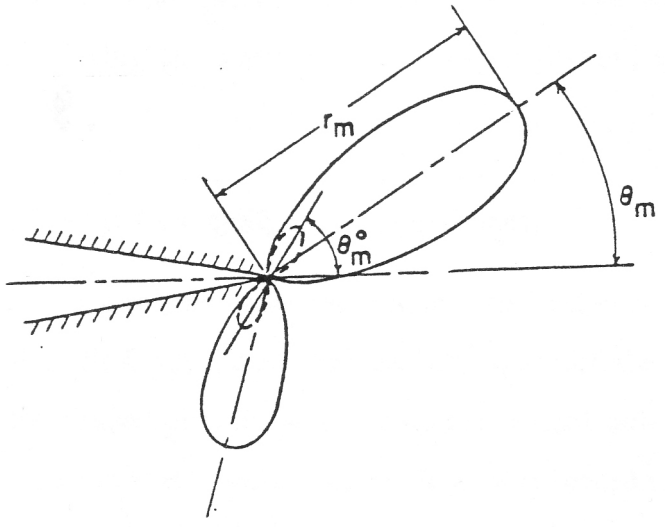

Figure 4.6: Near-tip fringe loops for the general mixed mode fracture.

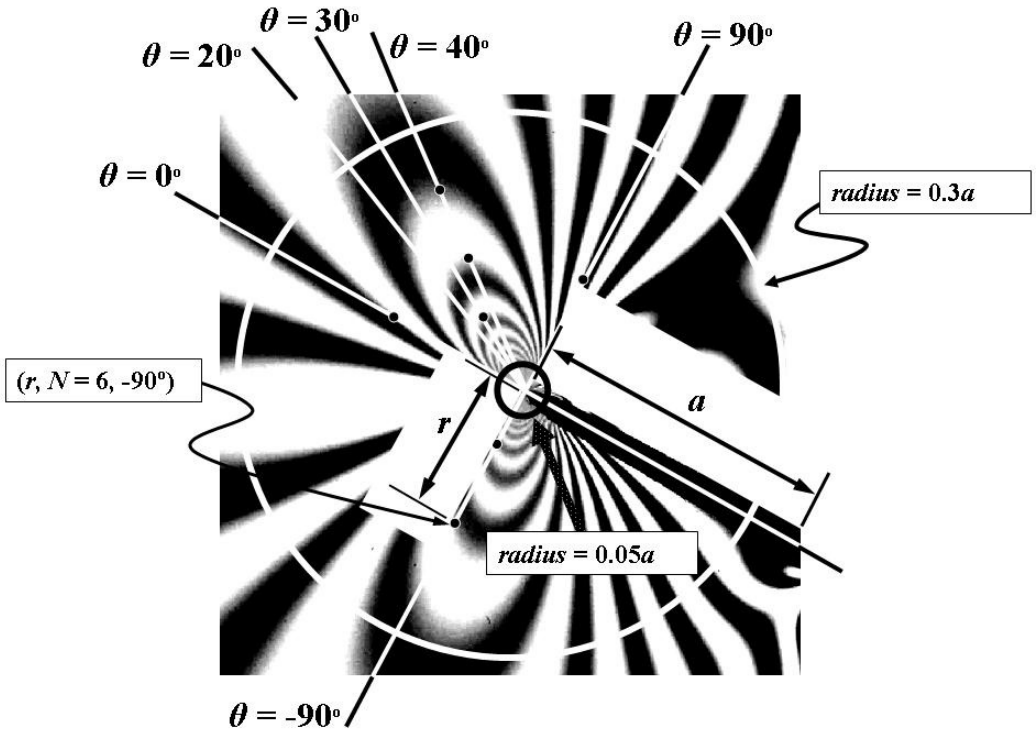

Figure 4.7: Data extraction technique for Sanford and Dally method.

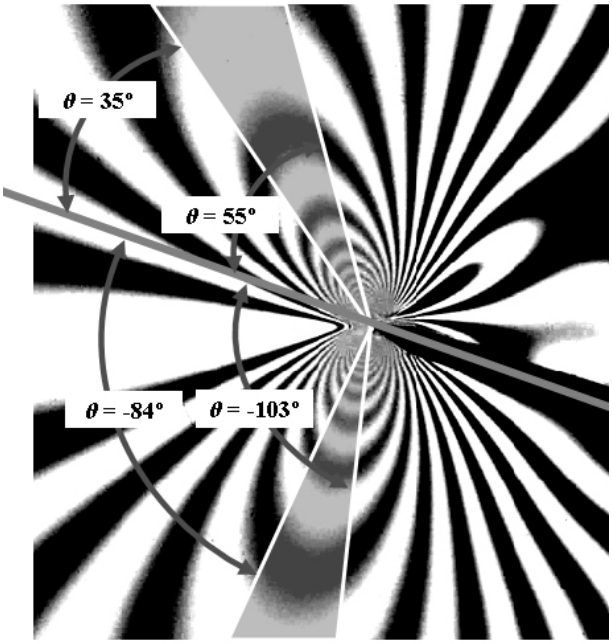

Figure 4.8: Regions in which the data are supposed to be analyzed by Smith and Smith method (Fringe pattern for $\beta = 20°$).

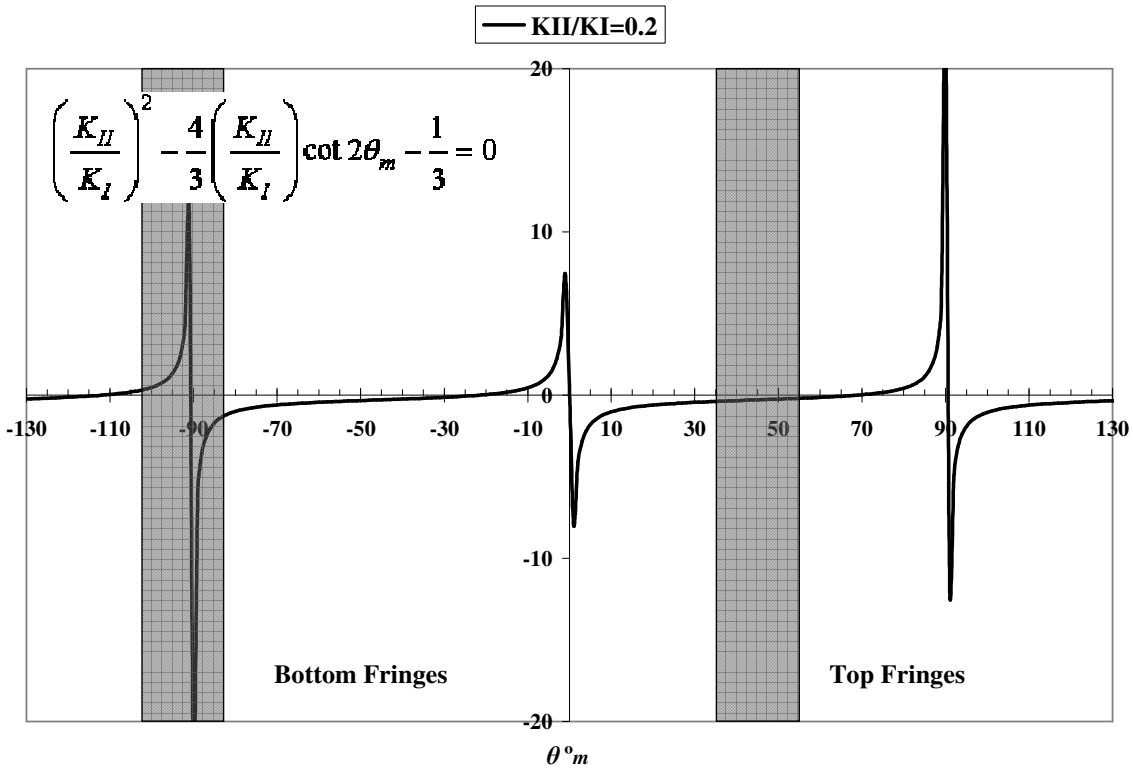

Figure 4.9: Regions in which the data are supposed to be analyzed by Smith and Smith method (β = 20º).

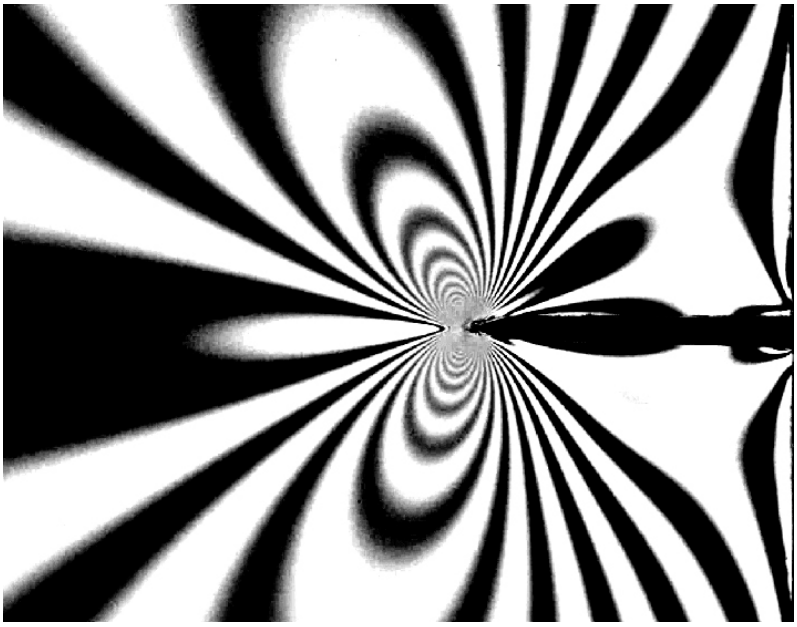

Figure 4.10: Isochromatic fringe pattern for straight crack $\beta = 0^{o}$, *Mag* ×8 (Specimen#1).

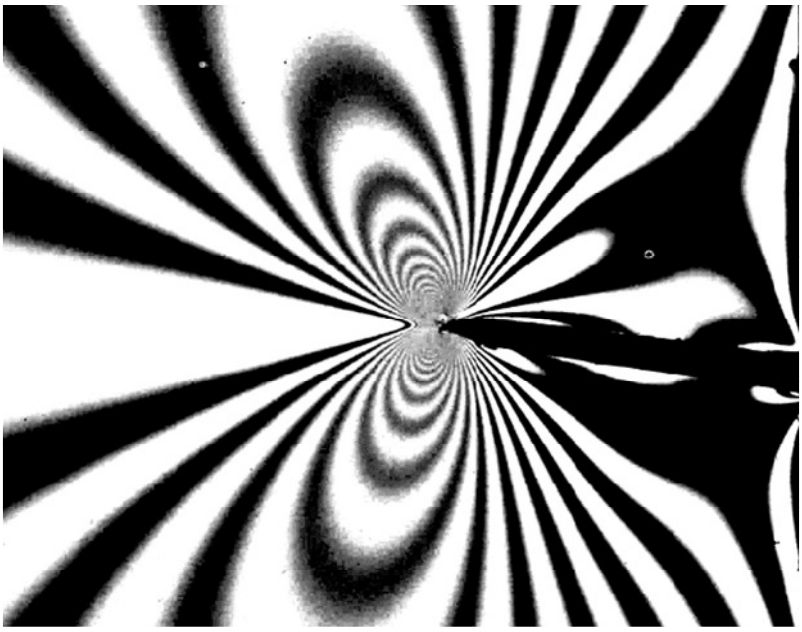

Figure 4.11: Isochromatic fringe pattern for $\beta = 10^{o}$, *Mag* ×8 (Specimen#1).

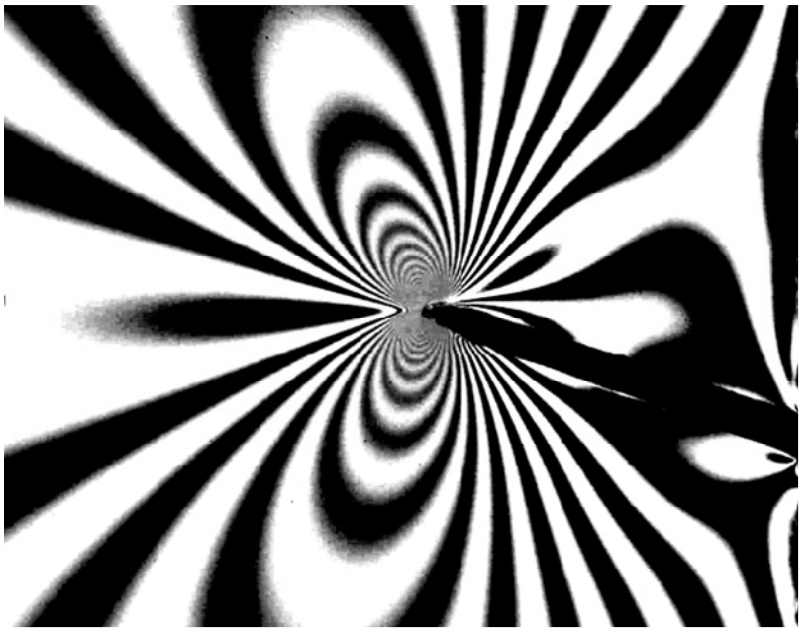

Figure 4.12: Isochromatic fringe pattern for $\beta = 20^{o}$, *Mag* ×8 (Specimen#1).

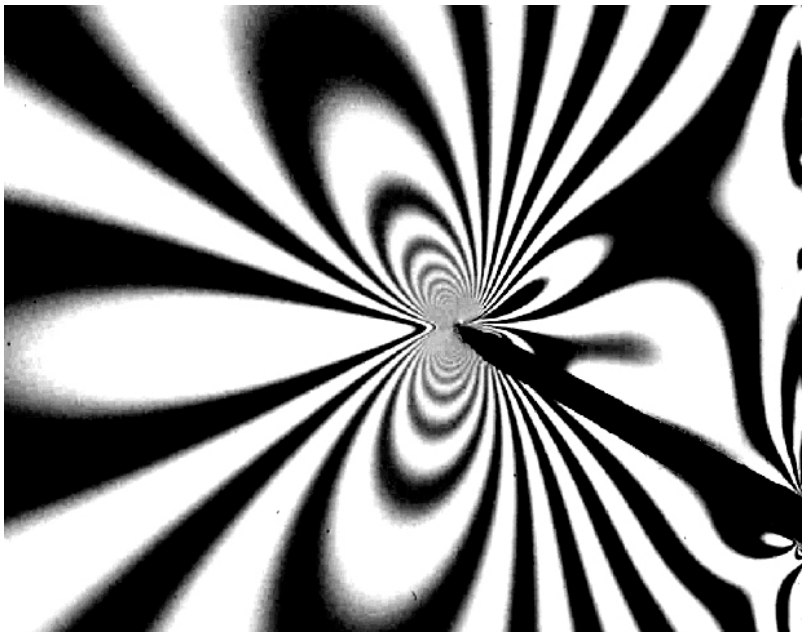

Figure 4.13: Isochromatic fringe pattern for $\beta = 30^{o}$, *Mag* ×8 (Specimen#1).

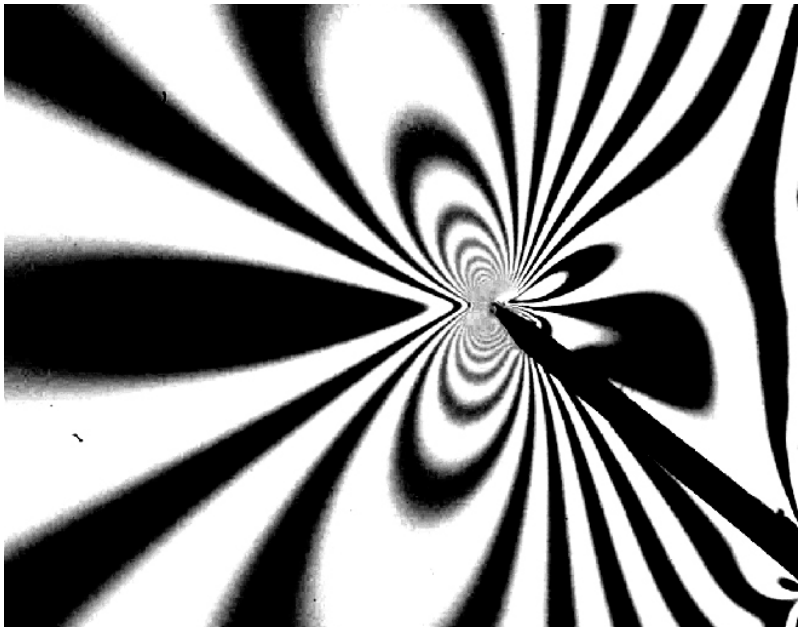

Figure 4.14: Isochromatic fringe pattern for $\beta = 40^{o}$, *Mag* ×8 (Specimen#1).

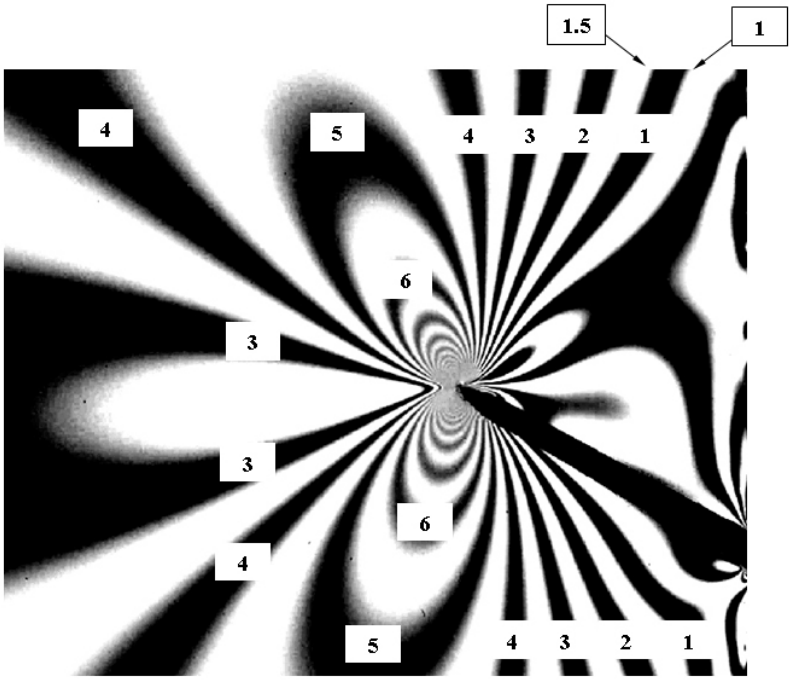

Figure 4.15: Example of fringes order determination.

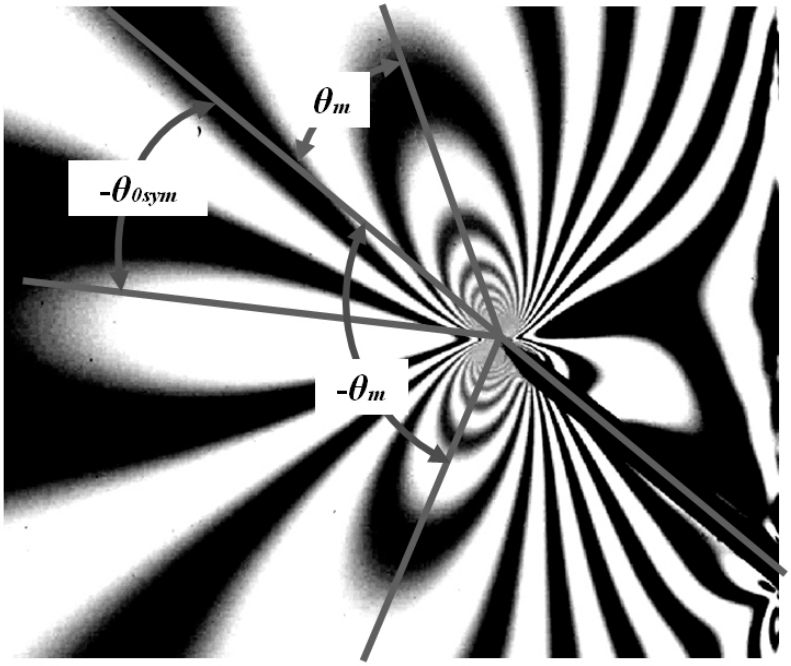

Figure 4.16: Determination of the crack initiation angle using fringe symmetry axis method (FSAM).

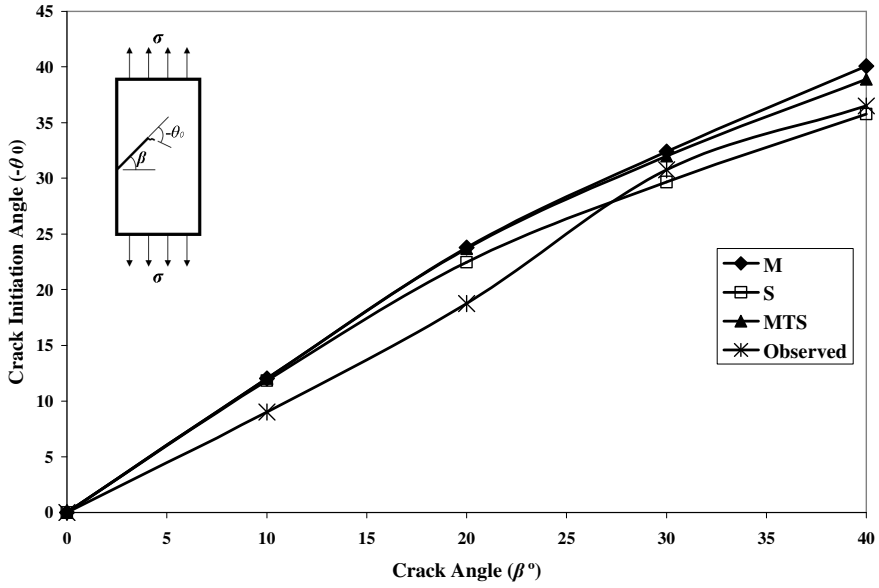

Figure 4.17: Comparison between observed and experimental crack initiation angles using M, S and MTS criteria.

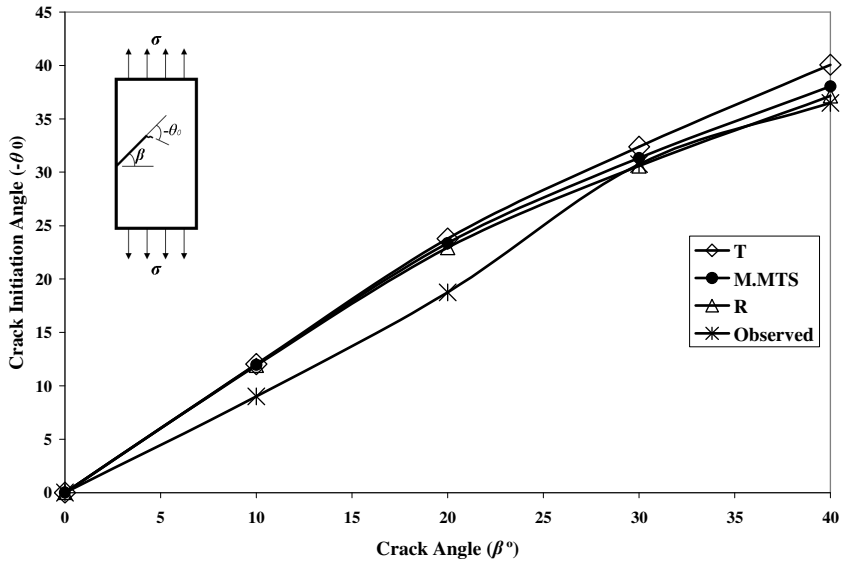

Figure 4.18: Comparison between observed and experimental crack initiation angles using T, M.MTS and R criteria.

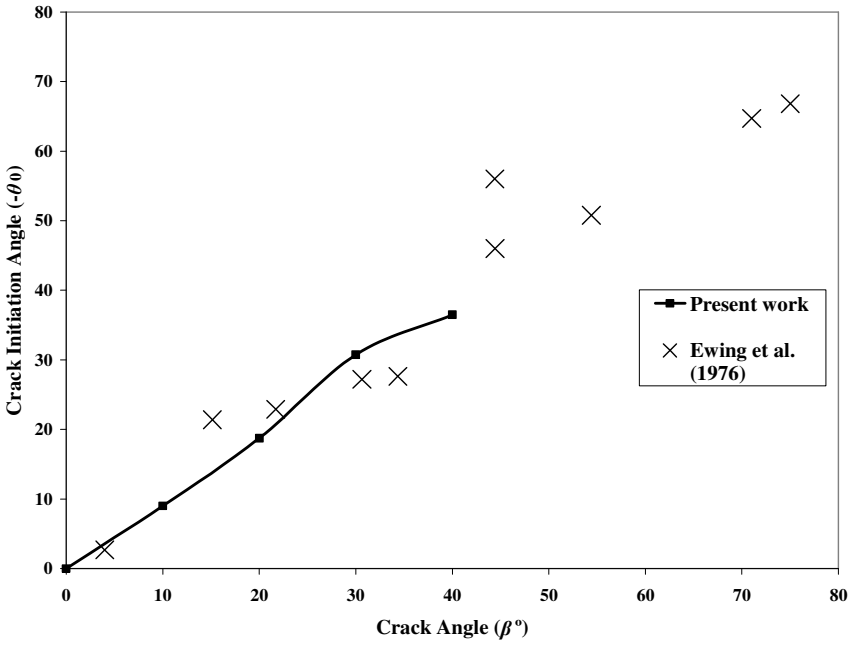

Figure 4.19: Comparison between experimental crack initiation angle of this study and Ewing *et al*. (1976).

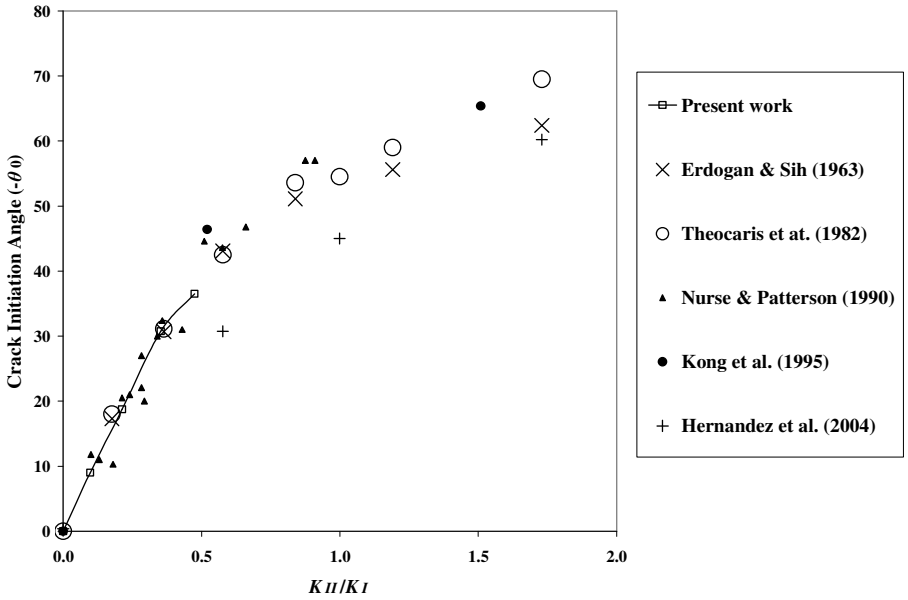

Figure 4.20: Comparison between experimental crack initiation angle of this study and available results in the literature.

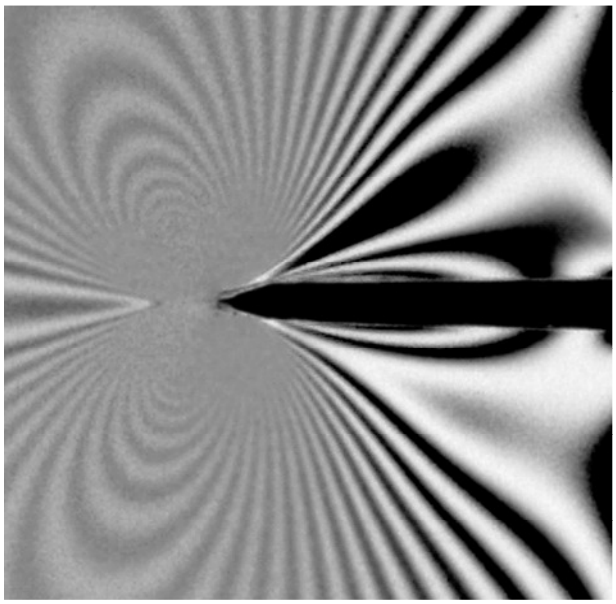

Figure 4.21: Crack initiation for β = 0º (Specimen #1).

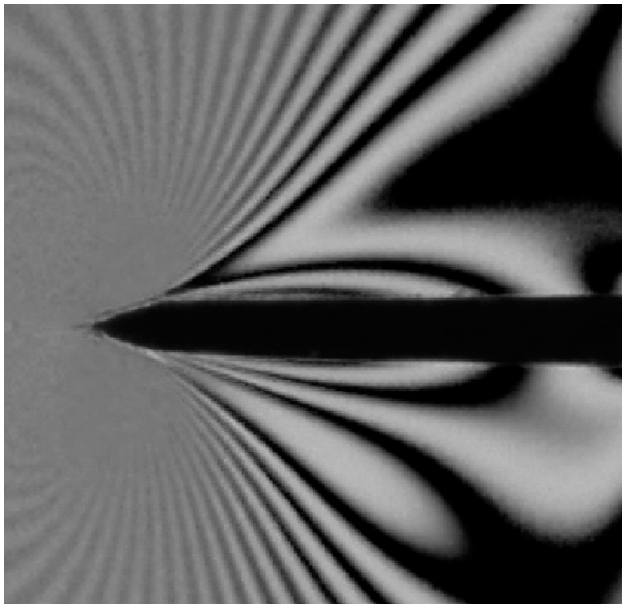

Figure 4.22: Crack initiation for β = 0º (Specimen #2).

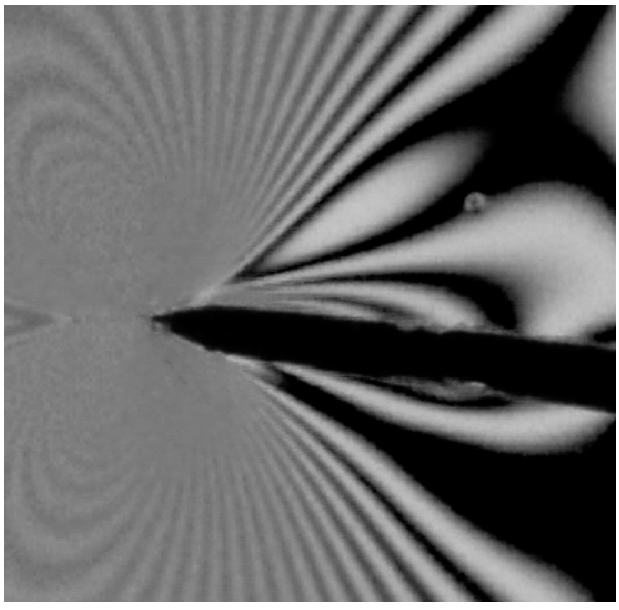

Figure 4.23: Crack initiation for β = 10º (Specimen #1).

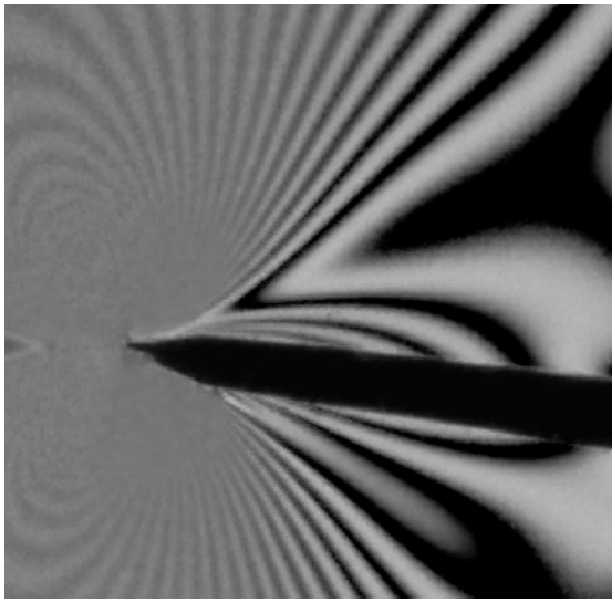

Figure 4.24: Crack initiation for β = 10º (Specimen #2).

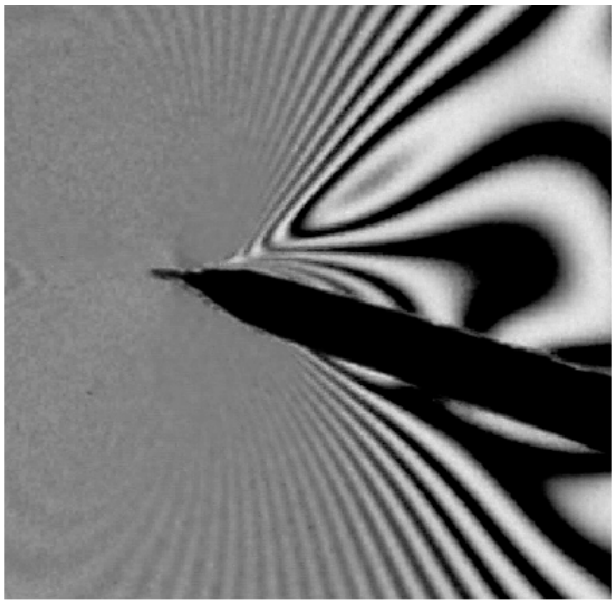

Figure 4.25: Crack initiation for β = 20º (Specimen #1).

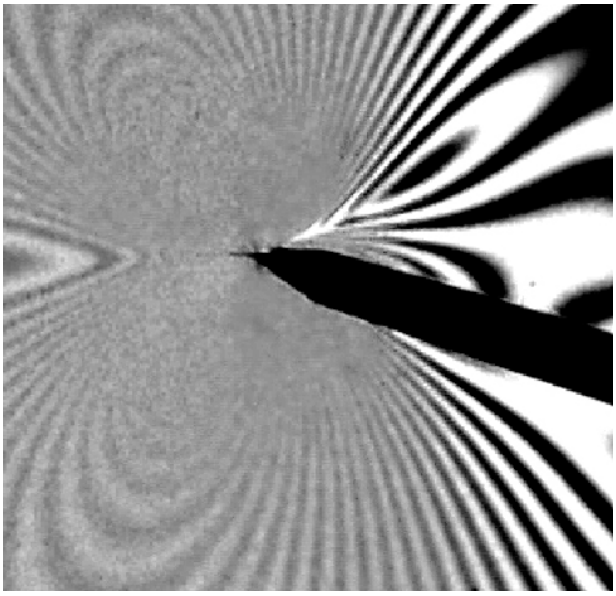

Figure 4.26: Crack initiation for β = 20º (Specimen #2).

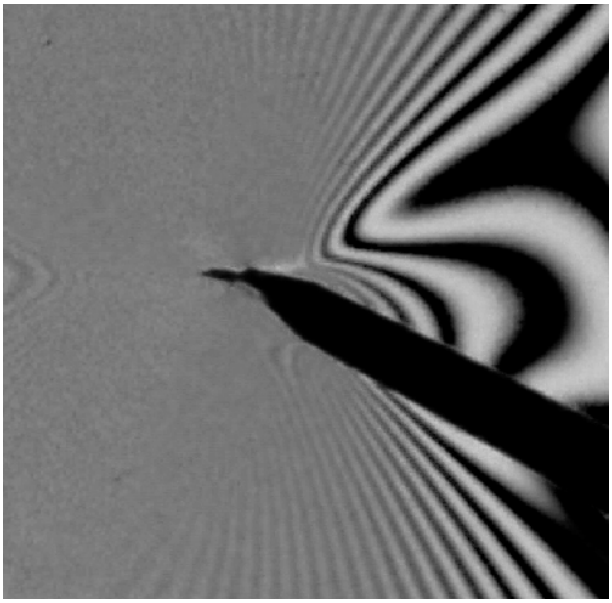

Figure 4.27: Crack initiation for β = 30º (Specimen #1).

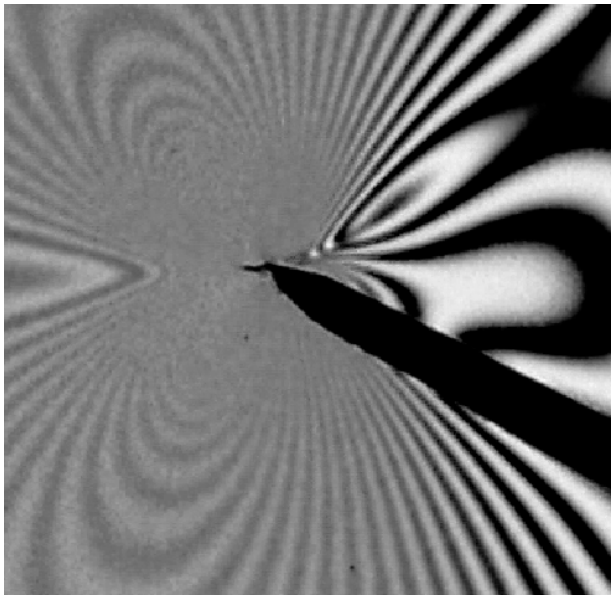

Figure 4.28: Crack initiation for $\beta = 30^{o}$ (Specimen #2).

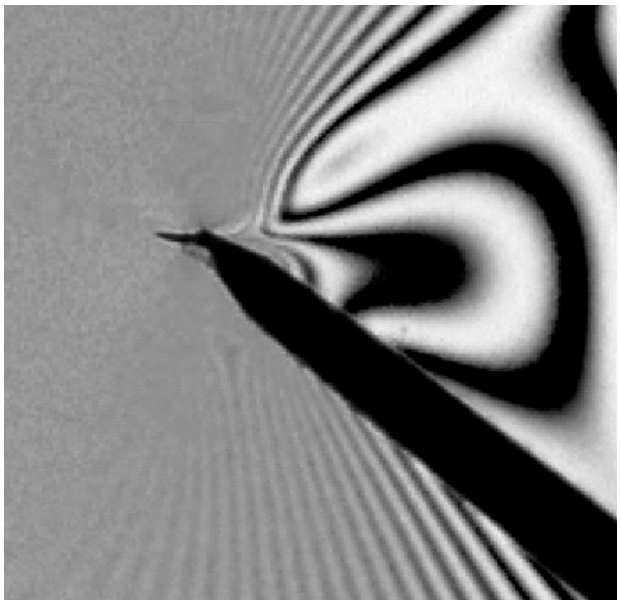

Figure 4.29: Crack initiation for $\beta = 40^{o}$ (Specimen #1).

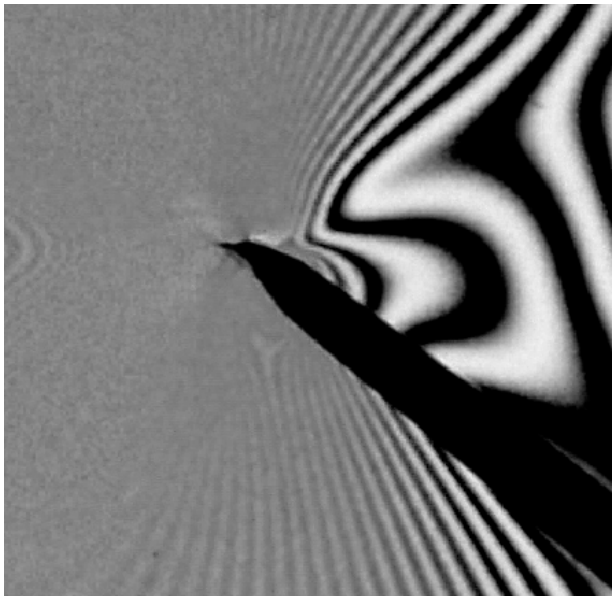

Figure 4.30: Crack initiation for $\beta = 40^{o}$ (Specimen #2).

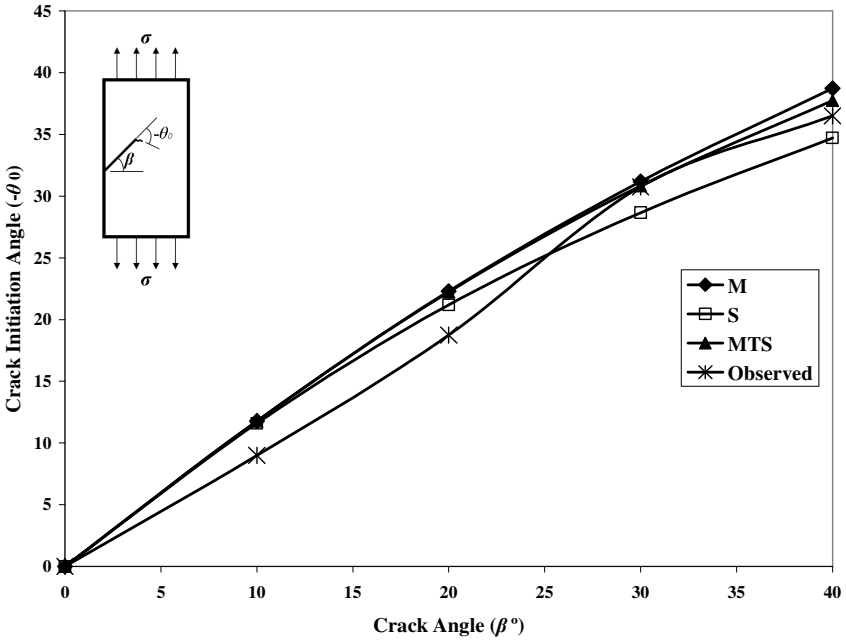

Figure 4.31: Comparison between observed and numerical crack initiation angles using M, S and MTS criteria.

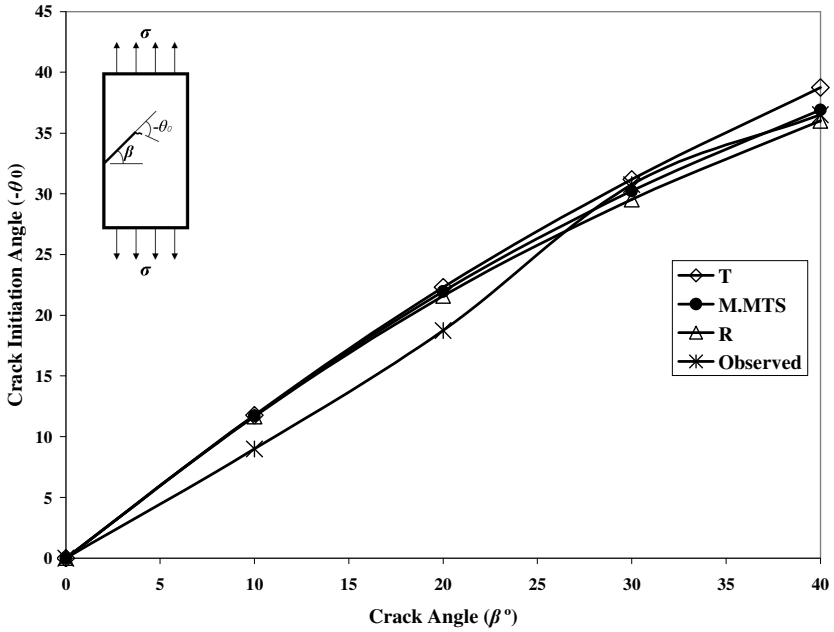

Figure 4.32: Comparison between observed and numerical crack initiation angles using T, M.MTS and R criteria.

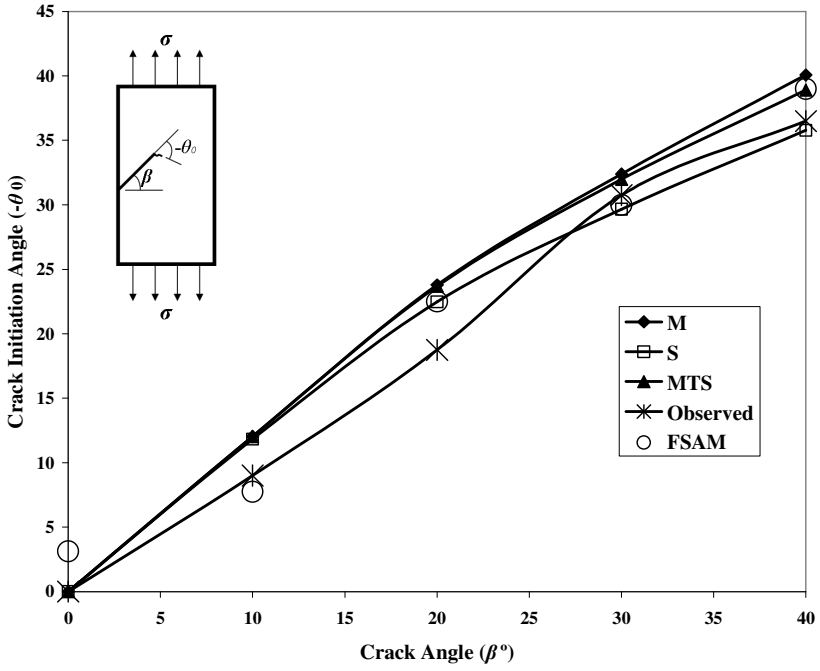

Figure 4.33: Comparison between observed, experimental and fringe symmetry axis crack initiation angles using M, S and MTS criteria.

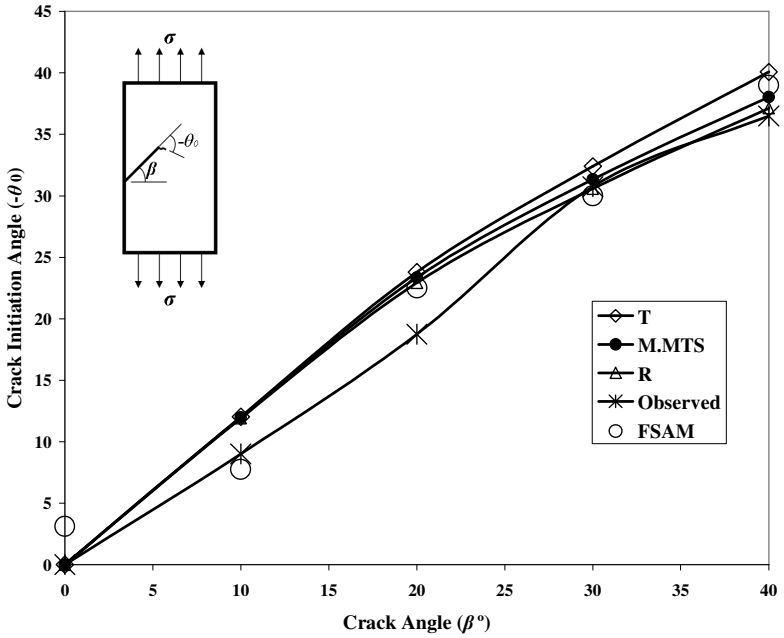

Figure 4.34: Comparison between observed, experimental and fringe symmetry axis crack initiation angles using T, M.MTS and R criteria.

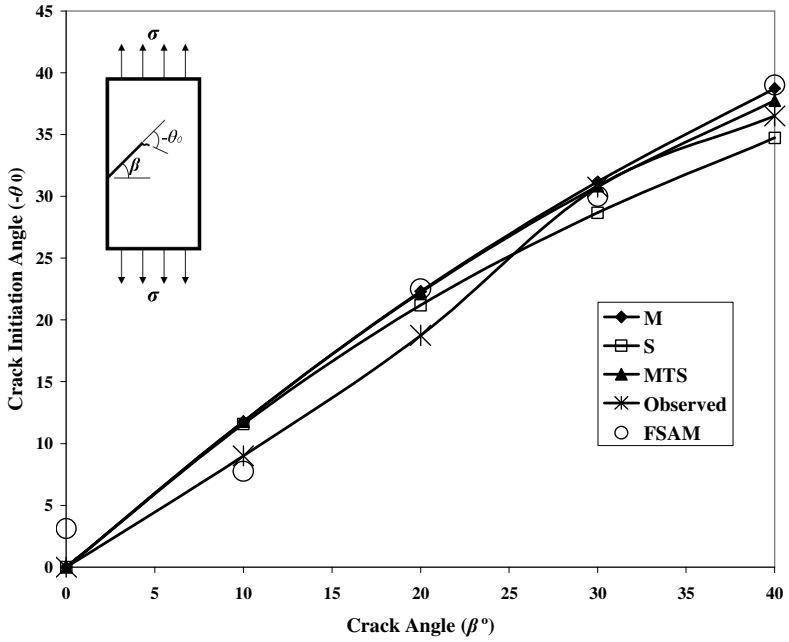

Figure 4.35: Comparison between observed, numerical and fringe symmetry axis crack initiation angles using M, S and MTS criteria.

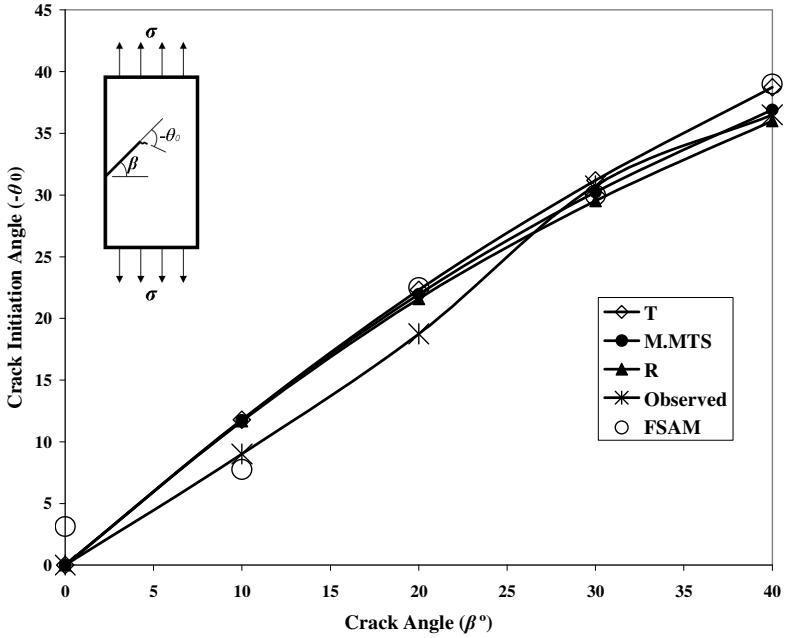

Figure 4.36: Comparison between observed, numerical and fringe symmetry axis crack initiation angles using T, M.MTS and R criteria.

CHAPTER 5

CONCLUSION AND RECOMMENDATIONS

5.1. Conclusion

The drawn conclusion from the presented experimental and numerical analyses can be summarized in the following pints:

1. ANSYS finite element code is an excellent numerical tool for estimating both pure and mixed mode SIF K_I and K_{II} for the case of an inclined edge crack panel subjected to tensile loading. The numerical estimation of the SIF compared very well with that obtained from photoelastic technique.

2. The finite element results were used to develop a new model for estimating the geometry correction factors for K_I and K_{II}. The proposed model for estimating the geometry correction factors of an inclined edge crack compared very well with the analytical solution for pure opening mode and with results available in the

literature for case of mixed mode fracture. Its validity was checked for the cases when a/w = 0, 0.1, 0.2, …, 0.7 and when β = 0°, 10°, 20°, …, 80°.

3. Photoelastic technique was used along with six criteria to estimate the crack initiation angle for an inclined edge crack. The results compared well with results available in the open literature.

4. Smith and Smith (1972) method for estimating the mixed mode stress intensity factors was tested and found to be not practical in determining the SIF because of the difficultly associated with limited area in which it is valid.

5. Sanford and Dally (1979) least squares method was used to estimate the mixed mode SIF K_I and K_{II}. In general, the method showed good accuracy in estimating the SIF but it its accuracy decreases for low inclination angle, especially for $\beta \leq 10°$. The method sensitivity in estimating the mixed mode SIF decreases as the crack inclination does.

6. Crack initiation angles estimated experimentally using the crack initiation criteria compared very well with observed crack initiation angles and with similar results available in the literature. In general, the measured crack initiation angles seem to be closest to those estimated from the S and R criteria. Fringe symmetry axis method (FSAM) was used to estimate the crack initiation angle. FSAM results

compared well with other experimental and numerical results of this study. This method was found to be the simplest of all the methods considered in this study.

7. The accuracy of the experimental results was found to be dependent on a number of factors including crack tip geometry, clarity of fringe image, method and type of criterion.

5.2. Recommendations

This research work involved analytical, experimental and numerical techniques for estimating crack initiation angle. Following are some recommendations that are useful for future investigations.

1. In photoelastic technique, manufacturing of a crack, especially the crack tip, is a vital issue which influences the accuracy of the results in terms of SIF and crack initiation prediction. The crack width should be small, approximately less than or equal to 0.5 *mm*. Otherwise, it will cause undesirable disturbances on the isochromatic fringe loops near the crack tip. This problem is more pronounced in the case of an inclined crack.

2. Serious care should be taken in photographing the isochromatic fringe field. If a digital camera is to be used, it should have the capability to be manually

controlled. Image size, focal length, aperture, focus and exposure time are all significant factors that can affect the quality of the image.

3. While using the fringe symmetry axis method it was found that the angle between the lines of fringe symmetry of the top and bottom fringes is approximately constant for all crack inclination angles. This angle can add extra degree of freedoms in the relations that govern the photoelastic determination of the mixed mode stress intensity factors. The importance of this point can be clarified by considering Smith and Smith (1972) method. In this method, the authors neglected the effect of the far field stress σ_{0x} because of lack in availability of relations. Smith and Smith used Eqs. 2.7 and 4.4 to express the maximum shear stress $\tau_{\max}$ in terms of r, θ, K_I and K_{II}. Since r, θ and $\tau_{\max}$ can be determined from a photoelastic experiment the only remaining variables are K_I and K_{II}, $\tau_{\max}$ can be calculated from Eq. (4.10). To resolve this, Smith and Smith used the idea proposed by Irwin (1958). Irwin observed the geometry of the fringe loops and noted that

$$\frac{\partial \tau_{\max}}{\partial \theta} = 0 \tag{5.1}$$

Combining Eqs. 4.11 and 5.1, give Eq. (4.12).

Hence, Eqs. 4.11,4.12 and 4.10 are used to estimate the mixed mode SIF K_I and K_{II}. Consequently, if the far field stress σ_{0x} is to be included additional relation is needed.

4. Real life problems involve multiaxial loadings. As a first step biaxial loading case needs also to be investigated experimentally and numerically.

5. FEA shows a good accuracy in estimating the stress intensity factors, hence, in describing the state of stress in the vicinity of the crack tip. It is well known that the crack propagation phenomenon is highly dependent on the state of stress at the crack tip. Accordingly, simulation of the crack initiation using FEA will add another dimension in analyzing and understanding such a problem. Incorporation of crack initiation criteria into FE codes will simplify the crack propagation simulation issue.

6. Simulation of the fringe patterns using FEA is already addressed in the literature. However, this issue did not take enough attention, especially for mixed mode fracture. A study that couples simulation of the fringe patterns and prediction of the crack initiation angle using fringe symmetry axis method (FSAM) is recommended.

7. Triaxiality effect, localized yielding and the size of the core region are all important factors that influence the values of the SIF as well as the crack initiation angle. Investigations of these factors that couple experimental and numerical techniques are needed.

8. The proposed model for estimating the geometry correction factors for an inclined edge crack was developed for uniaxial tensile loading. Other types of loadings need to be investigated.

REFERENCES

1 Albrecht, K., 1974, "Photoelastic Stress Analysis", John Wiley & Sons Ltd.

2 Anderson, T. L., 1995, "Fracture Mechanics: Fundamentals and Applications", CRS Press.

3 ANSYS ® Software, Version 10.0.

4 Ayatollahi, M. R., and Safari, H., 2003, "Evaluation of Crack tip Constraint Using Photoelasticity", Int. J. Pressure Vessels and Piping, Vol. 80, pp. 665-670.

5 Ayhan, A, O., 2004, "Mixed Mode Stress Intensity Factors for Deflected and Inclined Surface Cracks in Finite-Thickness Plates", Eng. Fracture Mech., Vol. 71, pp. 1059-1079.

6 Barsoum, R. S., 1976, "On the Use of Isoparametric Finite Elements in Linear Fracture Mechanics", Int. J. Num. Methods in Eng., Vol. 10, pp. 25-37.

7 Barsoum, R. S., 1977, "Triangular Quarter-point Elements as Elastic and Perfectly Plastic Crack Tip Elements", Int. J. Num. Methods in Eng., Vol. 11, pp. 85-98.

8 Bradley, W. B., and Kobayashi, A. S., 1970, "An Investigation of Propagating Cracks by Dynamic Photoelasticity", Exp. Mech., 10, pp. 106-113.

9 Broek, D., 1986, "Elementary Engineering Fracture Mechanics", Martinus Nijhoff Publishers, Dordrecht.

10 Callister, W. D., 2000, " Material Science and Engineering an Introduction" John Wiley & Sons, Inc.

11 Chan, W. Y., and Chow, C. L., 1979, "Notch Effects on Photoelastic Determination of Mixed-Mode Stress Intensity Factors", Eng. Fracture Mech., Vol. 12, pp. 253-265.

12 Dally, J. W., and Riley, W. F., 1991, "Experimental Stress Analysis", McGraw-Hill.

13 Durelli, A. J., and Riley, W. F., 1965, "Introduction to Photomechanics", Prentic-Hall, INC, / Englewood Cliffs, N.J.

14 Erdogan, F., and Shi GC., 1963, "On the Crack Extension in Plates under Plane Loading and Transverse shear", J. Basic Eng., Vol. 85, pp. 519-527.

15 Etherdige, J. M., and Dally, J. W., 1977, "A Critical Review of Methods for Determining Stress-Intensity Factors from Isochromatic Fringes", Exp. Mech., pp. 248-254.

16 Etherdige, J. M., and Dally, J. W., 1978, "A Three-Parameter Method for Determining Stress Intensity Factors from Isochromatic Fringe Loops", J. Strain Analysis, Vol. 13, No. 2, pp. 91-94.

17 Ewing, P. D., Swedlow, J. L., and Williams, J. G., 1976, "Further Results on the Angled Crack Problem", Int. J. Fracture, Vol. 12, No. 1, pp. 85-93.

18 Freese, C. E., and Baratta, F. I., 2006, “Single Edge-Crack Stress Intensity Factor Solutions", Eng. Fracture Mech., Vol. 73, pp. 616-625.

19 Gdoutos, E. E., 1980, "A Photoelastic Prediction of the Crack Propagation Angle", J. Phys. E: Sci. Instum., Vol. 13, pp. 776-778.

20 Gdoutos, E. E., 1984, "Problems of Mixed Mode Crack Propagation", Martinus Nijhoff Publishers, The Hague.

21 Griffith, A. A., 1921, Phil. Trans. Roy. Soc. London, Series A221, pp. 199.

22 Henshell, R. D., and Shaw, K. G., 1975, "Crack Tip Finite Element are Unnecessary", Int. J. Num. Methods in Eng., Vol. 9, pp. 495-507.

23 Hernandez-Gomez, L. H., Sauceda-Meza, I., Urriolagoitia-Calderon, G., Balankin, A. S., and Susarrey, O., 2004 "Evaluation of Crack Initiation Angle under Mixed Mode Loading at Diverse Strain Rates", Theoretical and Applied Fracture Mech., Vol. 42, pp. 53-61.

24 Hussain, M.A., Pu, S.L., and Underwood, J., 1974, “Strain Energy Release Rate for a Crack under Combined Mode I and Mode II", Fracture Analysis ASTM STP 560, pp. 2-28.

25 Irwin, G. R., 1958, Discussion of Ref., Proc. SESA, XVI(1), pp. 93-96.

26 James, F. D., and James, W. P., 1989, "Manual on Experimental Stress Analysis", Society for Exp. Mech.

27 Kong, X. M., Schluter, N., and Dahl, W., 1995, “Effect of Triaxial Stress on Mixed Mode-Facture", Eng. Fracture Mech., Vol. 52, No. 2, pp.379-388.

28 Madenci, E., and Guven, I., 2006, "The Finite Element Application in Engineering using ANSYS®", Springer.

29 MATLAB® Software, Version 7 (R14).

30 Nurse, A. D., and Patterson, E. A., 1990, "A Photoelastic Technique to Predict the Direction of Edge Crack Extension using Blunt Crack", Int. J. Mech. Sci., Vol. 32, No.3, pp. 253-264.

31 Peter, M., Haefele, and Lee, James D., 1995, "Combination of Finite Element Analysis and Analytical Crack Tip Solution for Mixed Mode Fracture", Eng. Fracture Mech., Vol. 50, No. 5/6, pp. 849-868.

32 Petit, C., Vergne, A., and Zhang, X., 1996, “A Comparative Numerical Review of Cracked Materials", Eng. Fracture Mech., Vol. 54, No. 3, pp. 423-439.

33 Photoelastic Stress Analysis Technical Bulletins, Measurement Group, Inc.

34 Post, D., 1954, "Photoelastic Stress Analysis of An Edge Crack in a Tensile Field", Proc. SESA, Vol. XII, No. 1, pp. 99-116.

35 Pu, S. L., Hussain, M. A., and Lorenson, W. E., 1978, "The Collapse Cubic Isoparamteric Elements as Singular Elements for Crack Problems", Int. J. Num. Methods in Eng., Vol. 12, pp. 1727-1742.

36 Ramesh, K., Gupta, S., and Kelkar, A. A., 1997, "Evaluation of Stress Field Parameters in Fracture Mechanics by Photoelasticity-Revisited", Eng. Fracture Mech., Vol. 56, No. 1, pp. 25-45

37 Rouhi, M. R., Evans, E. T., and Barr B. I. G., 1977, "Photoelastic Approach to Fracture Path Prediction", Int. J. Fracture, Vol. 13, pp. 370-6.

38 Rousseau, C. E., and Tippur, H. V., 2000, "Compositionally Graded Materials with Cracks Normal to the Elastic Gradient", Acta Materialia, Vol. 48, pp. 4021-4033.

39 Sanford, R. J., 1989, "Determining Fracture Parameters with Full-filed Optical Methods" Exp. Mech., pp. 241-247.

40 Sanford, R. J., 2003, “Principles of Fracture Mechanics”, Prentice Hall, Upper Saddle River, NJ.

41 Sanford, R. J., and Dally, J. W., 1979, "A General Method for Determining Mixed-Mode Stress Intensity Factors from Isochromatic Fringe Patterns", Eng. Fracture Mech., Vol. 1, pp. 621-633.

42 Schroedl, M. A., and Smith, C. W., 1973, "Local Stress Near Deep Surface Flaws under Cylindrical Bonding Fields" Progress in Flaw Growth and Fracture Toughness Testing, ASTM publication STP 536, pp. 45-63.

43 Schroedl, M. A., McGowan, J. J., and Smith, C.W., 1972, "An Assessment of Factors Influencing Data Obtained by the Photoelastic Stress Freezing Technique for Stress Fields Near Crack Tips", Eng. Fracture Mech., Vol.4, pp. 801-809.

44 Schroedl, M. A., Smith, C. W., "A Study of Near and Far Field Effects in Photoelastic Stress Intensity Determination", Eng. Fracture Mech., Vol. 7, pp. 341-355.

45 Shafique, M. A. K., 1999, "Investigation of Mixed Mode Crack Initiation Angles under Different Loading Conditions", MS Thesis, KFUPM.

46 Shafique, M. A., and Marwan, K., 2000, "Analysis of Mixed Mode Crack Initiation Angles under Various Loading Conditions", Eng. Fracture Mech., Vol. 67, pp. 397-419.

47 Shafique, M. A., and Marwan, K., 2004, "A New Criterion for Mixed Mode Fracture Initiation Based on Crack Tip Plastic Core Region", Int. J. Plasticity, Vol. 20, pp. 55-84.

48 Shan, Baoxiang, and Pelegri, Assimina A., 2003, "Assessment of the Fracture Behavior of An Asymmetrically Loaded Cantilever Composite Structure", J. Eng. Mat. and Tech., Vol. 125, pp. 353-360.

49 Shigley, J. E., 2004, "Mechanical Engineering Design", McGraw-Hill, Inc.

50 Sih, G. C., 1973, "Some Basic Problems in Fracture Mechanics and New Concepts", Eng. Fracture Mech., Vol. 5, pp. 365-377.

51 Sih, G. C., 1974, “Strain Energy Density Factor Applied to Mixed Mode Crack Problems", Int. J. Fracture, Vol. 10, No. 3, pp. 305-321.

52 Smith, D. G., and Smith, C. W., 1972, "Photoelastic Determination of Mixed Mode Stress Intensity Factors", Eng. Fracture Mech., Vol. 4, pp. 357-366.

53 Theocaris, P. S., and Andrianopoulous, N., P., 1982, "The Mises Elastic-Plastic Boundary as the Core Region in Fracture Criteria ", Eng. Fracture Mech., Vol. 16, No.3, pp. 425-432.

54 Theocaris, P. S., and Andrianopoulous, N., P., 1982, "The T-criterion Applied to Ductile Fracture", Int. J. Fracture, Vol. 20, pp. R125-R130.

55 Theocaris, P.S., and Gdoutos, E. E., 1975, "A Photoelastic Determination of KI Stress Intensity Factors", Eng. Fracture Mech., Vol. 7, pp. 331-339.

56 Tilbrook, M. T., Reimanis, I. E., Rozenburg, K., and Hoffman, M., 2005, "Effect of Plastic Yielding on Crack Propagation near Ductile/Brittle Interfaces", Acta Materialia, Vol. 53, pp. 3935-3949.

57 Ukadgaonker, V. G., and Awasare, P. J., 1995, "A New Criterion for Fracture Initiation", Eng. Fractrure Mech., Vol. 51, No.2, pp.265-274.

58 Wells, A., and Post, D., 1958, "The Dynamic Stress Distribution Surrounding a Running Crack- A Photoelastic Analysis", Proc. SESA, XVI(1), pp. 69-92

59 Westergaard, H. M., 1937, “Bearing Pressure and Cracks", J. Applied Mech., Vol. 6, pp. A49-53.

60 Wilson, W. K., 1969, Research Report 69-IE7-FMECH-RI, Westinghouse Research Laboratory, Pittsburg.

61 Yin, X. C., and Chen, T. G., 1991, "Photoelastic Investigation of Mixed-Mode Fracture Parameters with Full-Field Selected Line Method", Eng. Fracture Mech., Vol. 39, No. 6, pp. 965-975.

APPENDIX I

```
!                  ANSYS Command File


! Dimensions: Length (m), Stress (Pa), angles (degree)

! Inputs: 1) Specimen crack Length (a)
!         2) Specimen width (w)
!         3) Specimen length (L)
!         4) Crack angle of inclination (beta)
!         5) Applied stress (P)
!         6) Singular elements Radius (R)
!         7) Number of singular elements around the crack
!            tip (N)
!         8) Modulus of Elasticity (E)
!         9) Poisson's ratio (nu)


/PREP7                     ! Enter preprocessor

a=10.0e-3
w=60e-3
L=180e-3
beta=0
P=7.63e6
R=8e-4
N=12
E=2500e6
nu=0.38


*AFUN,DEG                  ! Switch to degree


ET,1,2                     ! Select element type
                           ! as PLANE2
KEYOPT,1,3,0               ! Plane stress behavior

MP,EX,1,E                  ! Elastic Modulus
MP,PRXY,1,nu               ! Poisson's ratio


y3= L/2+w*tan(beta)        ! Y-coordinate of KP3
x7= a*cos(beta)            ! X-coordinate of KP7
y7= a*sin(beta)+L/2        ! X-coordinate of KP7



! Create Keypoints
! as shown in Fig. 3.3
! listed in Table 3.1

K, ,,,,
```

```
K, ,w,0,,
K, ,w,y3,,
K, ,w,L,,
K, ,0,L,,
K, ,0,L/2,,
K, ,x7,y7,,                ! Crack tip
K, ,0,L/2,,

! Create Lines

L,1,2
L,2,3
L,3,7
L,7,8
L,8,1
L,7,6
L,6,5
L,5,4
L,4,3


! Create Areas

AL,1,2,3,4,5
AL,6,7,8,9,3



CSKP,11,0,7,3,5,1,1,       ! Define local coordinate
                           ! system at crack tip, KP7

CSYS,0                     ! Switch to Global Cartesian

KSCON,7,R,1,N/2,0,             ! Create concentration point
                           ! at the crack tip, KP7


KESIZE,ALL,0.005           ! Specify the edge lengths
                           ! of the elements nearest
                           ! keypoints



MSHKEY,0                   ! Free mesh
AMESH, ALL                 ! Area mesh



NSEL,S,LOC,X,0             ! Select node at (0,0) as
NSEL,R,LOC,Y,0             ! shown in Fig. 3.10
D,ALL,UX                   ! Restrict the disp. in X
ALLSEL                     ! Select everything


NSEL,S,LOC,Y,0             ! Select nodes at y = 0
D,ALL,UY                   ! Restrict the disp. in Y
ALLSEL                     ! Select everything


NSEL,S,LOC,Y,L             ! Select nodes at y = L
SF,ALL,PRES,-P             ! Apply pressure load
```

```
ALLSEL                    ! Select everything



/SOLU                     ! Enter solution phase
SOLVE                     ! Solve


/POST1                    ! Enter postprocessor

RSYS,11                   ! Activate local CS
CSYS,11,                  ! Switch to local CS 11

NPLOT                     ! Plot nodes


! Zoom the area around the crack tip then define the path
! as shown in Fig. 3.9 and refer to Section 3.2.1
! the menu path is: Main Menu>General Postproc>
!                   Path Operations>Define Path>By Nodes
! after that, execute the command below



KCALC,1,1,3,0             ! Calculate SIF
```

APPENDIX II

```
% Sanford and Dally (1979) Least Squares Method for
% Estimating the Mixed Mode SIF KI and KII


clear all


% Data point matrix P size is m×3
% "m" is the number of data

% P = [fringe order "N" ^ radial distance "r" (m) ^ angular position
%      "θ" (radians)]



P=[1.5      0.00262     2.093
    2       0.00135     2.093
    3       0.00207     1.918
   3.5      0.00166     1.918
    4       0.00266     1.744
.........................
.........................
.........................];


% Material fringe constant "fr" (Pa/fringe/m)
% Specimen thickness h (m)


fr=7e3;
h=3e-3;


% Initial guesses for "KI", "KII" and "Sox"
% Sox is the far field stress


KI=input ('KI = ');
KII=0;
Sox=0;

% Number of iteration "iter"


iter=input(' The Number of Iteration = ');
index=0;



while (index<iter)

% "N" is the fringe order, "r" is the radial distance and "t" is
% angular position




for j=1:m
```

```
        N=P(j,1);
        r=P(j,2);
        t=P(j,3);

% f is Eq. (4.15) a is matrix [c] in Eq. 4.19



f(j,1)=1/(2*pi*r)*((KI*sin(t)+2*KII*cos(t))^2+(KII*sin(t))^2)
            +2*Sox/sqrt(2*pi*r)*sin(t/2)*(KI*sin(t)*(1+2*cos(t))
            +KII*(1+2*(cos(t))^2+cos(t)))+Sox^2-(N*fr/h)^2;


a(j,1)=-(1/(pi*r)*(KI*(sin(t))^2+2*KII*cos(t)*sin(t))
            +2*Sox/sqrt(2*pi*r)*sin(t/2)*(sin(t)*(1+2*cos(t))));

a(j,2)=-(1/(pi*r)*(2*KI*sin(t)*cos(t)+4*KII*(cos(t))^2)
            +KII*(sin(t)^2)
            +2*Sox/sqrt(2*pi*r)*sin(t/2)*(1+2*(cos(t))^2+cos(t)));

a(j,3)=-(2/sqrt(2*pi*r)*sin(t/2)*(KI*sin(t)*(1+2*cos(t))
                  +KII*(1+2*(cos(t))^2+cos(t)))+2*Sox);


end


f;
a;


d=a'*f;
c=a'*a;

% dK is Eq. (4.21)


dK=inv(c)*d;


K1=KI+dK(1,1);
K2=KII+dK(2,1);
Stox=Sox+dK(3,1);


KI=K1;
KII=K2;
Sox=Stox;


index=index+1;
end


KI=KI/1000
KII=KII/1000
Sox=Sox/1000
```

VITAE

Name: Jafar Husain Ali Al Bin Mousa

Date of Birth: 30 Nov. 1980

Place of Birth: Al Hassa, Saudi Arabia

Marital Status: Married

Nationality: Saudi

Education: Bachelor of Applied Mechanical Engineering from KFUPM, June 2003.

Master of Science in Mechanical Engineering from KFUPM, June 2006.

Academic Rank: Graduate Assistant in Mechanical Engineering Department at KFUPM since October 2003.

Teaching Activities: Material Science (ME 205/215) Laboratory from February to June 2004 and from February to June 2006.

Machine Design (ME 308) Laboratory from September 2004 to February 2005, February to June 2005 and from September 2005 to January 2006.